THE DESIGN, ASSEMBLY, AND TESTING OF A
SHOCK TUBE FOR STUDY OF COAL
COMBUSTION KINETICS

by

WILLIAM RANDALL SEEKER

B. S., New Mexico State University, 1974

A MASTER'S THESIS

submitted in partial fulfillment of the
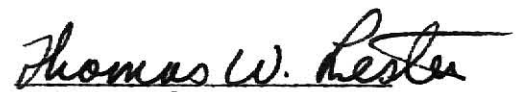requirements for the degree

MASTER OF SCIENCE

Department of Nuclear Engineering

KANSAS STATE UNIVERSITY

Manhattan, Kansas

1976

Approved by:

Major Professor

TABLE OF CONTENTS

1 2

NOMENCLATURE OF TERMS

a   Local speed of sound of gas; m/sec

C   Conductance of vacuum connection; 1/sec

C_p Specific heat at constant pressure; kcal/kg °K

C_v Specific heat at constant volume; kcal/kg °K

d   Inside diameter; in (cm)

d'   Outside diameter; in (cm)

H   Enthalpy per unit mass; J/kg (Btu/lbm)

L   Length of vacuum connection; ft(cm)

M_s Incident shock Mach number

M_s^* Analytical shock attenuation factor

P   Pressure; bars (psi), torr

P_{st} Standard pressure (one atmosphere)

R   Gas constant; J/kg °K (ft^2/s^2 °R)

S   Tensile strength; bars (psi)

S_1 Vacuum pump speed; 1/sec

S_n Speed of evacuation; 1/sec

T   Temperature, °K

t   Time, sec

U   Velocity in shock-fixed coordinates; m/sec

V   Tube volume, cm^3

v   Velocity in laboratory-fixed coordinates; m/sec

W_s Velocity of incident shock front; m/sec

W_R Velocity of reflected shock front; m/sec

X   Distance measured along tube from diaphragm; m

X_2 Distance of collision of contact surface and reflected shock front; m

X_c Distance from diaphragm when reflected rarefaction head overtakes contact surface; m

γ Specific heat ratio, C_p/C_v

ρ Gas density, gm/cm^3

τ_2 Time after diaphragm rupture when reflected shock collides with contact surface; msec

τ_c Time after diaphragm rupture that rarefaction overtakes contact surface; msec

$\Delta\tau$ Time interval between shock front arrival at end wall and its collision with the contact surface; msec

$\Delta\tau'$ Effective observation behind reflected shock; msec

SUBSCRIPTS

1   Region of undisturbed test gas

2   Region behind incident shock front to contact surface

3   Region between contact surface and rarefaction tail

4   Region of undisturbed driver gas

5   Region behind reflected shock front

s   Incident shock

LIST OF FIGURES

LIST OF TABLES

I. INTRODUCTION

Increased use of our domestic energy reserves will be possible only
if they can be consumed in a safe and environmentally sound manner. For
instance, one problem in the direct combustion of coal is minimizing the
emission of noxious pollutants. On the other hand, the continuing deploy-
ment of light water reactors will require a better understanding of
thermal-hydraulic behavior during abnormal occurences. The unique gas
dynamic characteristics of shock tubes make them suitable test vessels
for basic studies in both areas.

Implementation of control strategies in coal combustion, such as
flue-gas recirculation, reduction in primary air, and staged combustion
will demand an understanding of the kinetic processes involved. However,
knowledge of these reactions is non-existent due primarily to difficulties
in kinetic measurements in particle-laden flows. The traditional approach
in the research of pulverized coal combustion has been to utilize furnaces
and flames. However, velocity, concentration, and temperature gradients
inherent in the combustion zone of such apparatus and difficulties in their
use for pulverized fuels due to coagulation and blockage of ports, severely
limit the quality of kinetic results obtainable from these techniques.
The conventional shock tube does not suffer from these disadvantages. The
region behind the reflected shock is practically gradient free. Ideally,
gases in the reaction zone of a shock tube can be brought almost instan-
taneously (within nanoseconds) to any desired temperature and pressure and
held at these precisely controlled values for hundreds of microseconds.
The reaction zone of the shock tube can thus be probed by the various
optical and spectroscopic techniques developed previously for the investigation

of homogeneous reaction kinetics to determine time-resolved species concentrations. In this manner the complex chemical reaction kinetics of the pulverized coal combustion sequence may become more understandable.

Another, completely separate problem that can be studied is the breakage of a main coolant supply line to the pressure vessel of a pressurized water reactor (PWR). This causes rapid decompression and loss of coolant. Thus, the water in the reactor region, which was initially subcooled, becomes supersaturated and vaporizes. Therefore, a study of this boiling transition phenomenon is essential to the analysis of the accident outcome.

In a conventional shock tube the production of the shock wave results from the expansion of a gas at high pressure into a second chamber of initially much lower pressure. A possible approach to the study of phase transition would use the decompression of the high pressure section. In this novel technique, an additional chamber filled with water with an immersed heating element would be attached to the high pressure section. Characteristics of boiling are analyzed through the power dissipated by the heating element and through high speed photography.

The preliminary purpose of this investigation is to design a conventional shock tube facility to be used in subsequent chemical reaction kinetic studies. The critical design parameters, section lengths and internal diameter, were established from maximum conditions required in combustion processes (design basis criteria). The back up systems were designed and consist of the following:

(1) Tube: The tube material, flanging, dimensions, and diaphragm holder;

(2) Support System: The equipment used for mounting the tube including the adjustable support carts and channel retaining rail for the carts;

(3) Vacuum System: The complete valving and pumping
     system for evacuation of the test section;

(4) Gas Mixing System: The valving manifolds for
     selection of constituents for driver and test gases;

(5) Analysis Instrumentation; Includes thin film resis-
     tance shock front identification, time interval
     instrumentation, pressure transducer and observation
     ports.

Following the acquisition of all parts, construction of the facility,
and development of operating procedures, the actual phase began. This
consisted of measurement of shock speed at various initial conditions,
the determination of shock speed attenuation along the tube, and analysis
of pressure histories.

In the following sections a review of shock tube theory is covered.
After enumeration of the design considerations involved, the specific
design features are presented. Finally, the performance of the facility
is presented with emphasis on pressure histories and shock attenuation
results.

II. THEORY AND GOVERNING EQUATIONS

Since its inception by Vieille (1899) and its development to its
modern form by Bleakney's group at Princeton in the late 1940's, the
shock tube has developed into an invaluable research tool in diverse
areas. Basically, a conventional shock tube is a device in which a
plane shock wave is produced by the bursting of a diaphragm which se-
parates the high pressure driver from the driven (or test) gas at a
much lower pressure. This shock wave propagates down the tube into
test gas, heating it suddenly ($>10^5$ °K/sec) to a higher temperature.
The temperature step has associated with it, a pressure discontinuity.
The shock wave will eventually reach the end of the tube at which
point it will reflect into itself. This region behind the front of the
reflected shock is then further heated and brought to higher pressures.
This reaction zone is virtually free of velocity gradients and can be
brought to almost any desired temperature (<4000 °K).

Shock Waves in Ideal Gases

The gas flow theory in the shock tube for ideal gases has been well
investigated (Rankine, 1870; Hugoniot, 1877; Resler, Lin, and Kantrowitz,
1952; Gaydon and Hurle, 1963) and will be presented here only for com-
pleteness. To best illustrate the flow, the (X - t) diagram, of which
Fig. 1 is an example of the ideal case, is presented. It is apparent
from the diagram that the distance of a fan or wave from the diaphragm
is plotted along the horizontal axis with the corresponding time its
vertical component. The origin of the horizontal axis then is just at
the diaphragm.
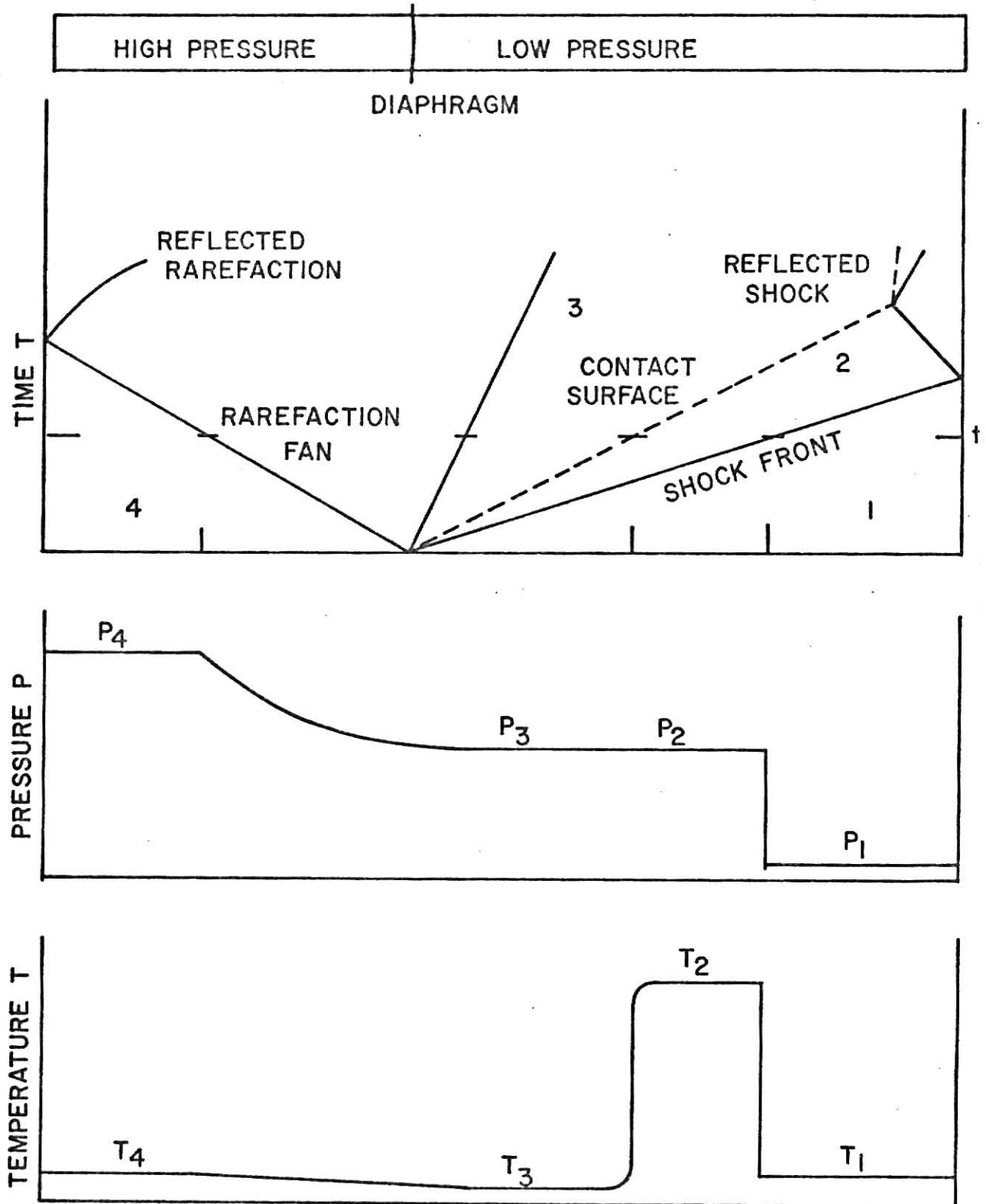
Fig. 1
EXAMPLE OF AN (X-t) DIAGRAM

At the origin of time there is no flow but immediately after the diaphragm has burst the (X - t) diagram shows the propagation of the right-moving shock front into the test gas. The actual bursting process is complicated but in oversimplified terms the diaphragm is assumed to be removed instantaneously. The compression waves, thus formed by the burst, rapidly steepen into the shock wave shown. The shock front moves into the stationary test gas with velocity W_s, which is greater than the local speed of sound of the test gas. The contact surface which marks the back edge of the shock wave is ideally a planar surface separating the test gas and the driver gas. Simultaneously a left-moving expansion fan moves into the driver gas with the local speed of sound of the driver.

The shock front continues down the tube until it reaches the end wall, at which point the shock wave reflects into itself. The secondary wave thus causes additional heating and pressure increases analogous to the original shock wave. The time available for observation behind the reflected shock, or the time during which the pressure and temperature remain relatively constant, is just the time required for the reflected shock front to rebound off the approaching contact surface and to reach the end wall for the second time. (see Fig. 2) The ultimate observation time is due to the reaction quenching properties of the rarefaction head which has arrived at the test section end wall by virture of its reflection off of the driver end wall and subsequent propagation into the test section.

A simple transformation of coordinate systems from the normal laboratory-fixed coordinates to one in which the shock front is at rest will simplify the unsteady flow equations. As can be seen in Fig. 3, in the laboratory-

Fig. 2

AVAILABLE OBSERVATION TIME IN THE REFLECTED SHOCK

LABORATORY-FIXED COORDINATES i.e. SHOCK TUBE AT REST

DRIVER GAS 3	SHOCK WAVE 2	TEST GAS 1
$P_2 = P_3$, ρ_3, T_3	V_2 $\longrightarrow$ P_2, ρ_2, T_2	W_s $\longrightarrow$ P_1, ρ_1, T_1
$V_3 = V_2$ $\longrightarrow$	V_2 $\longrightarrow$	

CONTACT
SURFACE
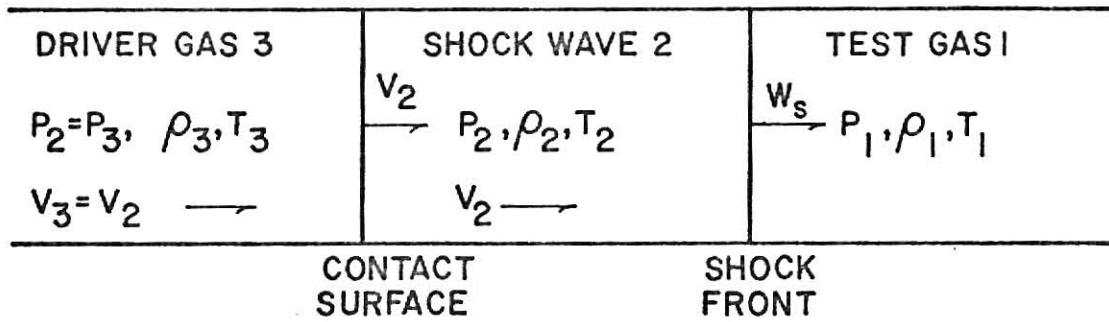
SHOCK
FRONT

SHOCK-FIXED COORDINATES i.e. SHOCK FRONT AT REST

$U_2 = W_s - V_2$ $\longleftarrow$ $\longleftarrow$ $U_1 = W_s$
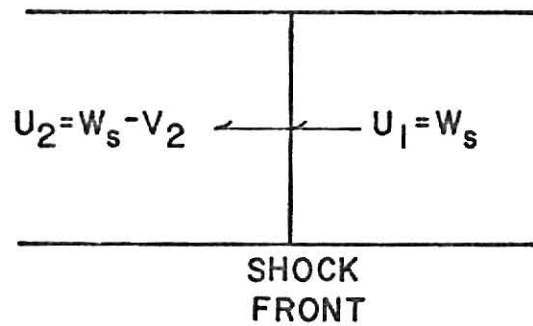
SHOCK
FRONT

Fig. 3

LABORATORY-FIXED AND SHOCK-FIXED COORDINATE SYSTEMS

fixed coordinate system the shock front moves into the test gas with a velocity W_s; while in a shock-fixed system the gas moves across the front with velocity $U_1=W_s$. The gas behind the shock, which is moving with velocity V_2 in the laboratory-fixed coordinate system is traveling away from the shock front at a speed of $U_2=W_s-V_2$ in shock-fixed coordinates.

The beginning fundamental equations are found from a straight forward treatment of the flow across the shock front. First, from the equation of continuity at constant area,

$$\rho_1 U_1 = \rho_2 U_2 \tag{1}$$

Also the conservation of momentum can be applied so that the force on the shock front is set equal to the product of the mass flow rate and velocity change. Thus for constant cross-sectional area this is

$$(P_2 - P_1) = (U_1\rho_1) \times (U_1 - U_2) \ ,$$

which can be written as

$$P_2 + (U_1\rho_1)U_2 = P_1 + \rho_1 U_1^2 \ .$$

Using equation (1), it follows that,

$$P_2 + \rho_2 U_2^2 = P_1 + \rho_1 U_1^2 \ . \tag{2}$$

Finally, the basic differential equation for the conservation of energy for the case of no change in heat, work, height or internal energy across the shock front can be written in the integrated form as,

$$H_2 + 1/2 \ U_2^2 = H_1 + 1/2 \ U_1^2 \ . \tag{3}$$

The basic fluid flow equations can be used to derive the so-called Rankine-Hugoniot equations (Rankine, 1870; Hugoniot, 1877). The enthalpy per unit mass can be written as the product of the temperature and the specific heat at constant pressure so that using the ideal gas law,

$$H = C_p T = \left(\frac{\gamma}{\gamma-1}\right)RT = \left(\frac{\gamma}{\gamma-1}\right)\frac{P}{\rho} . \tag{4}$$

Then from equations (3) and (4) we find

$$\left(\frac{\gamma}{\gamma-1}\right)\frac{P_1}{\rho_1} + 1/2\ U_1^2 = \left(\frac{\gamma}{\gamma-1}\right)\frac{P_2}{\rho_2} + 1/2\ U_2^2 . \tag{5}$$

Combining with the other basic equations and eliminating U_1 and U_2 and after rearranging, the following are arrived at:

$$\frac{P_2}{P_1} = \frac{1 - \left(\frac{\gamma-1}{\gamma+1}\right)\rho_1/\rho_2}{\rho_1/\rho_2 - \left(\frac{\gamma_1-1}{\gamma_1+1}\right)} \tag{6}$$

and

$$\frac{\rho_2}{\rho_1} = \frac{U_1}{U_2} = \frac{\left(\frac{\gamma-1}{\gamma+1}\right) + P_2/P_1}{\left(\frac{\gamma_1-1}{\gamma_1+1}\right) + 1} . \tag{7}$$

Equations (6) and (7) are known as the Rankine-Hugoniot equations.

Since the Mach number M_s, is the ratio of the speed of a disturbance or flow in a gas to the local speed of sound in the gas, the Mach number related to the shock front is:

$$M_s = \frac{U_1}{a_1} = \frac{W_s}{a_1} \tag{8}$$

The local sound speed is related to the square root of the temperature of the gas or from the ideal gas law

$$a_1 = \sqrt{\gamma_1 R T_1} = \sqrt{\gamma_1 P_1/\rho_1} \tag{9}$$

The thermodynamic parameter ratios across the incident shock front as a function of the incident shock Mach number are obtained from the Rankin-Hugoniot equations (6) and (7) and from equations (1), (2), (8) and (9).

$$\frac{P_2}{P_1} = \frac{2\gamma M_s^2 - (\gamma_1 - 1)}{\gamma_1 + 1} , \tag{10}$$

$$\frac{\rho_2}{\rho_1} = \frac{(\gamma_1 + 1) M_s^2}{(\gamma_1 - 1) M_s^2 + 2} , \tag{11}$$

$$\frac{T_2}{T_1} = \frac{P_2 \rho_1}{P_1 \rho_2} = \frac{(\gamma_1 M_s^2 - \frac{\gamma_1 - 1}{2})(\frac{\gamma_1 - 1}{2} M_s^2 + 1)}{(\frac{\gamma_1 + 1}{2})^2 M_s^2} . \tag{12}$$

The behavior of these equations as a function of M_s is demonstrated graphically in Fig. 4. Thus the strength of a shock i.e. P_2/P_1 is determined solely by its speed.

The dependence of the shock strength on the diaphragm bursting-pressure-to-initial-test-gas-pressure ratio is found to be (Appendix A):

$$\frac{P_4}{P_1} = \frac{2\gamma_1 M_s^2 - (\gamma_1 - 1)}{(\gamma_1 + 1)} \left\{ 1 - \frac{\gamma_4 - 1}{\gamma_1 + 1} (M_s - \frac{1}{M_s}) \right\}^{-2\gamma_4/(\gamma_4 - 1)} . \tag{13}$$

Although in practice the actual shock Mach number is less than that predicted by equation (13), it can be used to predict the shock strength for a bursting pressure ratio and a certain set of driver/test gases. Equation (13) is very useful in the choosing of the best driver gases, a procedure which will be discussed later.

Finally, the conditions behind the reflected shock front can be obtained in an analysis completely analagous to the incident shock front (Gaydon and Hurle, 1963, p. 25);

$$\frac{P_5}{P_1} = \left\{ \frac{2\gamma M_s^2 - (\gamma - 1)}{\gamma + 1} \right\} \left\{ \frac{(3\gamma - 1) M_s^2 - 2(\gamma - 1)}{(\gamma - 1) M_s^2 + 2} \right\} , \tag{14}$$

$$\frac{\rho_2}{\rho_1}$$

$$\frac{P_2}{P_1}$$

$$\frac{T_2}{T_1}$$
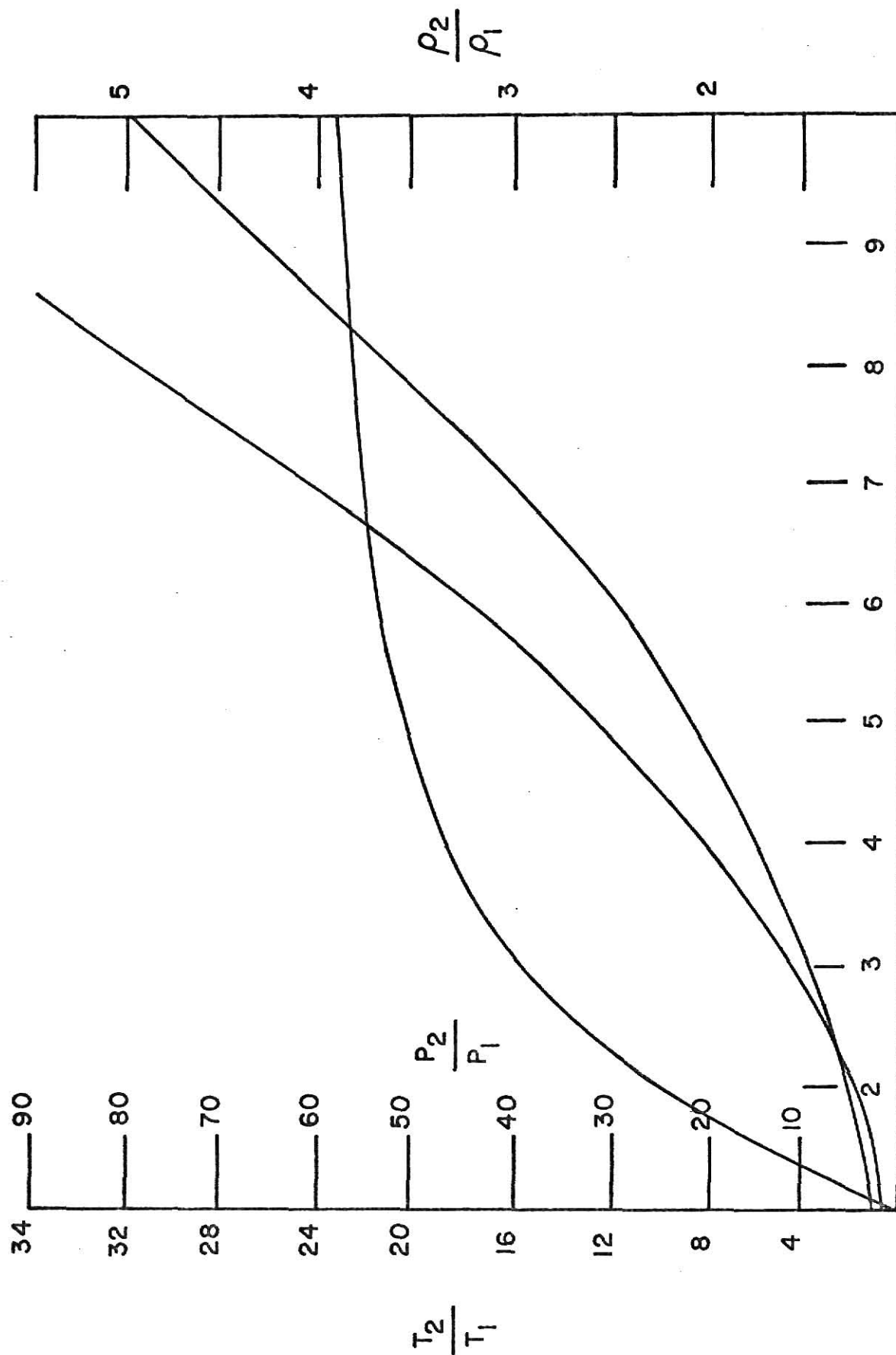
MACH NUMBER OF INCIDENT SHOCK

Fig. 4

VARIATION OF SHOCK PARAMETERS WITH INCIDENT MACH NUMBER

$$\frac{T_5}{T_1} = \frac{\{2(\gamma-1)M_s^2 + (3-\gamma)\} \ \{(3\gamma-1)M_s^2 - 2(\gamma-1)\}}{(\gamma+1)^2 \ M_s^2} . \qquad (15)$$

There are important considerations involved in the working behind the reflected shock front, as opposed to behind the incident shock, that are useful in the study of chemical reactions. First are the much larger obtainable increases in pressure and temperature. More importantly, since the gas is at rest behind the reflected shock, the molecules can be viewed for the entire observation time in the reflected case.

Shock Waves in Real Gases and Real Shock Tube Performance

There are three major causes for the inaccuracies in the above analysis: (i) non-ideality of gases; (ii) non-instantaneous diaphragm removal; and (iii) neglect of boundary layer effects. The effect of the non-ideality of the test gas is very pronounced especially with regard to the temperature behavior behind the shock front. The temperature ratio T_2/T_1 across the shock front is much greater in the ideal case, as demonstrated graphically in Fig. 5, than for a real diatomic gas.

The discrepancy arises from the transformation of kinetic energy across the shock front into the energy involved in internal modes of vibration of the molecules, accompanied by disassociation of the molecules into atoms and further in the ionization of the atoms. These energy modes are excited to a degree that depends on the temperature. From classical partition theory each degree of freedom for translational, rotational and vibrational modes contribute $1/2$ kT to the internal energy. The specific heat ratio for a polyatomic gas is therefore not a constant but decreases with temperature while the specific heats increase with
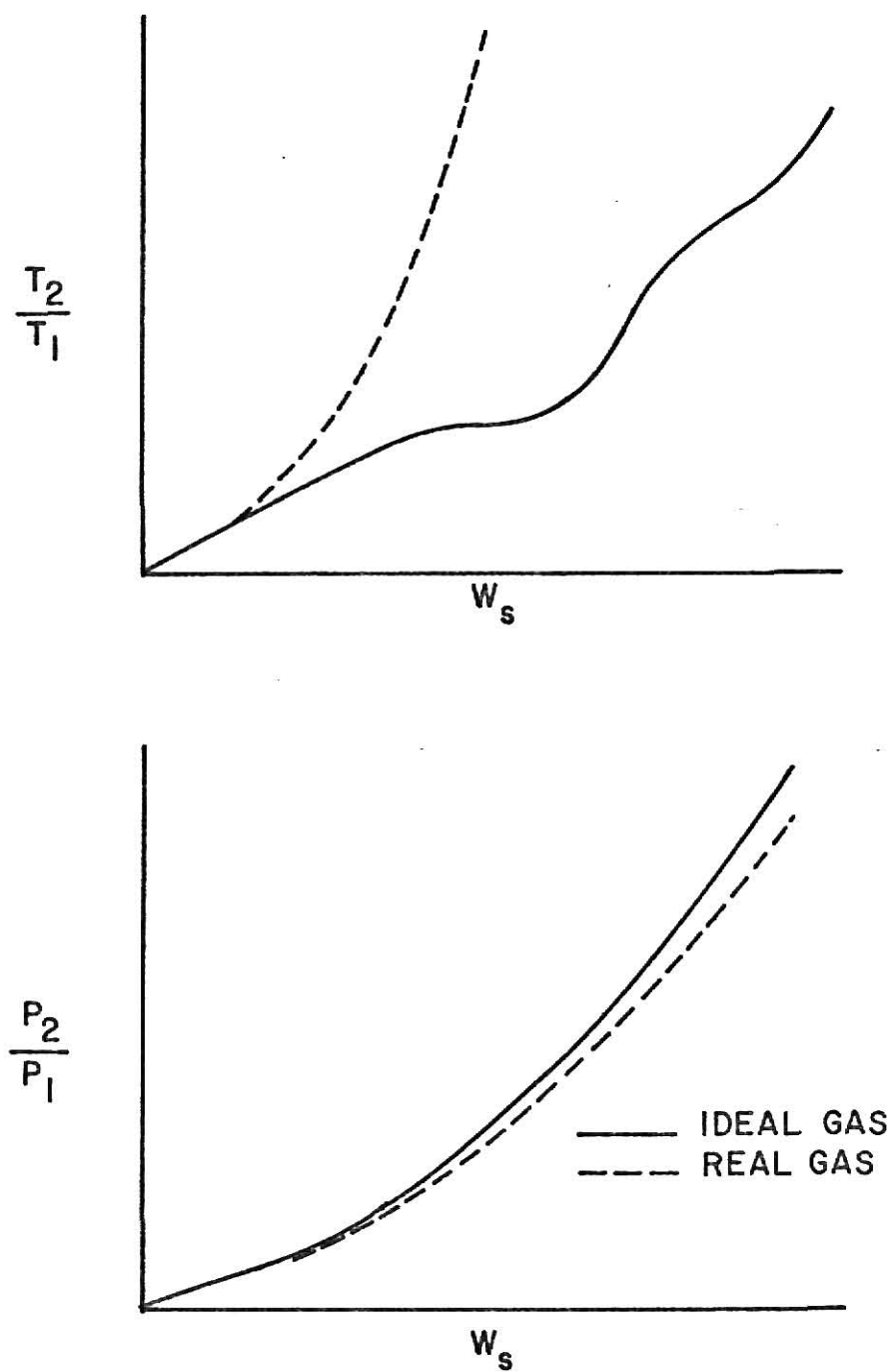
Fig. 5

VARIATION OF TEMPERATURE AND PRESSURE
WITH SHOCK SPEED IN IDEAL AND REAL
DIATOMIC GAS

temperature. Disassociation and ionization at much higher temperatures cause an additional decrease in the effective specific heat ratio. The calculation of the real equilibrium properties requires a straight forward iteration procedure (Gaydon and Hurle, 1963, p. 37-49). However, for many kinetic experiments, the shock heated gas temperature is not high enough for disassociation and ionization to be prevalent (<3000 °K) and the test gas is frozen so that the errors introduced by the assumption of ideal test gases are not severe. For these cases, equations (14) and (15) can be used to predict the conditions behind the reflected shock front to a sufficient degree of accuracy for the experimental investigation.

The influence of the diaphragm opening process on shock tube flows has been investigated competently by White (1958). He put forth a so-called 'formation from compression' model in which the shock formation process takes a finite time. It consists of compression waves being formed slowly as the diaphragm opens and finally coalescing to the shock wave with an upstream facing expansion wave being formed in the process. Also, the diaphragm opening process results in some mixing of the driver and driven gases due to the jet of driver gas through the first opening in the diaphragm. The magnitude of the mixing as well as the direction of its effect on the shock strength is influenced by many factors, including the gases used and the shock strength. The instantaneous removal prediction of the shock strength for a particular bursting-pressure ratio from equation (13) are too high for small ratios ($<10^3$) and too low for larger ratios ($\gtrsim 10^4$).

The final nonideality of the shock tube performance is due to the boundary layer effect. The contact surface is not actually a planar surface but rather there is a velocity gradient that exists normal to the

wall, close to the walls of the tube. At the tube walls, the velocity of the flow will be zero. This retarded region has zero thickness, δ, at the shock front and increases in thickness back through the contact surface into the driver gas. The removal of gas from the contact surface causes it to accelerate toward the shock front. The kinetic energy of the shocked gases is dissipated in the form of heat to the retarded layer causing the shock front to decelerate. The combination of decelerating and accelerating of the shock front and contact surface result in a severe limitation of available observation time as seen in Fig. 6. The analytical treatment of boundary layer effects on attenuation, flow nonuniformity, and observation time has been investigated thoroughly by Mirels (Mirels and Mullen, 1964; Mirels, 1971). The net effect of the diaphragm opening process and the boundary layer on the shock speed is shown schematically in Fig. 7.

The eventual use of the shock tube as a reaction chamber requires an experimental mapping of the shock speed to determine the extent of the above-mentioned non-idealities. The behavior of the shock speed near the diaphragm reveals the magnitude and direction of the effect from the diaphragm opening process while further down the tube, the character of the boundary layer is observable. Along with the mapping of the shock speed from the diaphragm to the end wall, the pressure history at the end wall will be investigated.
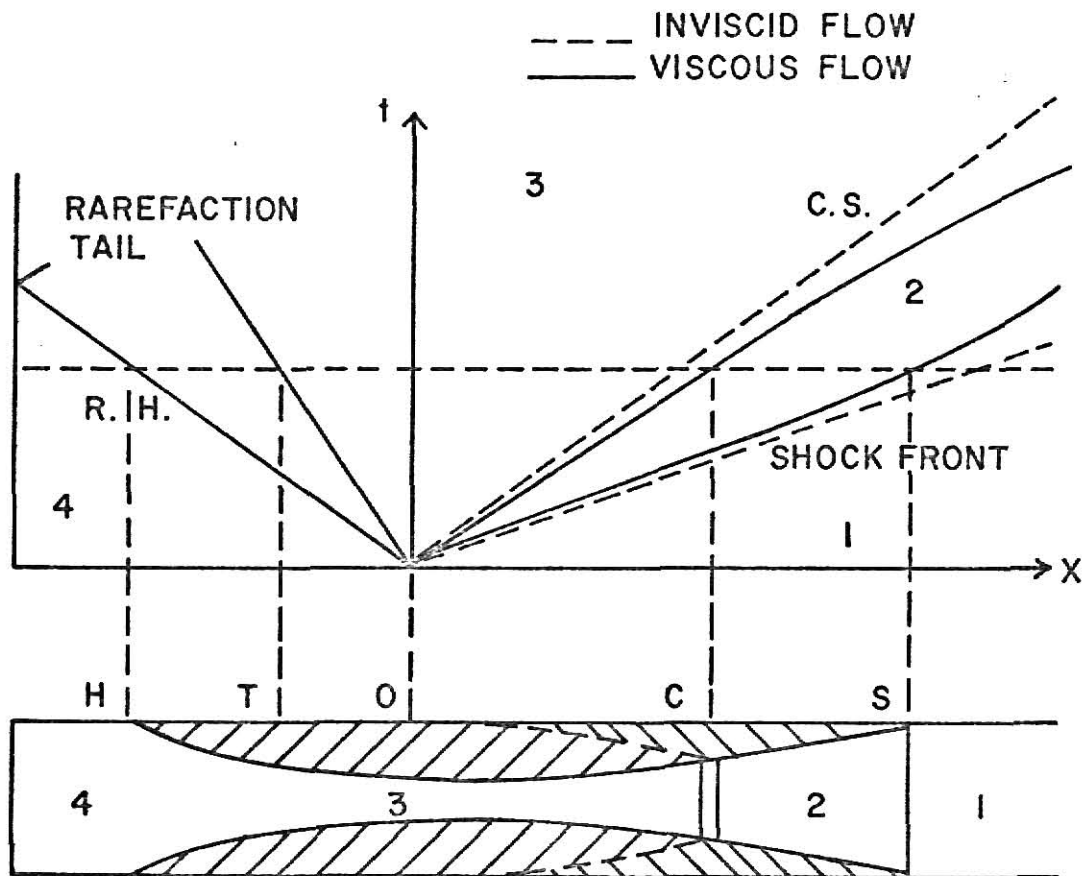
Fig. 6

(X-t) DIAGRAM SHOWING ACCELERATION OF CONTACT
SURFACE AND DECELERATION OF SHOCK FRONT
DUE TO BOUNDARY LAYER
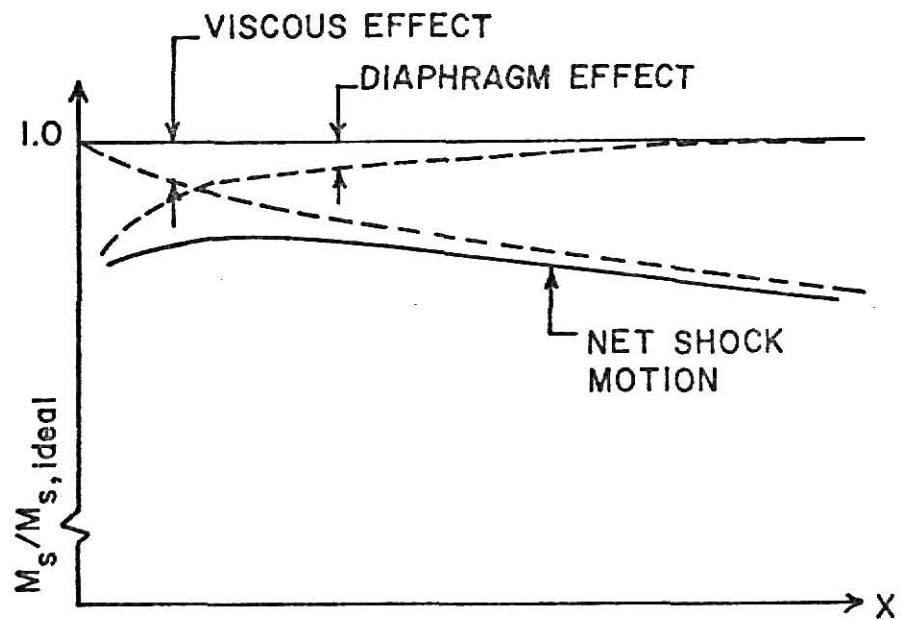
Fig. 7

EFFECT OF NONIDEAL DIAPHRAGM RUPTURE AND BOUNDARY
LAYER SHOCK ATTENUATION
(after Mirels, 1971)

III. APPARATUS DESIGN AND CONSTRUCTION

This section deals with the design and construction of the shock tube facility. The tube will be used mainly for coal combustion studies and eventually for studying two phase flow phenomenon. The character of the combustion of pulverized coal determines many of the design features required. Most importantly, the length of the driver section and test section is found solely from a consideration of the conditions behind the reflected shock needed for combustion studies. Further the deposition of particles on the tube wall after the combustion sequence necessitates aspects of the design that allow frequent cleaning of the tube's inner surface. Finally, the requirement of high purity in kinetic studies dictates high vacuum capabilities for the test section. More general features of the design that also are important are: pressure tightness, structural soundness and rigidity, ease in manipulation, ease in leveling, ease in fabrication, versatility, and regularity and smoothness of test section wall over its entire length.

Tube Selection

The determination of the test section length is dependent upon the desired observation time behind the reflected shock front, along with the test gas used and the shock strength. Therefore, in order for the test section length to be found, design basis shock conditions must first be decided upon.

A reflection upon equation (13) reveals that for a given bursting pressure ratio P_4/P_1 the shock strength in a given test gas is dependent upon the specific heat ratio and sound speed in the high pressure gas. The best driver gas is one for which M_s is the largest for the given ratio

P_4/P_1. The largest shocks occur when P_4/P_1 approaches infinity for which equation (13) implies that the quantity

$$[1 - \frac{\gamma_4 - 1}{\gamma_1 + 1} \frac{a_1}{a_4} (M_s - \frac{1}{M_s})] \rightarrow 0 ,$$

or the maximum Mach number approaches

$$\frac{\gamma_1 + 1}{\gamma_4 - 1} \frac{a_4}{a_1} .$$

Hence, the maximum obtainable Mach number occurs when the driver gas has the highest value of $\frac{a_4}{\gamma_4 - 1}$, which is the criteria to be used for the driver selection. The speed of sound is just $a_4 = \sqrt{\gamma_4 P_4/\rho_4}$ so that the criteria points to low density gases, and the best driver gases are thus hydrogen and helium (see Table 1). However, the inflammable character of hydrogen causes venting problems after the tube has been fired, and increases the danger involved in leaks from the gas system. For this reason the primary driver gas to be used will be helium.

The consideration of the subsequent gas kinetic studies of combustion of coal further restrict the design basis conditions.

TABLE 1
SOUND SPEED, SPECIFIC HEAT RATIO, MOLECULAR WEIGHT
AND DRIVER GAS CRITERIA OF VARIOUS GASES AT 298 K

Gas	Sound Speed in km/sec	Specific Heat Ratio	Molecular Weight in gm/mole	Driver Criteria $a_4/(\gamma_4 - 1)$
H_2	1.324	1.407	2.016	3.253
He	1.062	1.667	4.003	1.592
CO_2	0.269	1.291	44.01	0.924
N_2	0.350	1.404	28.02	0.866
Air	0.345	1.404	28.96	0.854
O_2	0.328	1.401	32.00	0.817
A	0.321	1.667	39.94	0.481

For these type experiments the maximum temperature required in the reaction zone should be about 3000 °K with an observation time in the range of two milliseconds (Field, et al, 1969). Also, the total pressure needs to be on the order of ten atmospheres. The test gas, for combustion processes, is air or oxygen; although for the design basis, air will be chosen. The design basis conditions are summarized in Table 2 along with appropriate gas constants and initial conditions.

The requirement of the temperature of 3000 °K in the reflected shock region requires a specific Mach number of the incident shock as given by equation (16). By substituting the ratio $T_5/T_1 = 10$ into equation (16) along with constants from Table 2 the shock Mach number can be evaluated by using the quadratic formula to give a design basis Mach number of 4.54. Using this incident Mach number, the pressure ratio across the reflected shock is given by equation (15) as $P_5/P_1 = 151$. Consequently, to obtain the design basis pressure of 10.1 bars (147 psi), the initial test section pressure must be:

$$P_1 = \frac{10.1}{151} = 0.067 \text{bar} \simeq 50 \text{ torr}.$$

From consideration of Fig. 2, it is seen that the time interval $\Delta\tau$ between when the shock front strikes the end wall and when the reflected shock front strikes the contact surface is

$$\Delta\tau = \frac{X_2 - X_1}{W_R} = \frac{X_2}{v_2} - \frac{X_1}{W_s} . \tag{17}$$

For large shocks ($M_s^2 \gg 1$) this becomes, to a good approximation

$$\Delta\tau \simeq \frac{X_1}{M_s a_1} \left(\frac{\gamma_1 - 1}{2\gamma_1}\right) \tag{18}$$

TABLE 2
DESIGN BASIS CONDITIONS AND CONSTANTS

==

Initial Conditions	Shock Conditions	Gas Constants	
$T_1 = 300 \, °K$	$T_5 = 3000 \, °K$	$\gamma_1 = 1.404$	
$T_4 = 300 \, °K$	$P_5 = 10.1 \text{ bars}$ (147 psi)	$a_1 = 345 \text{ m/sec}$	
$P_1 \, \& \, P_4$ determined later	$\Delta\tau = 2.0 \text{ msec}$ (Fig. 2)	$\gamma_4 = 1.667$	
		$a_4 = 1062 \text{ m/sec}$	

The relationship between this time interval and the actual observation time $\Delta\tau'$ is somewhat complicated by the uncertainty in the behavior of the first reflected disturbance, S_I. In fact, the character of S_I can range from a secondary reflected shock to a rarefaction wave, depending on the conditions across the contact surface interface. It can be shown (Gaydon and Hurle, 1963, p. 67) however, that the disturbance S_I for shocks into ideal air always has a velocity about one half the speed of the reflected shock front so that the true observation time is

$$\Delta\tau' = \frac{X_2-X_1}{W_R} + \frac{X_2-X_1}{W_{S_I}} \simeq \frac{X_2-X_1}{W_2} + \frac{X_2-X_1}{1/2W_R} = 3\Delta\tau \qquad (19)$$

Therefore, the design basis for the time interval $\Delta\tau$ is $(1/3)(2.0) = .67$ msec, and from equation (18) the required test section length to obtain this interval for the shock Mach number of 4.54 into ideal air is:

$$X_1 = (\Delta\tau)M_s a_1 \left(\frac{2\gamma_1}{\gamma_1-1}\right) = 4.84 \text{ meters.}$$

This value of the test section length was found by neglecting nonideal effects alluded to previously. However, some estimate of the magnitude of these must be made in order to modify this test section

length appropriately. Since the design basis conditions are not limited to specific values but rather represent ranges of appropriate values, the estimates of real effects can be somewhat crude. An estimate of real gas effects can be made by comparing the incident shock density ratio as predicated experimentally and theoretically. For the 4.54 Mach number, the density ratio for ideal air as given by equation (11) is 4.8, while the experimental value for real air is 5.1 as determined by Byron (1957; repeated in Gaydon and Hurle, 1963, Fig. III. 4, p. 53). Gaydon and Hurle (1963) further predict that the test section length must be increased by a factor of one-third to correct for the boundary layer effect. Thus, the total real effect results in a correction factor of about 1.4, or the test section length should be increased to seven meters.

There is a minimum driver length $(X_4)_{min}$ which ensures noninteraction of the reflected rarefaction head with uniform flow during the observation time. The driver must be made long enough so the rarefaction head does not reach the contact surface before interaction of the contact surface and the reflected shock front. If (X_c, τ_c) are the (X-t) diagram coordinates of the rarefaction-head contact-surface interaction and (X_2, τ_2) the coordinates of the contact-surface reflected-shock-front collision, then the minimum driver length satisfies $\tau_c = \tau_2$. The consideration of the relative speed of the rarefaction head and the contact surface reveals that (Gaydon and Hurle, 1963, p. 60-63)

$$\tau_c = \frac{2X_4}{a_4} \left[1 - \frac{\gamma_4 - 1}{\gamma_1 + 1} \frac{a_1}{a_4} \left(\frac{M_s^2 - 1}{M_s^2} \right) \right]^{-(\gamma_4 - 1)/2(\gamma_4 - 1)}, \qquad (20)$$

and by studying Fig. 2 it is seen that

$$\tau_2 = \frac{X_1}{M_s \alpha_1} + \Delta\tau \qquad (21)$$

The calculated design parameters are:

$$M_s = 4.54$$

$$X_1 = 7m$$

$$\Delta\tau = 0.67msec.$$

Thus from equation (21) the time at which the reflected shock collides

with the contact surface, τ_2, is 5.14msec. When this is set equal to

the right hand side of equation (20) the minimum acceptable driver

length is $(X_4)_{min} = 2.3m$. To ensure noninteraction of the rarefaction

fan during the observation time, the driver length is increased to three

meters.

The tube design thus consists of a three meter driver with a seven

meter test section. The design basis (X-t) diagram for this ten meter

shock tube is shown in Fig. 8. In Fig. 9, an (X-t) diagram for diatomic

nitrogen as a test gas is shown for this tube for $T_5 = 2000$ °K and

$P_5 = 10.1bar$ (147psi) behind the reflected shock.

The remaining features of the basic tube to be considered are the

tube material, internal dimensions and wall thickness. The material

chosen was type 304 stainless steel for the obvious advantages of strength,

inexpensiveness, machinability and ease of cleaning. The major disad-

vantage is the relatively complex spectrum of the always present iron

impurity which interferes in any optical spectroscopic measurements.

The tube diameter of two inches (5.08cm) is large enough to prevent

boundary layer closure and to allow a sufficient optical path length;

Fig. 8

DESIGN BASIS (X-t) DIAGRAM

N_2 driven/He driver
$T_5 = 2000$ K
$P_5 = 147$ psi (10.1 bar)

$v_3 + a_3 = 1715$ m/s

RAREFACTION TAIL

CONTACT SURFACE

$W_R = 500$ m/s

$v_2 = 980$ m/s

SHOCK FRONT

$v_3 - a_3 = 240$ m/s

$W_s = 1270$ m/s

8.89 ms

6.54 ms

5.49 ms

t (msec)

RAREFACTION HEAD

2.83 ms

$a_4 = 1062$ m/s
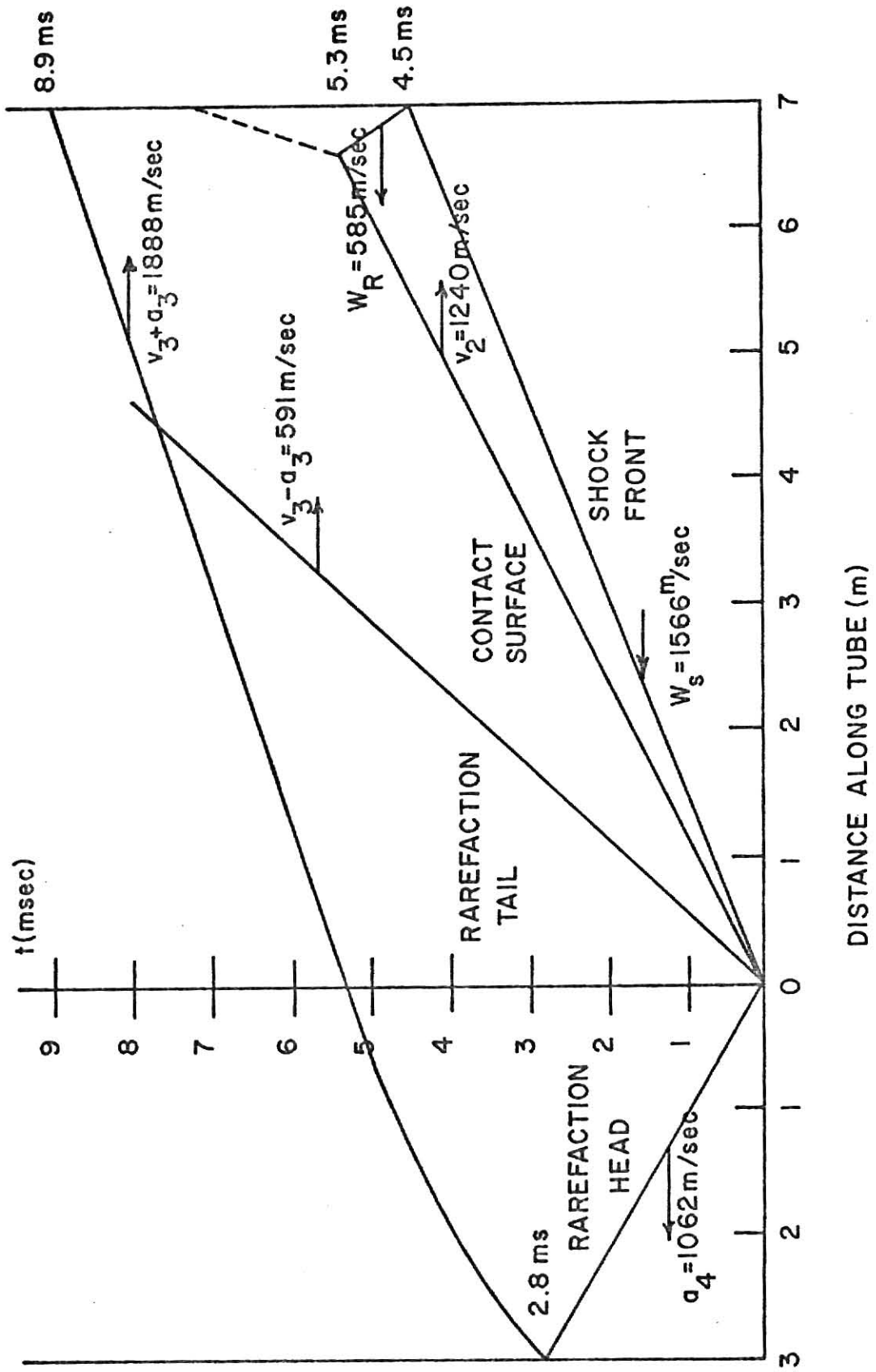
DISTANCE ALONG TUBE (m)
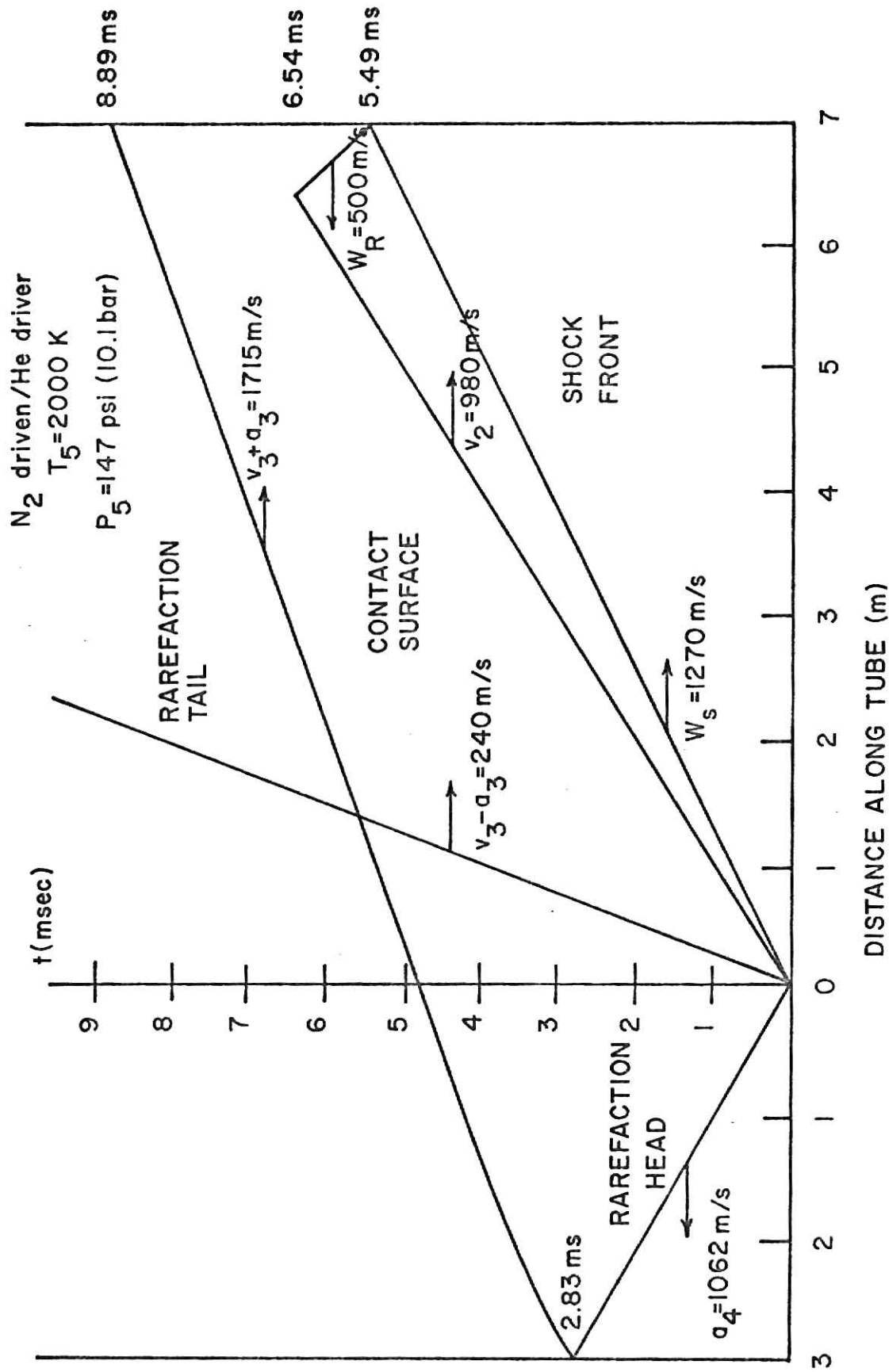
Fig. 9

(X-t) DIAGRAM OF SHOCK EXAMPLE

although it is small enough not to be exorbitantly expensive or to use large amounts of gas in each run. The circular tube has the greatest structural strength and allows for greater ease in cleaning than the rectangular counterpart, which is especially important after particle deposition in coal combustion.

The tube wall thickness must be sufficient to withstand, primarily, the static pressure in the driver, which could be as much as the full gas bottle pressure of 151.6 bars (2200 psi). The required wall thickness can be estimated from Barlow's formula for the theoretical bursting pressure of seamless tubing, as given in the ASME Boiler Code,

$$P = \frac{2S(d'-d)}{d'} \quad ,$$

where:

        P = maximum allowable working pressure,

        S = tube tensile strength divided by the factor of safety,

        d' = tube outside diameter,

        d = tube inside diameter.

The tensile strength of type 304 seamless stainless steel tubing is 5170bars (75,000 psi) at room temperature so that for a maximum working pressure of 206.8 bars (3000 psi) and an outside diameter of 6.35cm (2 1/2 inches), the 5.08cm (2 inches) tubing has a factor of safety of five. The normal noncode requirement for the factor of safety for air and gas is three, so that the 1.27cm (0.25 inch) wall thickness is sufficient. The chosen tubing was seamless hollow bar stainless mechanical tubing purchased from A. B. Murray and Co. (see Appendix B for information on all ordered material) meeting specification ASTM A-511 for straightness tolerances (0.030 inches maximum curvature in any

three feet) and permissible variations in outside diameter ($\pm$ 0.010 inches) and wall thickness ($\pm$ 10 percent).

The test and driver sections were subdivided into several sections (Fig. 10). For the driver, this was done so the sections would not be too large to machine in a three-meter-bed lathe. However, the experiment being performed dictates the test section length so that subsections are required for length versatility. Also the cleaning process after combustion is made easier with smaller subsections.

The driver consists of two sections, one and two meters in length. The test section consists fo five sections: an observation station of one half meter length containing shock analysis instrumentation, a section having the diaphragm holder of one meter and three interchangeable and removable sections of 1, 2 and 2 1/2 meter length. This sectioning allows for the test section length to vary from a minimum length of 1 1/2 meters to the designed 7 meters with six intermediate lengths: 2 1/2, 3 1/2, 4, 4 1/2, 5 and 6 meters.

The connection of these sections poses an unusual problem. For those experiments requiring high purity, the test section must be evacuated to pressures as low as $10^{-3} - 10^{-5}$ torr. Thus the connections must have high vacuum and high pressure integrity. For this reason the tube sections are connected using six inch diameter slip-on flanges (150 pound) with 3 3/8 inch diameter by 1/8 inch thick O-rings. The flanges use four 3/4 inch heat-treated bolts, each. During fabrication, the flanges were welded on both sides leaving a bead on the front face. This was followed by the facing of the O-ring surface so that it is

DRIVER   DIAPHRAGM   TEST   END
          FLANGE   FLANGE

END FLANGE

OBSERVATION
STATION:
2 THIN FILM
GAUGE MOUNTINGS
OBSERVATION
BLOCK
(PRESSURE
TRANSDUCER
AND
WINDOWS)

CONTAINS:
2 THIN
FILM
GAUGE
MOUNTINGS

PORTS:
MAIN VACUUM
OUTLET
TEST SECTION
VACUUM GAUGE
TEST FILLING
INLET

PORTS:
--DRIVER FILLING
--VENT OUTLET
--PRESSURE GAUGE
--DRIVER VACUUM
OUTLETS

.5m   1m   2.5m   2m   1m   2m   1m
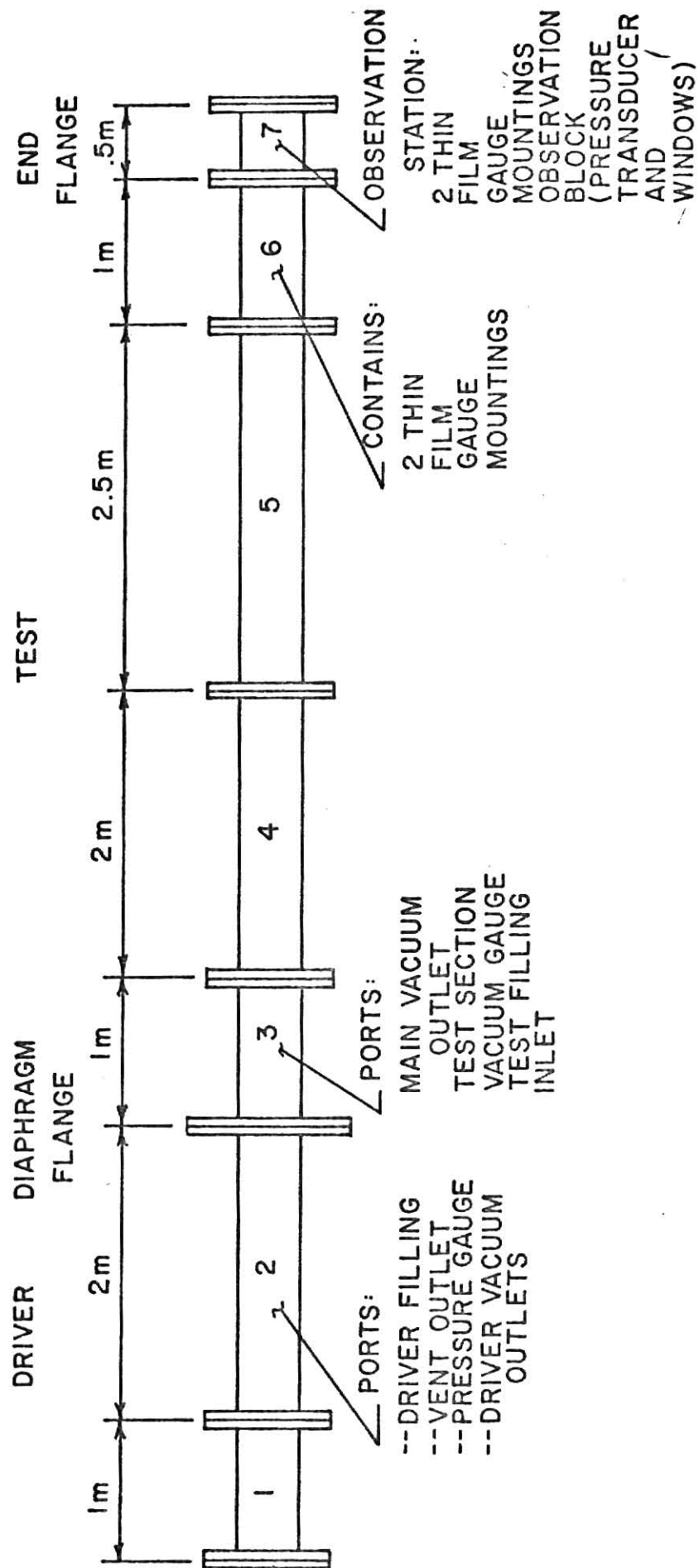
Fig. 10

TUBE SECTIONING

extremely flat and perpendicular to the tube axis. This process caused the tube internal diameter to be up to 0.05cm (0.020 in) larger at the flange face, tapering to the original diameter in about 8cm. Consequently, there is a gentle widening and closing as the shock progresses down the tube but no sharp transitions such as steps. Finally, the O-ring grooves are machined into one of the matched flanges. All sections were hydrostatically tested to pressures up to 206.8 bars (3000 psi).

The diaphragm is ruptured by overpressure. The material used is mylar, which is available in various thicknesses; however, metals such as copper, aluminum and steel, may also be employed. The diaphragm for a particular run may be a single thickness or a combination of thicknesses since the natural bursting pressure of a particular material is proportional to its thickness whether a single piece or multiple layers are used. Therefore, practically any bursting pressure, and thus any pressure ratio P_4/P_1, can be obtained with only a few different material thicknesses.

Just before bursting, the diaphragm may have as much as three to six tons of force on it due to the driver pressure, and hence, the diaphragm must be clamped securely to prevent slippage. The diaphragm holder must also afford a vacuum tight seal. Therefore, the diaphragm is held between two O-rings of different sizes, so that the diaphragm itself is the O-ring surface. The diaphragm holder consists of three parts (Fig. 11): a seven-inch-diameter diaphragm flange with a 4 1/2 inch square indentation, a 4 1/2 inch diameter circular insert, and a seven-inch-diameter clamping flange, with a 4 1/2 inch circular indentation. The diaphragm is sandwiched between the diaphragm flange in the indentation

O-RING GROOVES

TUBE
WALL

INSERT

DIAPHRAGM
POSITION

DIAPHRAGM FLANGE
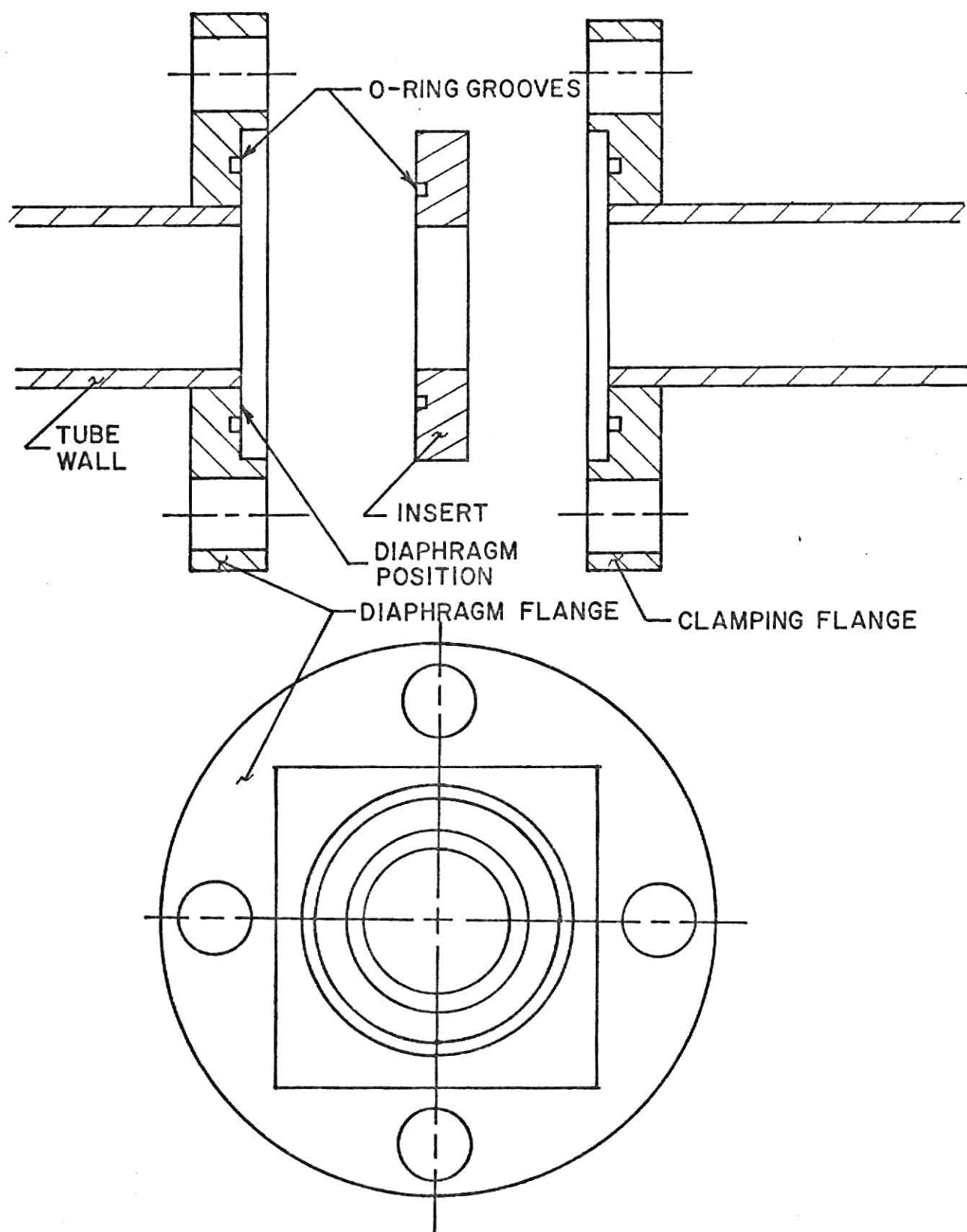
CLAMPING FLANGE

Fig. 11
DIAPHRAGM HOLDER ASSEMBLY

and the insert. The diaphragm flange and clamping flange are clamped together with the insert and diaphragm between them using four 3/4 inch heat-treated bolts. The diaphragm is thus restrained from moving by surface contact with the diaphragm flange and the insert.

Support System

The design of the support system is extremely important and involves several considerations. For instance, the gas flow, after the diaphragm has burst, results in very large changes in momentum from the diaphragm bursting as well as the gas striking the test section end wall. Thus, some design feature must prevent the accompanying recoil, especially when the shock heated gases are being optically probed through a parallel window system, since a shift in the tube would result in misallignment of the optical system. Further, the tube material, section connections, probe analysis mountings, and valve mountings each contribute to the weight of the individual tube sections. These sections can become restrictively heavy to move easily and design features must allow for the ease of manipulation so that sections can be separated for cleaning purposes, for section interchange and for diaphragm replacement. Finally, it is necessary that the sections interface correctly with no internal dimension shift (or 'steps') and it is desirable that the tube run horizontally.

The support system used is one in which a 35 foot (10.67m) length of aluminum extruded channel obtained from Metal Goods, six inches in width, by 0.314 inch web and 2.034 inch flange width is supported 91.4 cm above the floor on eleven unistrut channeling legs. (see Fig. 12)

ALUMINUM CHANNEL

1/2" X 1/2" ANGLE IRON

P1726 FLAT
PLATE FITTING

P1100 CHANNELLING

P2072A POST BASE
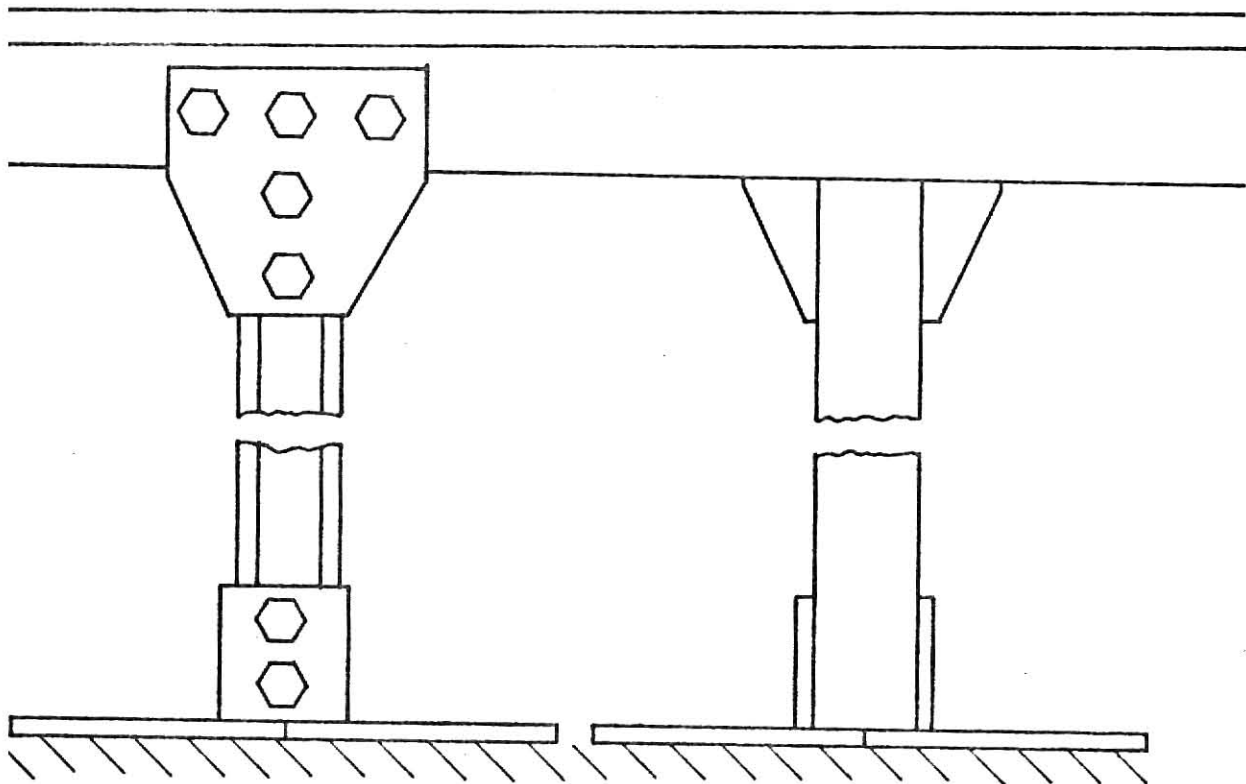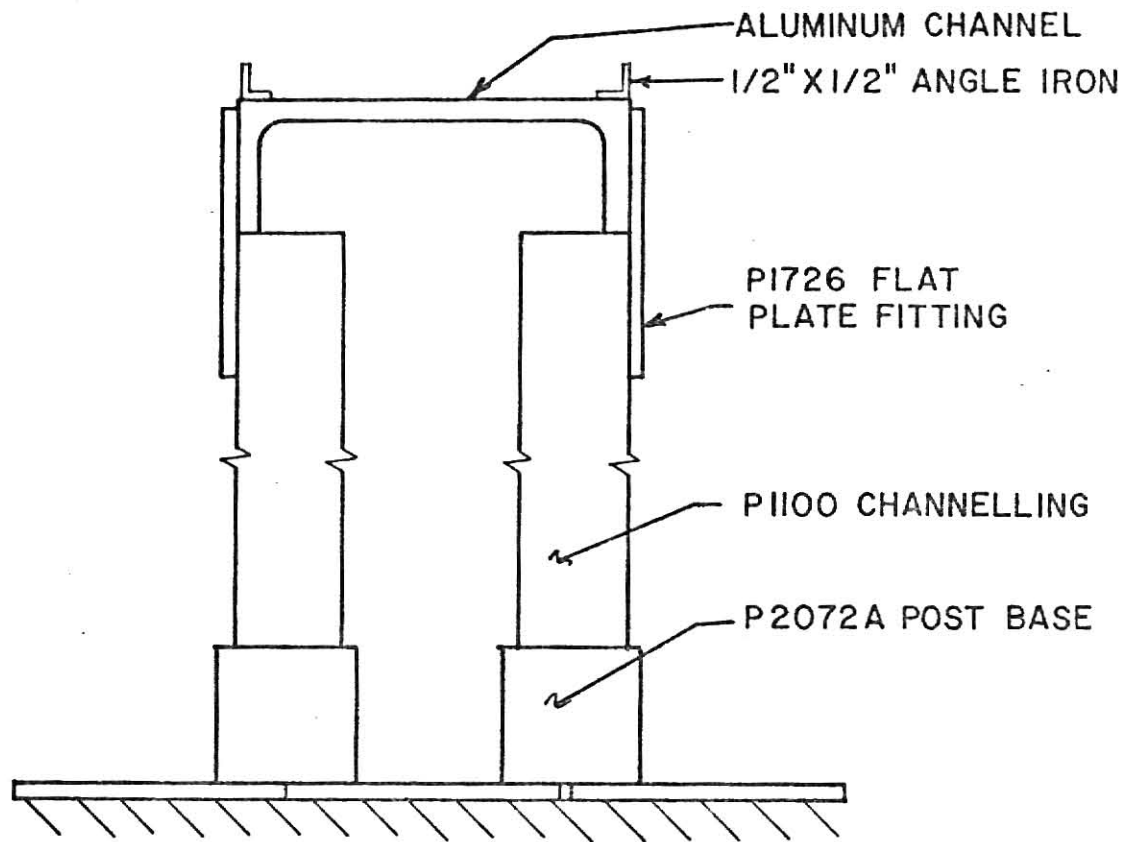
Fig. 12

CART TRACK SUPPORT SYSTEM

The legs are secured to post bases which are mounted to the floor by two 1/2" x 1 1/2" bolts into lead slag expanding nuts. Half inch angle iron is attached along the entire length and on both sides of the channel forming a retaining wall. The cart track was leveled using a standard air bubble level.

The tube is actually supported on carts which have assembly-line-trolley-type wheels which run in the track formed by the angle iron retainer. The carts, as shown in Fig. 13, were designed so that the tube height could be adjusted by taking off the retaining bracket, loosening the lock nut, and turning the support bar at least a half turn clockwise to lower the tube, and counterclockwise to raise it. During the tube firing sequence, the tube is held rigidly by clamping one of the carts to the aluminum channel using two standard six inch C-clamps.

The tube was alligned by use of a laser-transit procedure. The laser light was directed down the tube with the end flanges removed and without a diaphragm. The surveyors-type transit was set up and leveled at a position appropriate to view the face of the laser and the spot produced by the light from the laser passing through the tube and striking the far laboratory wall. The laser was then adjusted so that the spot on the wall and the outlet window of the laser were at the same height as viewed through the transit. Over each flange set was placed on opaque material with a small hole ($\sim$8mm) positioned exactly at the tube center. Each tube section height was adjusted using the support carts until the laser light passed through the entire length of the tube. After removal of the screens and the laser, the transit

RETAINING BRACKET

SUPPORT BAR

LOCK NUT

BASE

TROLLEY TYPE WHEELS
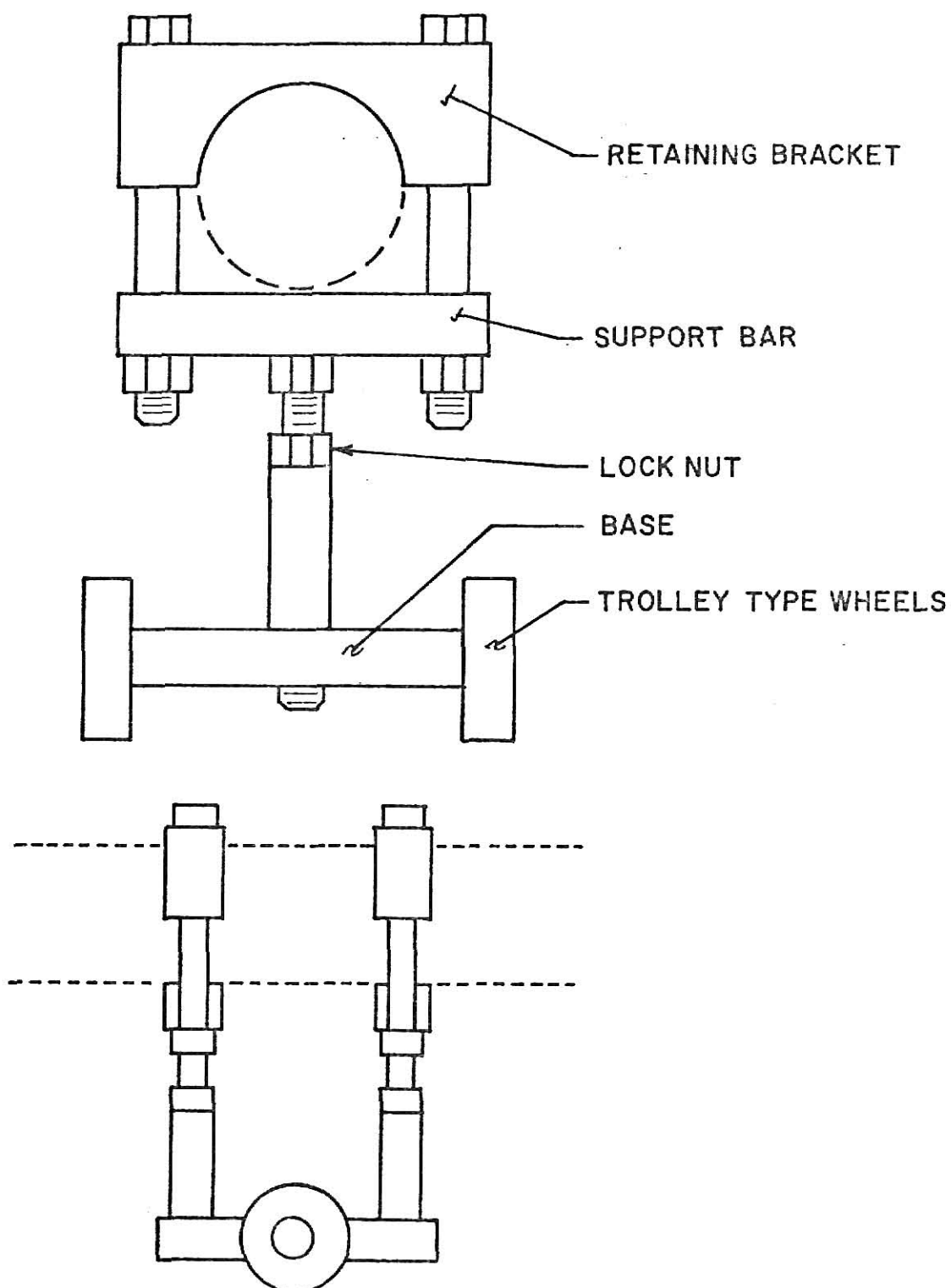
Fig. 13

CART DESIGN

was positioned so that the inside of the tube could be observed. By

placing a diffusing light source, an ordinary light bulb, at the other

end of the tube, the transit could be focused at each flange set and

the slight displacement of the internal dimension of adjacent sections

could be corrected as the flange set was coupled.

Vacuum System

The time required for evacuation of the test section is over-

whelmingly the most lengthy operation in the firing sequence. In

order for the turnover time between shocks to be as short as possible,

the vacuum system must be matched with some care to the test section

volume and ultimate pressure required. The time required to evacuate

a chamber of volume V from an initial pressure of P_i to a final pressure

P_f with a speed of evacuation S_n is given by the Gaede equation (Dayton,

1967)

$$t = 2.3 \frac{V}{S_n} \log \frac{P_i}{P_f} .$$ (23)

The speed of evacuation is related to the pump speed through the con-

ductance

$$\frac{1}{S_n} = \frac{1}{C} + \frac{1}{S_1}$$ (24)

where the conductance C is a function of the dimensions of the connection

between the tube and the pump. An empirical formula (Dayton, 1967) for

the conductance of air in liters per second for circular pipe of length

L in feet and inside diameter d in inches is

$$C = 6.6d^3 / (L + 0.11d)$$ (25)

where each right angle bend increases L by 0.05d. Thus in order to

increase C and have a maximum evacuation speed, the connection must

have as large a diameter and as short a length, as possible.

The ultimate pressure of the system is dependent upon the maximum permissable impurity concentration to ensure noninterference with measureable species concentrations. To keep impurity concentrations much below one part per million (1 ppm) requires pressures as low as 10^{-4} to 10^{-5} torr. However, there is no single vacuum pump which has a satisfactory pumping speed over the entire range, 760 to 10^{-5} torr. For this reason, the evacuation requires two separate pumping sequences using two separate types of vacuum pumps. The roughing sequence (760 to 10^{-2} torr) is performed by a Welch 1402 roughing pump with an average speed of 1.67 l/sec and the ultimate sequence (10^{-2} to 10^{-5} torr) uses a Veeco two-inch water cooled oil diffusion pump with an average speed of 70 l/sec. The valving of the main vacuum system (see Fig. 14 and Fig. 15) uses two Huntington 1 1/2 inch right angle bellows valves and one Vacao 3/8 inch brass bellows valve. The calculated conductance of the tube to the roughing pump connection is 0.62 l/sec and of the tube to the diffusion pump connection is 3.52 l/sec. The estimated total evacuation time to an ultimate pressure of 10^{-5} torr is 6.4 minutes. The outlet to the vacuum system is located close to the diaphragm, within the shock formation region, in order to lessen interference with completely developed shock flow.

Gas Mixing System

The gas filling manifolds are shown in Fig. 15. The low pressure and high pressure systems both use quarter inch stainless steel tubing with quarter inch taper seal valves from High Pressure Equipment Co. The driver gas mixtures presently use commercial grade helium and nitrogen obtained in standard gas bottles equipped with Matheson high pressure

Index to Numbered Items on Fig. 14

1. Main vacuum inlet bellows valve (valve number 1)

2. Safety interlock microswitch

3. Roughing valve (valve number 3)

4. Diffusion sequence bellows valve (valve number 2)

5. Veeco two-inch water-cooled, oil diffusion pump

6. Welch 1402 roughing pump

7. Hasting thermocouple vacuum gauge

THIS BOOK CONTAINS NUMEROUS PICTURES THAT ARE ATTACHED TO DOCUMENTS CROOKED.

THIS IS AS RECEIVED FROM CUSTOMER.
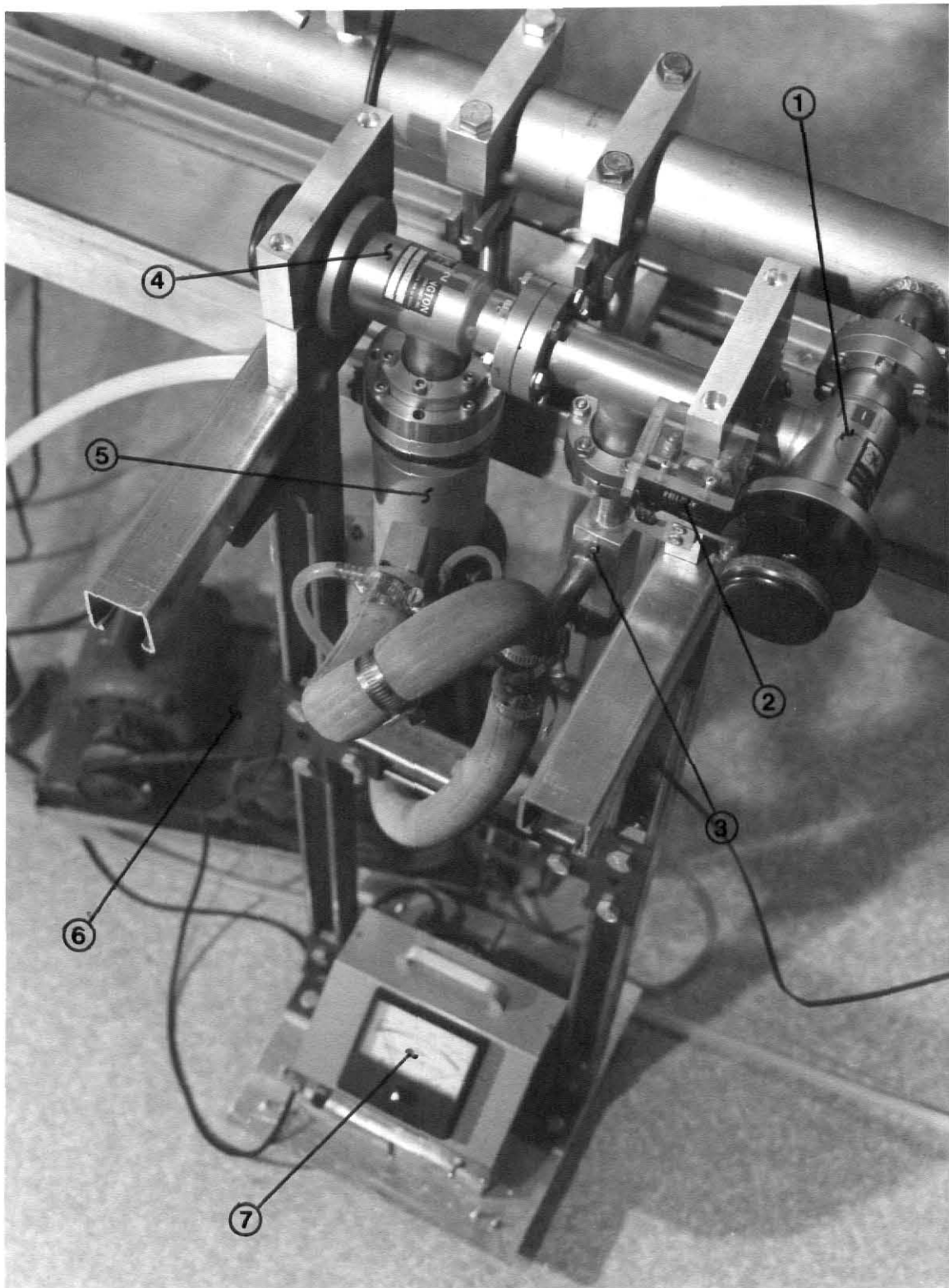
Fig. 14
Picture of Main Vacuum System
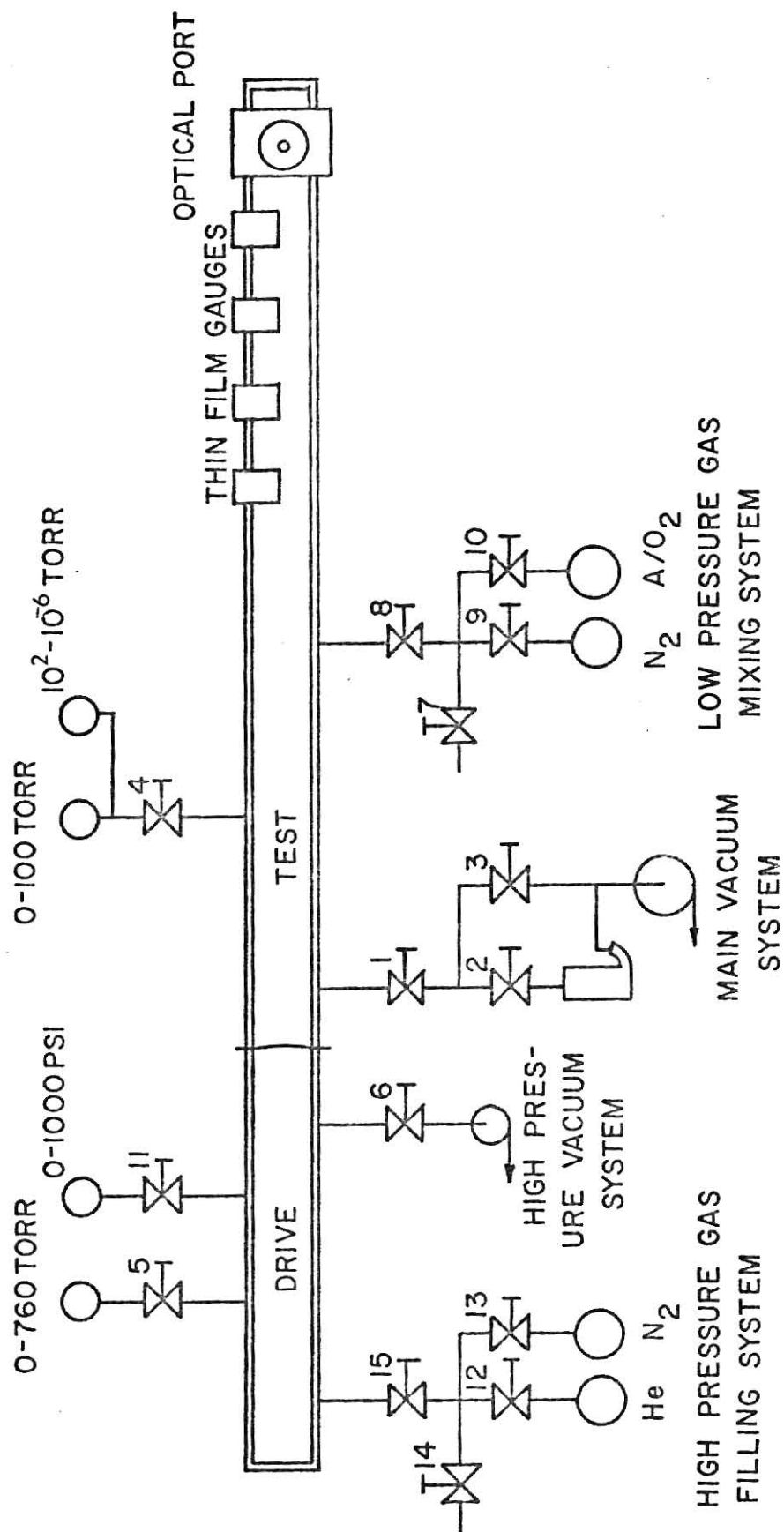
Fig. 15

SCHEMATIC OF PUMPING AND GAS HANDLING SYSTEMS

regulators. Eventually for high purity kinetic studies, the grade
of gas used will be improved. The high pressure manifold, valve
numbers 12, 13 and 14, is connected through quarter inch hydraulic
hosing to the firing solenoid valve 15. This solenoid valve is inter-
locked with the main vacuum valve number 1. A microswitch on valve
number 1 disengages the supply power to the solenoid valve when the
vacuum valve is open. Thus, the driver can not be filled unless the
vacuum system is isolated from the test section by valve 1. A com-
plete firing sequence check list was developed and is given in Appen-
dix D.

Diagnostics

There are certain parameters which can be measured during the
normal operation of the tube which reflect the character of the par-
ticular shock wave. Primarily, the shock strength can be determined
directly from a measurement of the shock velocity. The pressure
history of the shock wave is a second parameter which reveals infor-
mation about the shock formation and uniformity. Once the character
of shock is known, it is repeatable by matching initial pressures,
gas compositions, diaphragms and high pressure filling rates. Finally,
many experiments in reaction kinetics involve the use of optical
probing techniques so that the tube facility must have both parts and
optical paths for observing emission and absorption by the shock heated
gases.

If the time interval between arrival of the shock front at two
points along the tube separated by a known distance can be measured,
then the shock speed can be determined. Since the shock front has a

large temperature discontinuity, a detector which responds to the temperature rise will respond to the shock front arrival. Such a detector is a thin metal film to which the shock front can transfer heat causing a detectable decrease in resistance.

The use of thin film gauges is well documented in the literature. Gaydon and Hurle (1963), Jahn and Weimer (1958), and Hall and Hertzberg (1958) give excellent reviews of their design and use. The metal film of which gold, platinum and nickel are examples, are generally sputtered or evaporated as well as painted followed by baking on a suitable dielectric backing.

A process of manufacturing thin film gauges was adapted from the literature and is presented in Appendix E. A thin strip of Liquid Bright Platinum #05-X from Engelhard Industries was painted across the end, over the edges and down the length of short pyrex rods. The pyrex rods were then oven-baked so that the agent holding the platinum was driven off and the platinum was bonded to the pyrex backing. After leads were soldered to the gauges, they were epoxied into plexiglass holders. These holders were designed to fit into vacuum tight mountings which hold the end surface of the thin film gauge flush with the tube wall as shown in Fig. 16.

Several distinctive features of the thin film gauge mounting warrant discussion. Foremost among these is the preservation of tube wall regularity to prevent disturbance of the shock flow. This is accomplished by matching the shape of the plexiglass holder to the curvature of the tube inner wall (Fig. 16). Four gauge mountings were silver brazed to the tube thus allowing for the possibility of having

BNC CONNECTOR

PLEXIGLASS

ALUMINUM

ALUMINUM

STAINLESS STEEL
PLEXIGLASS
THIN FILM GAUGE

SILVER
BRAZED

TUBE WALL
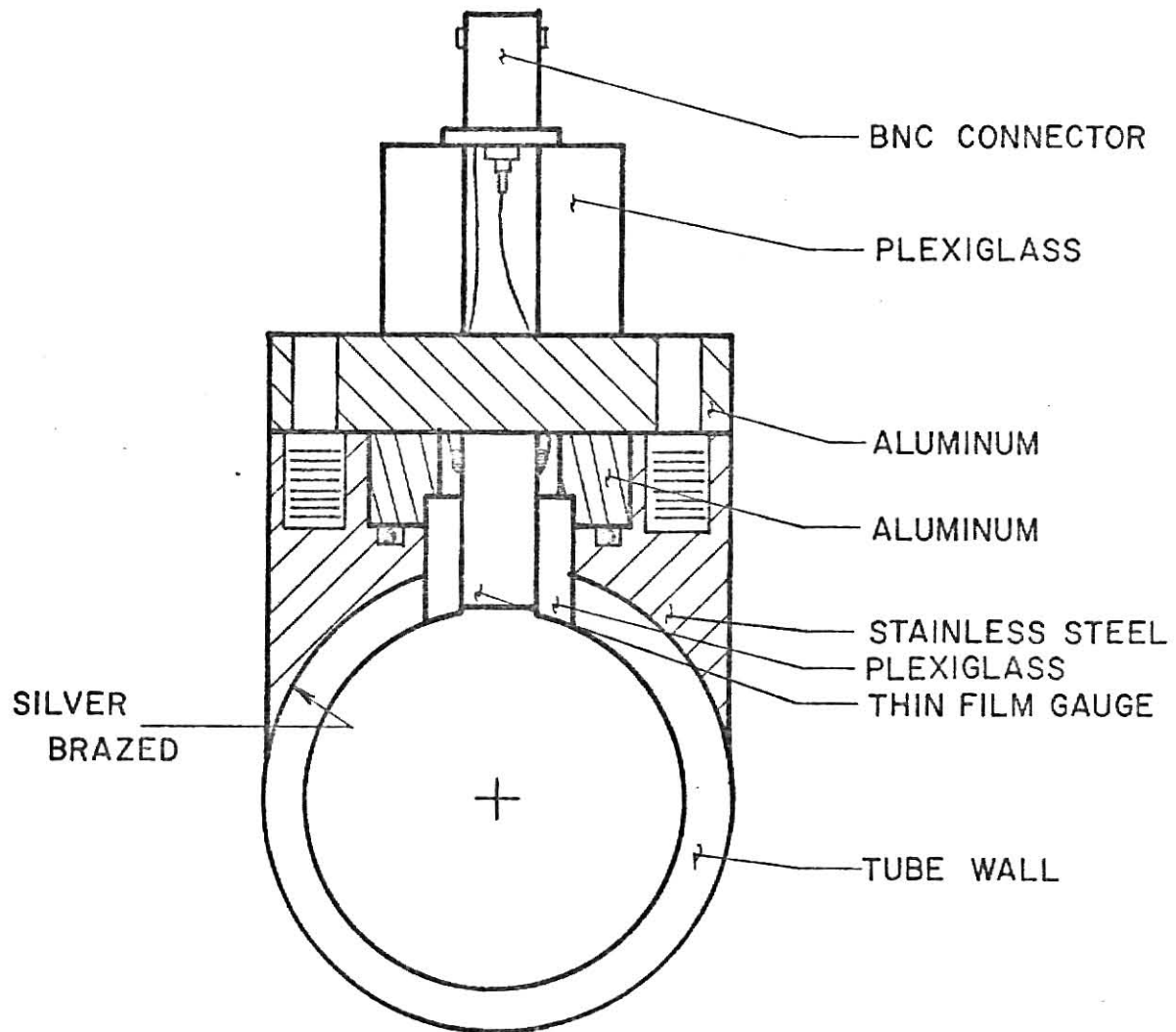
Fig. 16

THIN FILM GAUGE MOUNTING

three intervals over which the speed can be measured. This would give a direct measure of the shock speed attenuation on each run. The spacing of the mountings is a trade off between the need for accuracy and the need for an instantaneous velocity measurement due to the shock deceleration. The former dictates a large separation while the latter necessitates a very small spacing. The shock front decelerates a small amount over eight inches while this spacing still affords excellent accuracy for time interval capabilities in the microsecond range. Finally, since the shock strength varies along the tube, the mountings must normally be grouped close to the end wall to obtain as good an estimate of the shock strength before reflection as possible. Two of the mountings are in the observation section and two in the preceeding section (see Fig. 17).

The time interval counting system is shown schematically in Fig. 18 and the actual instrumentation is seen in Fig. 19. The thin film gauges are connected directly to a preamp designed to produce a voltage step output when the input resistance changes. This preamp was designed by Zallen (1973) and a schematic is given in Appendix G. The signal from the preamp, which is connected to the first thin film gauge, is amplified by the Ortec 410 shaping amp to give a sufficient voltage to fire the gate generator. This amplifier also shapes the signal so that it will have an extremely short rise time and be of short enough duration to not interfere with the stop signal from the second thin film gauge. The signal from the second preamp is amplified to enable it to have a short rise time and sufficient voltage to stop the gate output. The gate generator thus produces an output voltage between the arrival of the shock at the first thin film gauge and its arrival at the second thin film gauge. The gate generator is connected to the enable-disable input of the scaler so that the scaler is only able to count during the gate signal. Then, by connecting

Index to Numbered Items on Fig. 17

1. Observation section

2. Thin film gauge mounting positions

3. Observation block

4. Location of lateral wall pressure transducer mounting

5. Quartz window holder
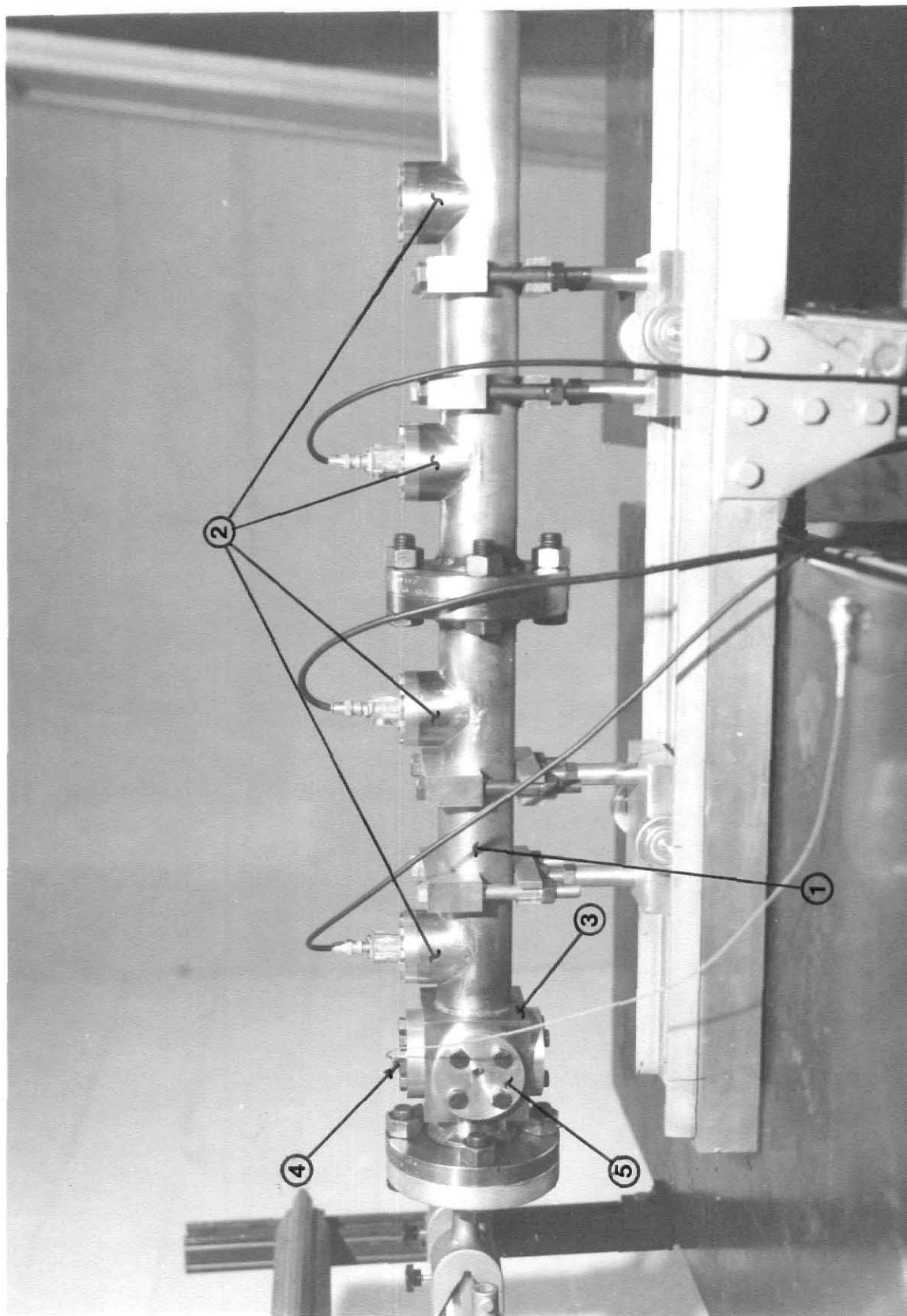
Fig. 17
OBSERVATION SECTION

1 THIN FILM GAUGES

2 THIN FILM G
   GAUGE PREAMP

3 PAR AMPLIFIER

4 ORTEC 410
   SHAPING AMP

5 E,G&G MODEL GG,
   2200/M

6 DATAPULSE 110B
   PULSE GENERATOR

7 NUCLEAR 700
   SCALER
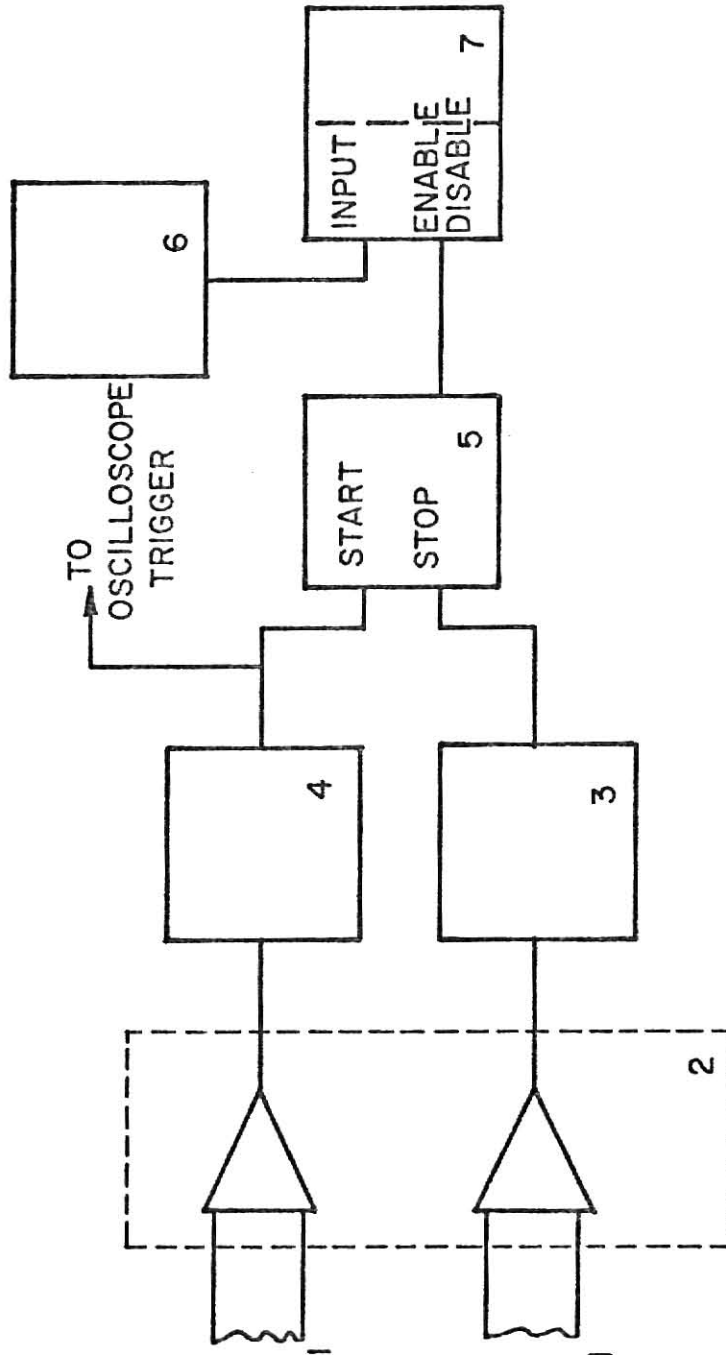
Fig. 18

SCHEMATIC OF THIN FILM GAUGE TIME INTERVAL COUNTING INSTRUMENTATION

Index to Numbered Items on Fig. 19

1. Thin film gauge preamp

2. Gate generator (G & G Model GG200/N)

3. Thin film gauge amplifier (PAR 211)

4. Photomultiplier tube supply current (ORTEC Model 456)

5. Pulse generator (DATAPULSE 110B)

6. Pressure transducer charge senitive amplifier (Kistler 1255)

7. Scalers (Nuclear 700)

8. Thin film gauge shaping amps (ORTEC Model 410)

9. Oscilloscope camera (Hewlett Packard Model 196A)

10. Oscilloscope (Tektronix Type 551)
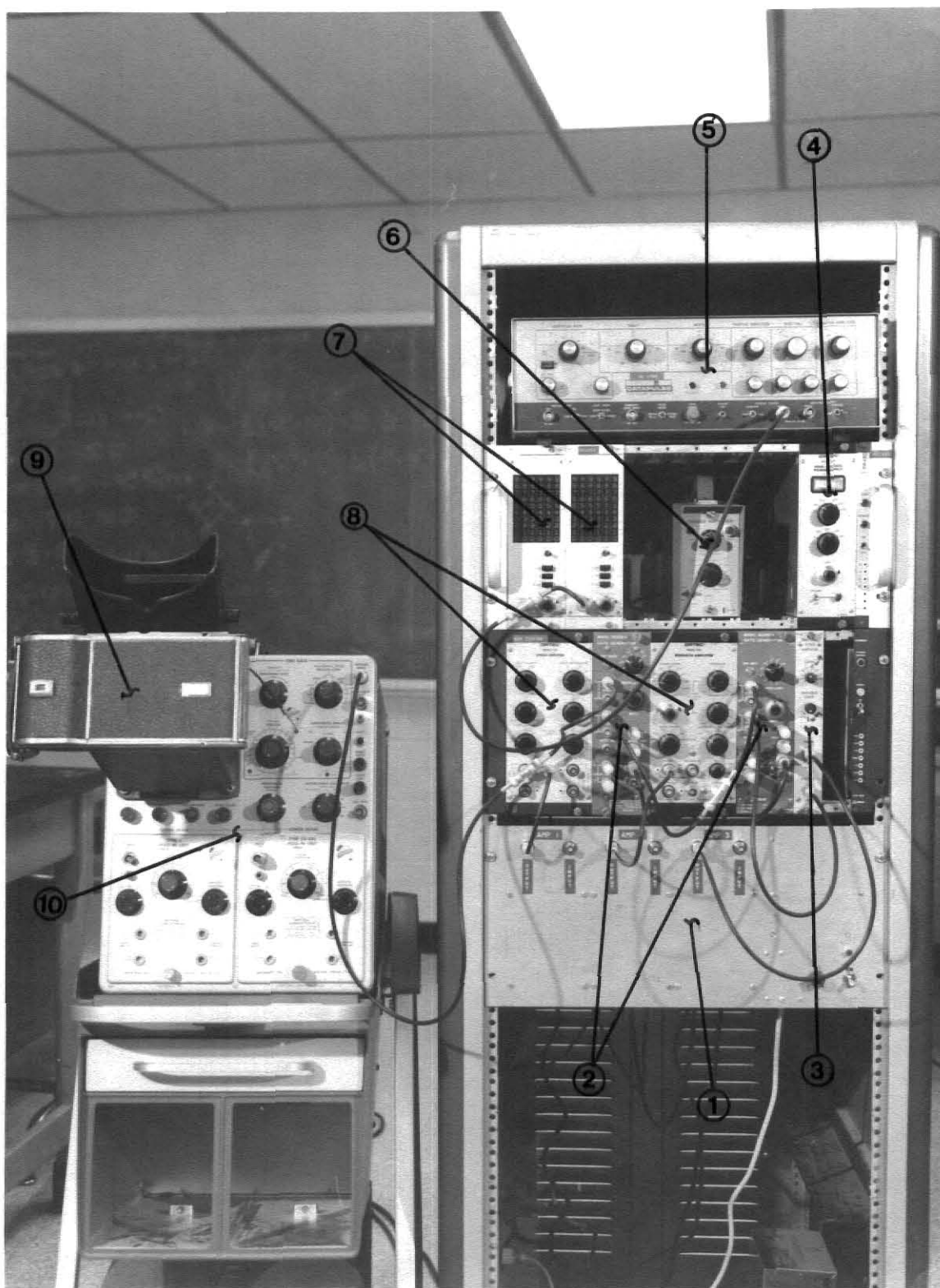
Fig. 19
SHOCK ANALYSIS INSTRUMENTATION

the input of the scaler to an oscillator at a frequency of one megahertz, the scaler records, in microseconds, the time interval for the shock front to pass across both thin film gauges. The use of this system allows the Mach number of the incident shock to be measured with greater than one percent percision.

The most appropriate dynamic characteristic to be measured in complex shock tube experiments is the pressure. If the pressure can be measured with high time resolution and accuracy, then the complicated wave inter-actions and nonuniform flow behavior behind the shock waves can be studied directly. In order to be useful, the pressure transducer used must have an ultra fast rise time and have a linear response over an extremely large range of pressure values (10 torr to 500 psi). Also, the transducer must not respond to extreme changes in temperature, such as that accompanying the shock wave, and it must be free from response to mechanical shock as transmitted by shock tube walls (acceleration response).

A Kistler miniature quartz pressure transducer model 603A obtained from Pivan Engineering is used because of its internal accelerometer which eliminates vibration response and its rise time of one microsecond. It may be used for pressures up to 3000 psi, and its sensitivity is 0.366 picocoulombs per psi. With a temperature sensivity of only 0.02 percent per degree farenheit, it is very well suited for high temperature shock tube work.

The transducer can be mounted in two positions. The most appropriate mounting is in the center of the end flange where it responds to the pressure in the central core region of the shock without interference from boundary layer disturbances. However, as can be noted in Fig. 17, the observation window is separated from the end flange by about 10cm. Thus, in order to

increase the observation time and to improve the shock structure at the window, the blank flange is replaced with a flange which has a variable length plug inside the tube. In this manner, the effective end wall of the shock tube is movable and can be located within a centimeter of the window. The use of this flange makes the end wall mounting impossible and necessitates a mounting in the lateral wall. The transducer is held in a plug (see Appendix C) which has O-ring type vacuum sealing and is retained in the observation block of the observation station. The design and construction of the observation block is discussed below.

Several methods of amplifications of the transducer signal have been attempted, including straight voltage amplification with a research amp, a FET charge sensitive preamp and a Kistler charge sensitivity amp, with only the latter having satisfactory response characteristics. The pressure signal from the Kistler amp is displayed on a Tektronix type 555 dual-beam oscilloscope, and is photographed with a Hewlett Packard model 196A oscilloscope camera. With the camera shutter held open, the oscilloscope, in the single sweep mode, is triggered externally by the first thin film gauge signal. The pressure history at the observation station, starting when the shock front reaches the first thin film, is thus photographed.

The shock tube produces a controlled temperature in which excited species can be formed by the energetic collision processes. The emission of these excited species is often used for chemical kinetic diagnostics, (Gaydon and Hurle, 1963; Nicholls and Pritchard, 1969). The spectrum may either be recorded photographically or photo-electrically in emission as well as absorption. The shock tube facility must therefore have optical ports for viewing such emission as well as an optical path through the tube to monitor absorption. If, in addition, a spectrum line reversal

temperature determination technique, using double beam methods (Clouston, Gaydon and Hurle, 1959; Faizullov, et. al., 1960) is to be used, then the tube must have two separate optical paths.

Changes in the electronic energy level of a molecule accompanied by changes in its vibrational and rotational energy occur by absorption of electromagnetic radiation in the visible and ultraviolet regions. Absorption in the infrared region of the spectrum corresponds to transitions of the vibrational levels with accompanying rotational level transitions. (Daniels and Alberty, 1975, p. 489) Thus, if a particular set of bands or lines are to be observed, the window material must not be opaque at the associated wavelengths. There is no one material which will transmit all of the appropriate spectrum from the near infrared region to ultraviolet region. However, quartz will cover much of the ultraviolet and all of the visible region. Another material such as ruby can then be used for vibration and rotation transitions in the infrared.

The window material presently used is supersil 2 fused silica from Amersil and the actual window size is one-half inch diameter and one-half inch thick. This material has excellent transmission characteristics from 170 millimicrons to 2 microns. The windows are epoxied into aluminum plugs similar to the pressure transducer plug and the plugs are held in a stainless steel observation window mounting block as shown in Fig. 20 & Fig. 17. This block was formed from a 3 1/2 inch (8.89 cm) cube of stainless steel bored through one face to the tube outside diameter (6.35 cm). The block was then slipped on the tube observation section and silver brazed on the tube by heating the tube and block until flow by capillary action of the silver solder into the gap between the tube and the block. The holes for the plugs were then bored into the four faces of the block and through

ALUMINUM WINDOW HOLDER
STAINLESS STEEL SILVER

BRAZED TO TUBE

FUSED SILICA WINDOWS

TUBE WALL

HOLDER FOR PRESSURE
TRANSDUCER
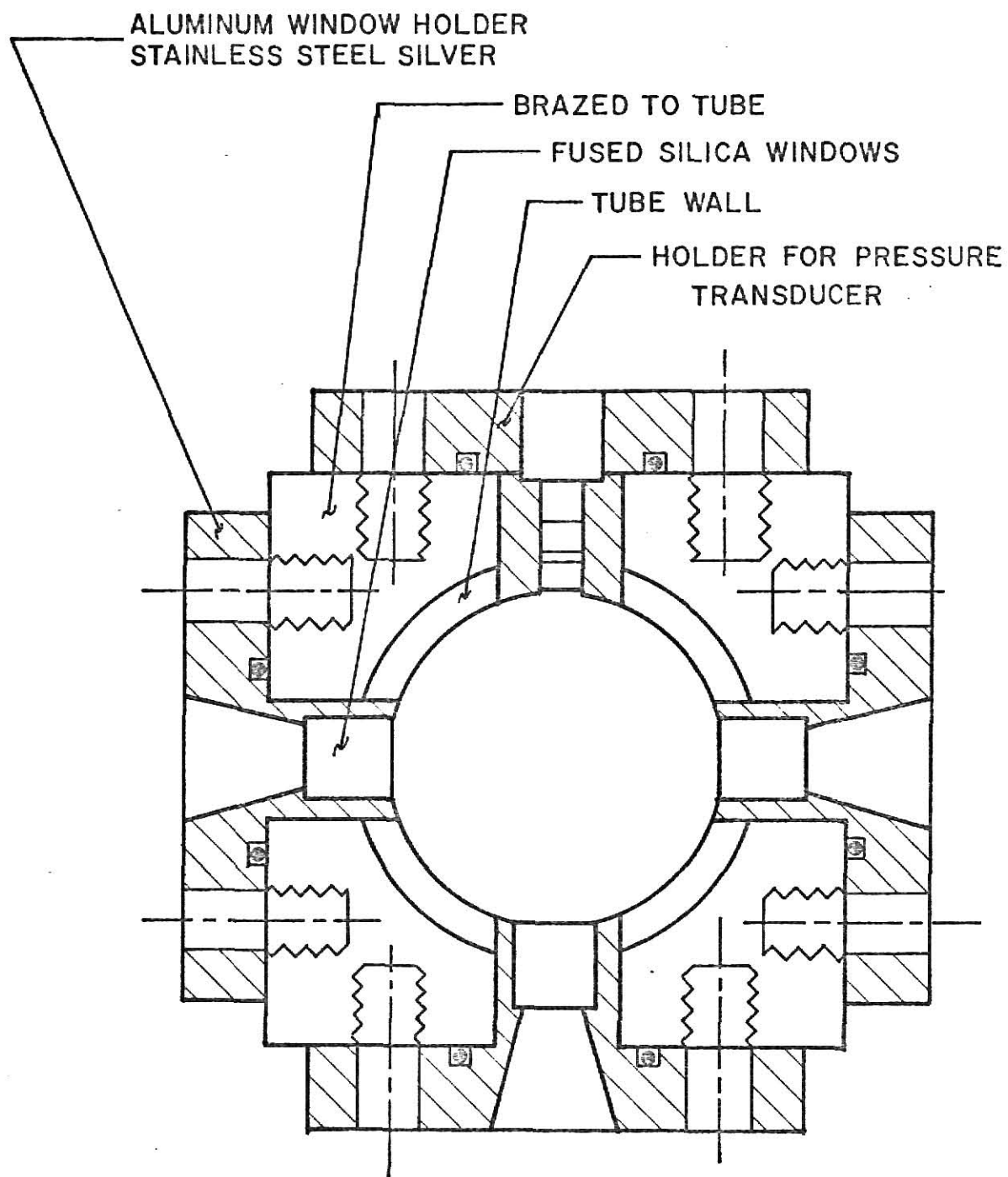
Fig. 20

OBSERVATION WINDOW AND PRESSURE
TRANSDUCER MOUNTING

the tube. The plugs, when mounted, thus hold the windows flush with the tube wall and allow a solid angel of .049 steradians to be subtended at the tube center. When the pressure transducer plug is replaced by a fourth window plug, there are two perpendicular path lengths available.

The shock tube facility uses several pressure gauges as part of the diagnostics as well as integral components in the firing sequency (Fig. 15). The driver pressure is measured with a Matheson stainless steel test gauge with a pressure range of 5-1000 psig (.35-68.93bars). It is used to determine the bursting pressure of diaphragm thicknesses and for monitoring the high pressure filling (see Appendix D). A "Speedivac" capsule dial gauge has also been used to assure the vacuum integrity of the driver section for the range 2-760 torr.

The test section uses several vacuum gauges. The initial evacuation of the tube for purity purposes requires extremely sensitive vacuum gauges. For preliminary tests the pressure is lowered to about a millitorr which can be measured using a Hastings thermocouple-type vacuum gage (model VC-13). However, for the high purity required in kinetic studies, the tube must be evacuated to 10^{-4} to 10^{-5} torr which requires replacement of the thermocouple tube with a Veeco ionization gauge type RG-2A. The tube is then filled with the experimental gas to the initial pressure dictated by the desired final conditions behind the shock wave. This pressure is determined using an Edwards "Speedivac" capsule dial gauge which has a range of 2-100 torr and an accuracy of $\pm$ 2 torr.

IV. EXPERIMENTAL PROCEDURES AND RESULTS

Procedures

It is necessary to develop procedures for the normal operation of the shock tube facility which will ensure correct shock structure, repeatability of shock strength, minimum turnover time, and most importantly, safety. The procedures developed here will be used in all subsequent applications of the tube. Also, computer programs using the ideal shock relationships of section I were developed and are discussed below.

Before each run the test section was evacuated to an ultimate pressure dictated by the purity requirements of the subsequent experiment. For extreme high purity, this was followed by flushing the test section with the test gas to be used and reevacuating. However, for experiments concerned only with the gas dynamic performance of the facility this was not necessary. After closing the main vacuum valve number 1 (Fig. 15), the test section was filled to the chosen pressure with the desired composition using the test section manifold (valve numbers 9, 10 and 11) and inlet valve number 8. The "Speedivac" 2-100 torr vacuum gage was used to determine this pressure. The tube was then isolated by closing all inlet valves to the test section (numbers 1, 4, and 8). The importance of this last step can not be over-emphasized. Failure to close these valves before firing the tube could result in oblique shocks propagating into the vacuum system and vacuum gauges causing possible detonations and injuries and at least destruction of all gauges. For this reason, the firing sequence check list (Appendix D) provided for double check for these valves.

A firing procedure was developed to produce maximum shock strength repeatability. This involved opening the appropriate driver gas manifold

valve, either valve 12 or 13 (Fig. 15), the same amount on each firing, one-half of a full turn. The regulator, whose delivery pressure must be set above the diaphragm bursting pressure, could then maintain the same flow rate for each firing. The actual firing occurred after the firing solenoid valve, number 15, was opened and the pressure in the driver section rose above the diaphragm bursting pressure. If a mixture of gases was to be used, the driver was initially filled manually with the first component and the second component was used for firing. This process was used to obtain Mach numbers for individual runs within 5 percent of each other. The bursting pressure for the various thicknesses and combination of thicknesses of mylar diaphragm was determined and is shown in Fig. 21.

Two computer programs were written which predict the ideal conditions behind the incident and reflected shock waves from the measured shock speed. They use equations (10), (11), and (12) for the incident shock region and (15) and (16) for reflected shock region. The input data consists of the speed of sound and specific heat ratio of the driver and test gases, the initial pressure in the test section, the bursting pressure of the diaphragm, the initial temperature of the test gas, the measured time interval and the distance over which the time was measured. The first program, which was written in WATFOR for an IBM 370 computer, also predicts the ideal Mach number from the bursting pressure ratio. The second program was stored on magnetic tape for use in a Tektronix desk top programmable calculator. The listings for both programs are given in Appendix F.
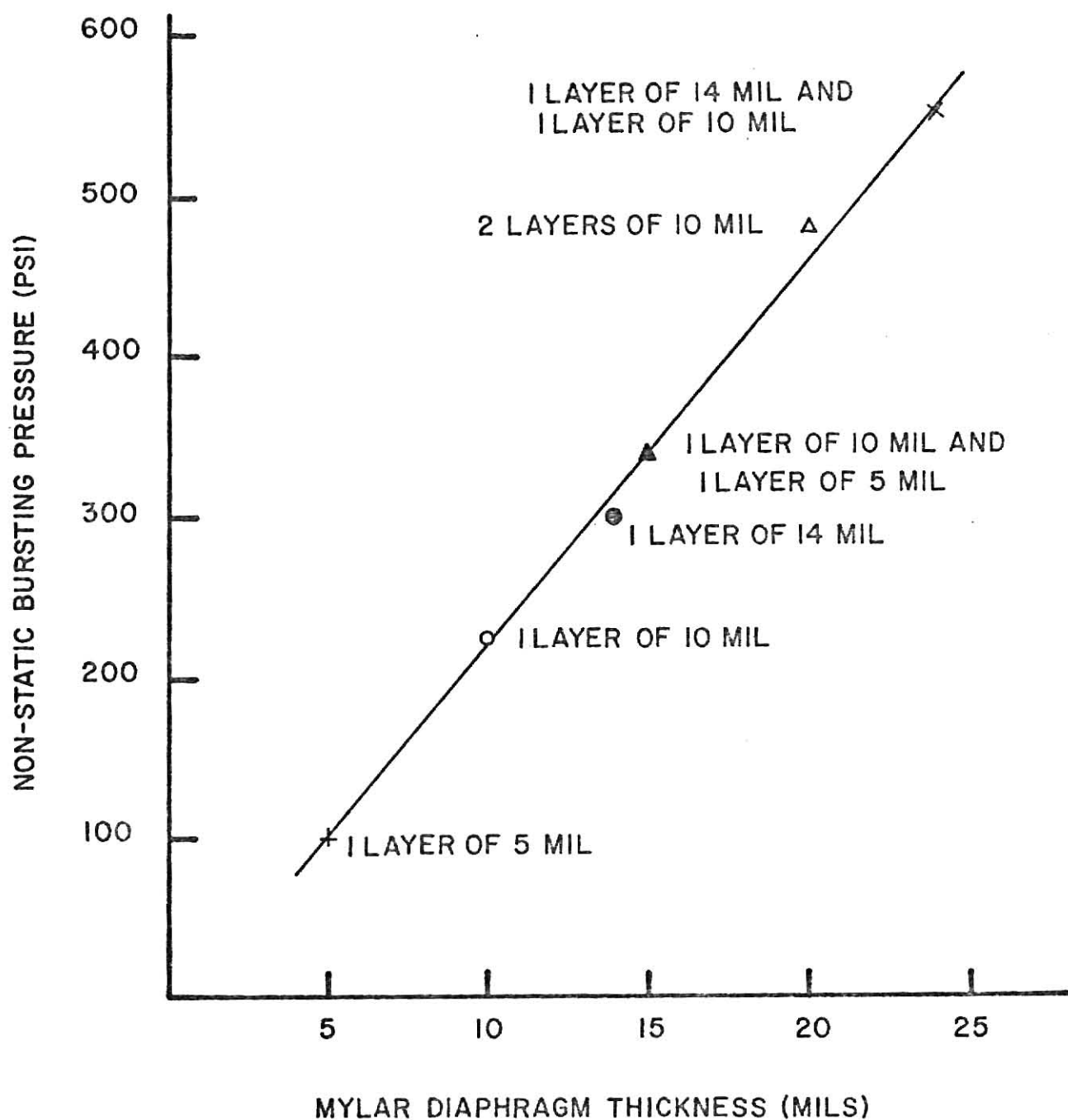
Fig. 21

BURSTING CHARACTERISTICS OF MYLAR DIAPHRAGMS

Pressure Histories

Several examples of the reflected shock pressure history, which was measured with the transducer mounted in the center of the end wall flange, are shown in Fig. 22. At this location, the transducer recorded the pressure transients of the core region of the tube without any interference from the boundary layer which would be present if the mounting was in a lateral wall. The strong discontinuity in pressure was seen as the shock front struck the end flange and pressure transducer, demonstrating the extremely quick response time of the transducer-amplifier-oscilloscope system. The transients following the discontinuity were assumed to be due to tube ringing or to the crystal vibration and not to actual pressure transients.

The pressure stayed very constant after the shock front had arrived for nearly 1.5 milliseconds in cases where the initial test gas pressure was not too low (above 50 torr) as shown in Fig. 22 (a), (b) and (d). The pressure rise due to shock attenuation was almost imperceptible (see below).

A physical interpretation of the reflected shock pressure history is difficult due to the complex wave interactions involved. The reflection from the contact surface-reflected shock interaction can be either a shock or a rarefaction depending on the shock strength. For strong shocks the first disturbance, S_1, is a shock wave and for weak shocks it is a rarefaction. The condition for which there is no disturbance is said to be "tailored". However, the real contact surface is not a surface at all, but rather, has a finite width with temperature, concentration and pressure gradients across it. The contact region has been modeled as a series of surfaces with all the changes in properties lumped at that surface (Zallen, 1973). Thus the reflection of the

(a)
He/Air
$P_4 = 100 \, psi$
$P_1 = 50 \, torr$

(b)
He/Air
$P_4 = 225 \, psi$
$P_1 = 100 \, torr$

(c)
He/Air
$P_4 = 225 \, psi$
$P_1 = 10 \, torr$

(d)
He/Air
$P_4 = 225 \, psi$
$P_1 = 100 \, torr$
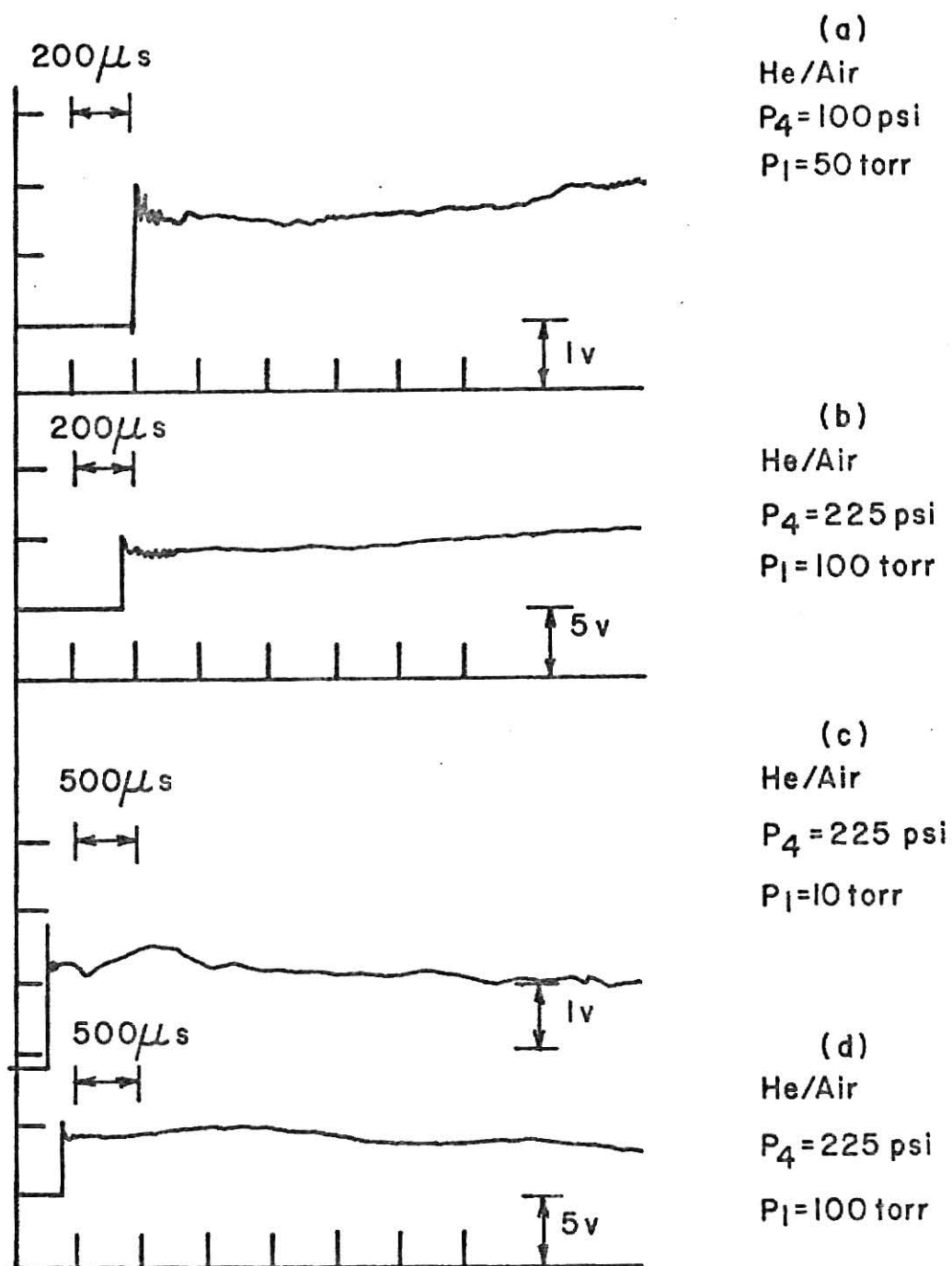
Fig. 22

REFLECTED SHOCK PRESSURE HISTORY

reflected shock off the contact region is not a discrete wave but rather a series of tightly spaced waves. In fact, the character of the first disturbance may change from a shock to a rarefaction due to this interaction with the various layers of the contact region.

In all cases shown in Fig. 22, the shock speed was below that necessary for ideal tailoring (Witliff, Wilson, and Hertzberg, 1959), i.e. undertailored, so that S_I should be a rarefaction. For Fig. 22 (d), the pressure decreased about 1.5 milliseconds behind the reflected shock indicating the arrival of a rarefaction. At much lower initial test gas pressures the time of uniform flow was very much less (Fig. 22(c)) due to the increased speed of the reflected shock and the pronounced boundary layer effects. The observable "hump" in the lower initial pressure case (Fig. 22 (c)) may be due to the smearing of the first disturbance from a finite width contact region. The degradation of the constant pressure time interval was dramatic for initial test gas pressures below 50 torr.

The interaction of the rarefaction head with the reflected shock pressure history and the driver pressure history is shown in Fig. 23. In part (a) the reflected shock pressure was relatively constant for nearly five milli-seconds until the arrival of the reflected rarefaction significantly lowered the pressure. The driver pressure history was measured by locating the observation section between the two driver sections so that the transducer was about 2 1/2 meters from the diaphragm and 1 meter from the driver end wall. The oscilloscope single sweep was triggered by the transducer signal. Two distinct rarefactions are evident in Fig. 21 (b). The incident rarefaction head passed by the
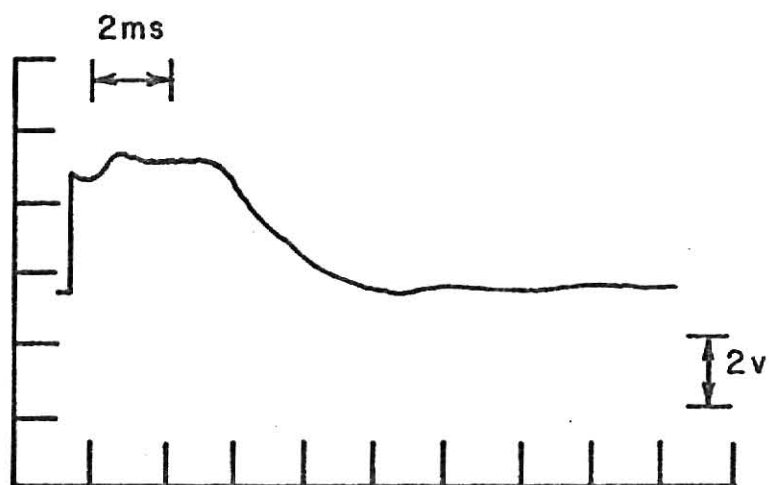
(a) TEST PRESSURE
    HISTORY

He/Air

P_4=225 psi

P_I=50 torr

M_s=2.78

2ms

2v

(b) DRIVER PRESSUR
    HISTORY

He/Argon

P_4=480 psi

P_I=100 torr

1ms

5v

Fig. 23

RAREFACTION EFFECT ON PRESSURE (a) IN TEST SECTION
AND (b) IN MIDDLE OF DRIVER SECTION
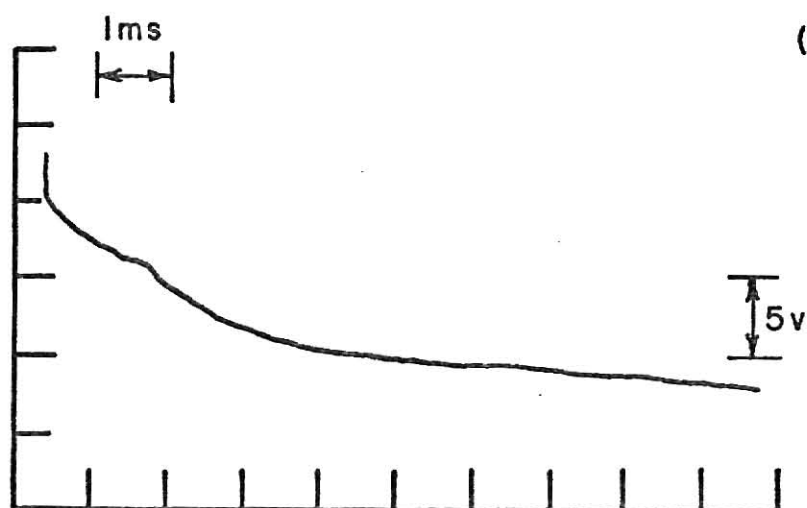
transducer station as demonstrated by the large decrease in pressure and the arrival of the reflected rarefaction head was denoted by the increased rate of pressure decline about 1.4 msec behind the incident rarefaction head. The calibration constant of the transducer system, 13 v/psi, was found by comparing the output of the Kistler with the predicted output from the measured shock strength of previous runs. Thus, the passage of the incident rarefaction brought the pressure down almost 100 psi in 1.4 milliseconds after which the reflected rarefaction lowered the pressure an additional 70 psi in the first two milliseconds after its passage. The large initial decrease after the reflected rarefaction was followed by a smaller, linear decrease at a rate of around 5 psi/msec.

As mentioned earlier, the pressure transducer can be mounted either in the end wall or in the lateral wall. For most applications, the end flange will be replaced by a flange which has a variable length plug inside the tube allowing the effective end wall of the shock tube to be as close to the observation ports as possible. This necessitates a lateral wall mounting. Two separate lateral mountings, shown in Fig. 24, were used and machined into plugs described originally in section III. The recessed mounting was designed to prevent disturbance of the flow by the transducer itself and is often used in hypersonic wind tunnel experiments (Sage, 1975).

Sage (1975) has examined the response time of a recessed mounting of the type shown in Fig. 24 (b) for pressure steps. It was found that the time required to reach 95 percent of the initial pressure difference between the chamber and the transducer signal was dependent upon the connecting canal length and diameter. For a canal diameter of 1.075 mm and length of 3 mm the time required to go from 0.01 torr to 95 percent of the final pressure of 1000 torr was found to be about 3 milliseconds.

(a) RECESSED MOUNTING

STAINLESS STEEL
SEAL

1.59mm

(b) FLUSH MOUNTING

—TEFLON SEAL

5.55mm
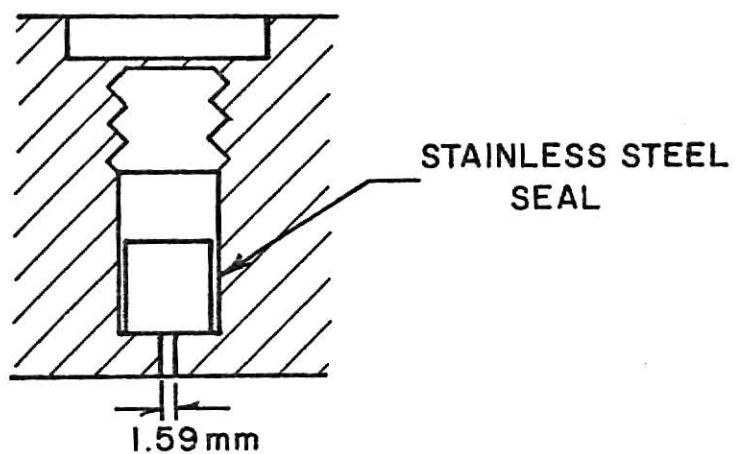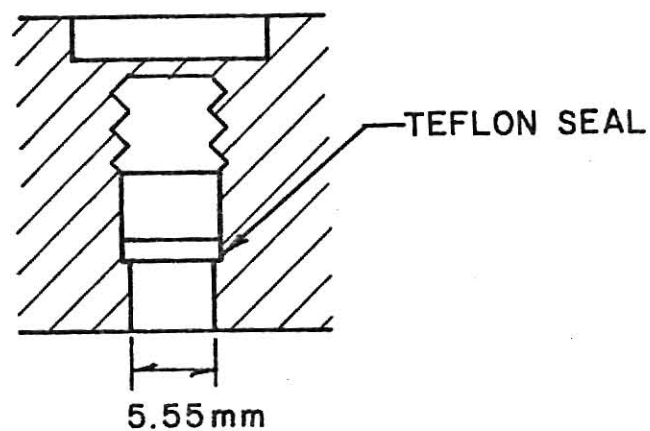
Fig. 24
PRESSURE TRANSDUCER MOUNTINGS

In the shock tube application, this lag time was again observed with the addition of a discontinuity in the pressure signal (Fig. 25) due to a small shock front which propagated down the canal. This canal connection of 1.6 mm diameter and 3.2 mm in length was observed to cause a delay time of several hundred microseconds to a millisecond before the transducer in the recessed mounting had a signal corresponding to that received from the end flange mounting.

This delay was not inherent in the lateral wall position itself. The flush mounting in the lateral wall and the end flange mounting gave similar results (Fig. 26), especially at initial test pressures above 10 torr. Below about 10 torr the reflected shock front moves faster in the stagnate boundary layer than in the fast moving inner core. This phenomenon, known as bifurcation, results in shock front "forking" as it propogates back down the tube, and is only observed for non-inert test gases. Dumitrescu, Popescu, and Brun (1969) reported extreme distortion of the pressure plateau near and below 10 torr using lateral wall pressure transducer mountings. This gradual increase in pressure was found to become more prominent as P_1 was decreased and the shock strength was increased. This present study revealed a much smaller effect as seen in Fig. 26 (a) probably due to the fact that the transducer was mounted very near the effective end wall ($\sim$1mm) so the bifurcated foot was not well formed.

Shock Attenuation

The loss of the driver gas and kinetic energy to the boundary layer causes the front to decelerate as it progresses down the shock tube. The flow of the driver gas expanding through the ruptured diaphragm causes

(a)

He/AIR
P4=480 PSI
PI=60 torr

(b)

He/AIR
P4=480 PSI
PI=100 torr

(c)

He/AIR
P4=225 PSI
PI=50 torr

(d)

He/AIR
P4=225 PSI
PI=50 torr
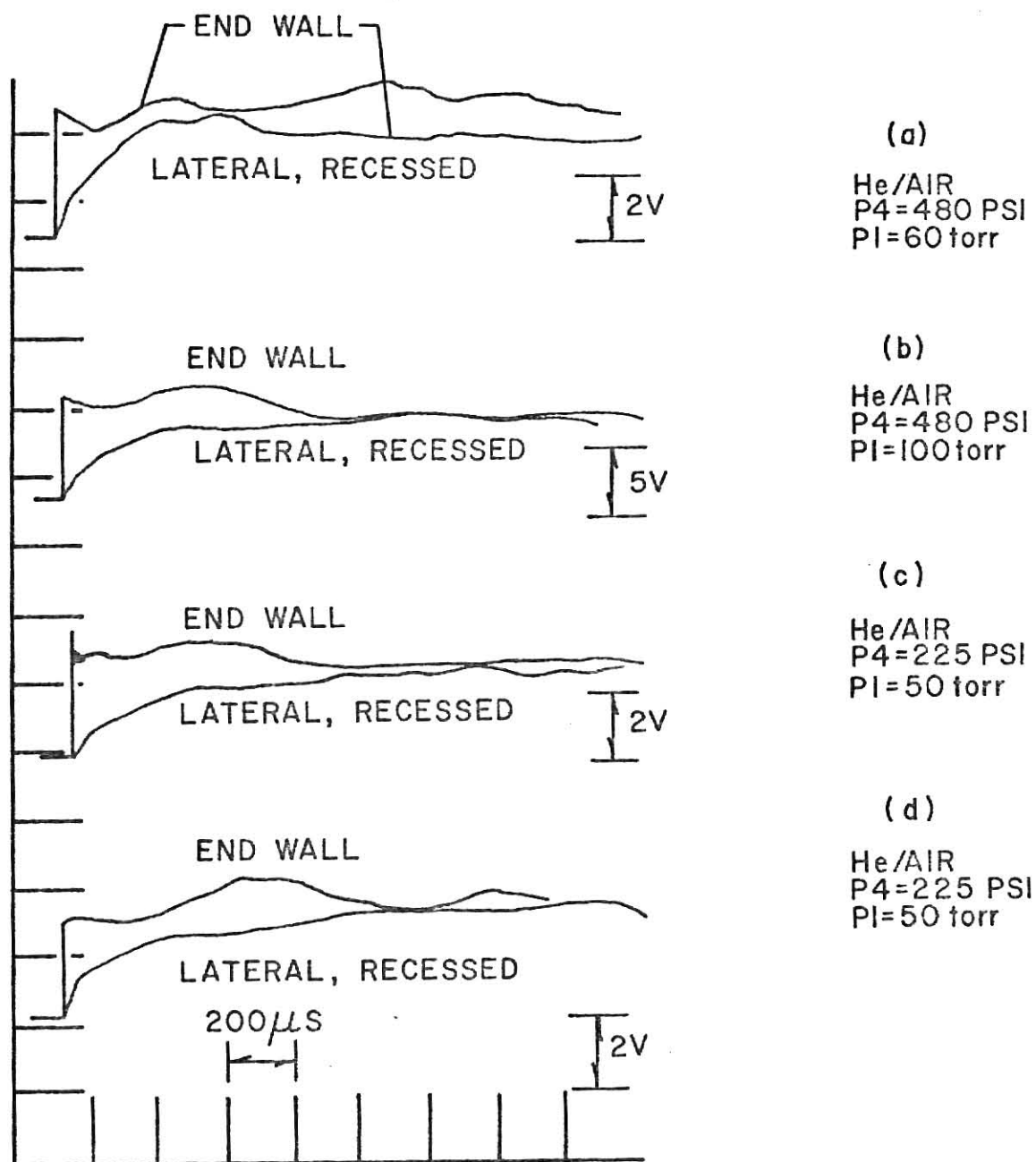
Fig. 25

COMPARISON OF REFLECTED SHOCK PRESSURE HISTORIES FROM
TRANSDUCER MOUNTED IN END FLANGE AND A
LATERAL WALL RECESSED MOUNTING
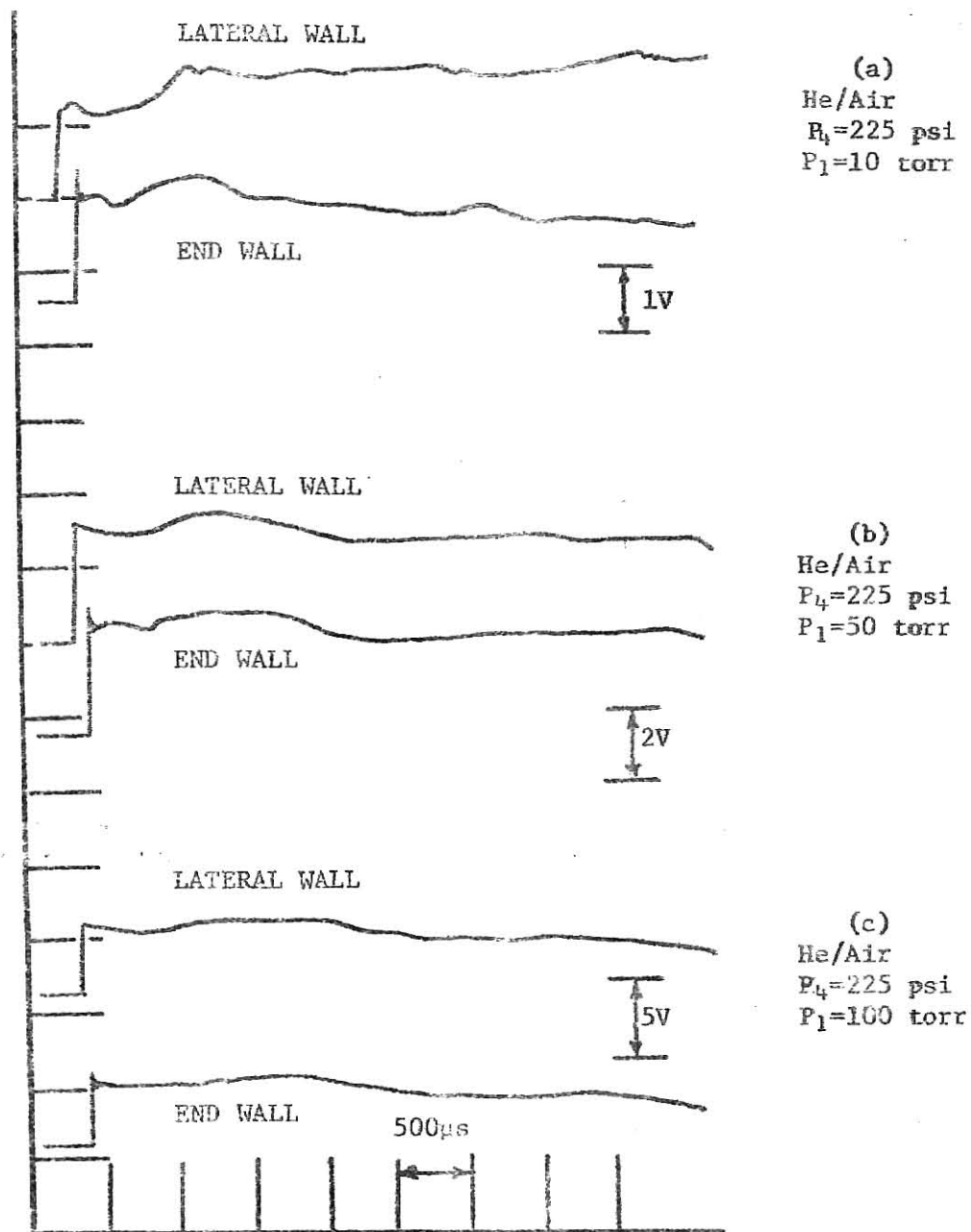
Fig. 26

COMPARISON OF REFLECTED SHOCK PRESSURE HISTORIES
FROM TRANSDUCER MOUNTED IN END FLANGE AND
LATERAL WALL FLUSH MOUNTING

turbulence and eddying in the boundary layer contributes to the shock attenuation. However, as discussed in section II, the diaphragm opening process may actually cause acceleration of the shock wave.

A knowledge of the character of the attenuation is very important. Since the shock front is moving faster near the diaphragm, the gases nearer the diaphragm are heated more strongly by the faster shock than gases away from the diaphragm and further down the tube. Thus, the gases in the shock will be cooler near the front and hotter near the contact surface. As the shock heated gases pass by an observation station as they due in experiments in the incident shock, the temperature will appear to rise slightly. This same effect occurs for the pressure. Dumitrescu, Popescu, and Brun (1969) stress the importance of this gradual rise in pressure and especially in temperature on the assessment of non-uniformities in hypersonic flow. Also, the magnitude of the attenuation indicates the degree of development of the boundary layer and whether the boundary layer is in the laminar or turbulent regime (Mirels and Mullen, 1964). Finally, it is desirable to measure the shock attenuation and local pressure in order to facilitate correction of shock tube kinetic data for wall boundary effects (Holbeche and Spence, 1964).

The shock attenuation was determined by moving the half-meter observation section to different positions along the tube. The observation section had two thin film gauges so that the shock speed at each position could be measured for various driver/test gas combinations and pressures. The observation station also contained the pressure transducer so that the incident shock pressure history could be monitored.

The nine cases investigated are given in Table 3. The variations of the Mach number along the tube are shown in Fig. 27, 28, and 29. The variation of the measured Mach number at each position in Fig. 27 was due to the manual shock firing which caused a lack of repeatability. The subsequent measurements, cases 4 through 9, used the firing procedure discussed previously with its inherent good repeatability characteristics. The definite shock attenuation is evident in each case. Further, cases 5, 6, and 7 demonstrate dramatically the increase in deceleration as the shock moves away from the diaphragm. This is due to the decreased effect of the diaphragm opening processes and the transition from a laminar to a wholly turbulent boundary layer regime further down the tube.

The average attenuation was determined by a least squares fit for the full tube length, the first 3 1/2 meters from the diaphragm, and the last 3 1/2 meters. The attenuation, as listed in Table 4, increased markedly over the second half of the tube where the turbulent boundary layer may be expected to be the prominent nonideal effect. The attenuation in the first half of the tube was remarkably small, and in case 6, was even an acceleration. These data also indicate that the attenuation in the second half of the tube is relatively constant for the same driver bursting pressure over various initial test pressures. The attenuation for the less efficient driver (50 percent HE-50 percent N_2) was severe as compared to the pure helium driver. Finally a comparison of the attenuation over the last half of the tube for cases 5 and 8, and cases 6 and 9 reveals that the attenuation for approximately the same shock strength decreases significantly with increasing initial test gas pressure.

TABLE 3
SHOCK ATTENUATION RUNS

Case	Driver Gas	Test Gas	P_4 in Bars (psi)	P_1 in torr	P_4/P_1	Mylar Diaphragm
1	50%He-50%N$_2$	Argon	20.7 (300)	10	1551	1-14
2	50%He-50%N$_2$	Argon	20.7 (300)	50	310	1-14
3	50%He-50%N$_2$	Argon	20.7 (300)	100	155	1-14
4	Helium	Air	15.5 (225)	10	1163	1-10
5	Helium	Air	15.5 (225)	30	388	1-10
6	Helium	Air	15.5 (225)	50	233	1-10
7	Helium	Air	33.1 (480)	20	1241	2-10
8	Helium	Air	33.1 (480)	60	414	2-10
9	Helium	Air	33.1 (480)	100	248	2-10

The attenuation due to the wall boundary layer can be predicted analytically using small pertubation theory (Mirels & Mullen, 1964). This method assumes ideal driver and test gases. The shock attenuation for this method is:

$$\Delta M_s = M_s M_s^* \left(\frac{P_{st}}{dP_1}\right)^{-n} \left(\frac{d}{x}\right)^{-(n+1)}$$ (26)

where the exponent n is $-1/5$ or $-1/2$ depending on whether the boundary layer is wholly turbulent or wholly laminar, respectively. The analytical shock attenuation factor M_s^* is a complicated function of the driver/test gas combination and the measured Mach number at the position X_s. From the graphs from Mirels and Mullen (1964), this factor was determined for the ideal-He/ideal-air cases and the predicted attenuation is given in Table 4 for the laminar and turbulent extremes.

A comparison of the measured average shock attenuations over the second half of the tube with the wholly turbulent predictions reveals that the boundary layer was approaching the turbulent regime for weaker shock strengths with higher initial test gas pressures. For stronger shocks into lower test gas pressures, the laminar boundary layer persisted further down the tube as evidenced by the attenuation comparison.
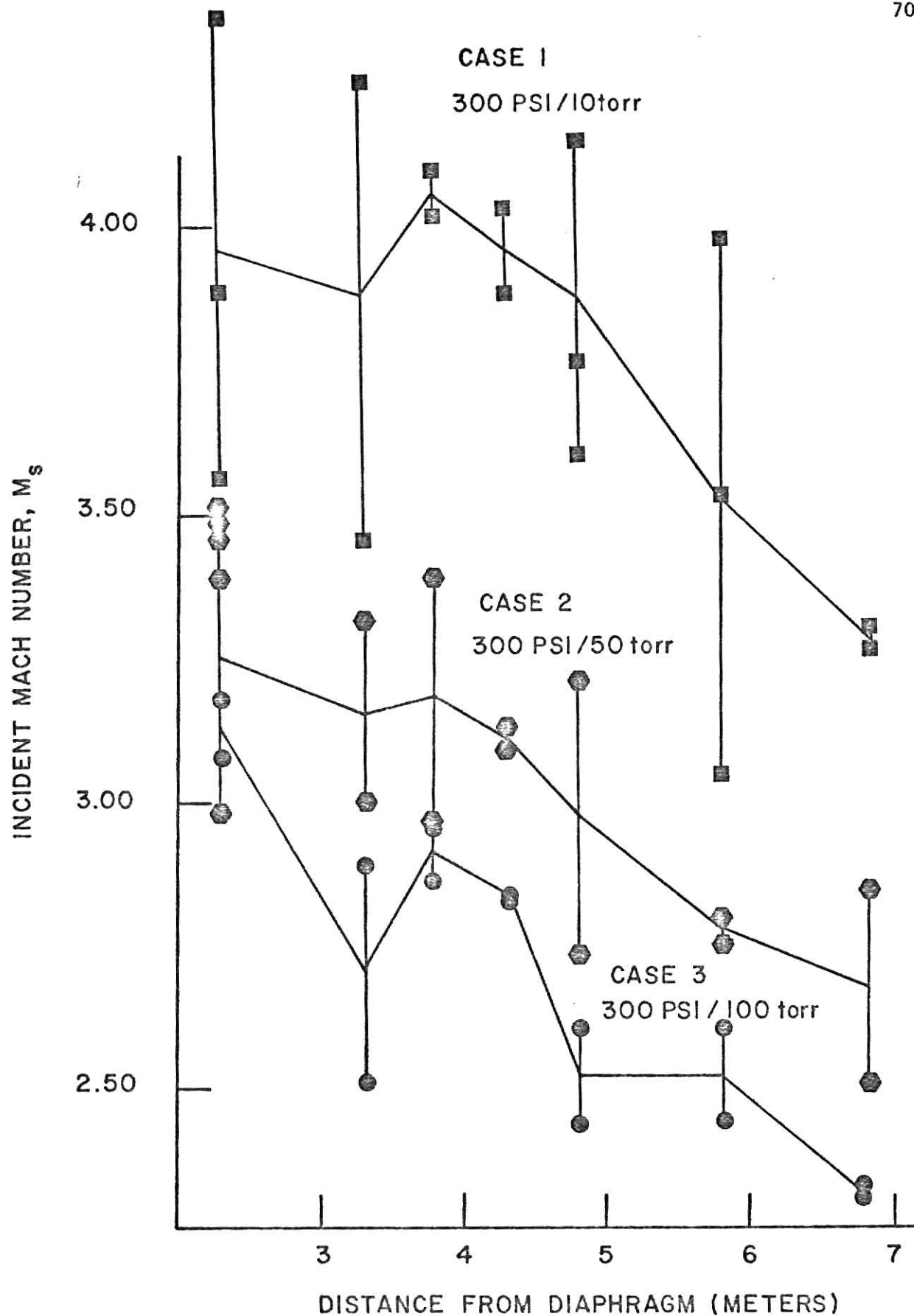
Fig. 27
SHOCK ATTENUATION FOR HELIUM-NITROGEN /ARGON
SHOCKS; CASES 1,2,and 3
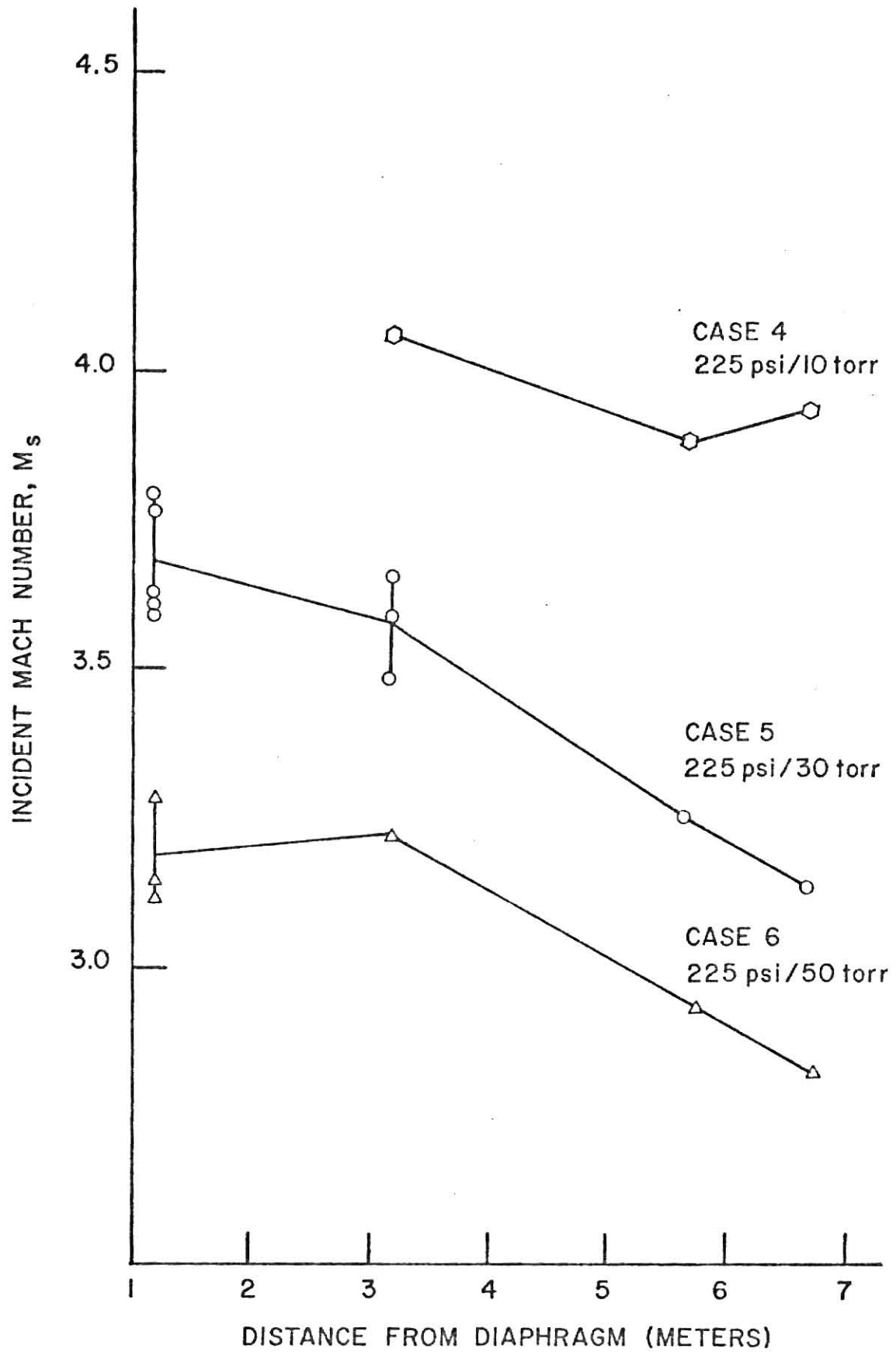
Fig. 28
SHOCK ATTENUATION FOR HELIUM/AIR
SHOCKS; CASES 4,5, and 6
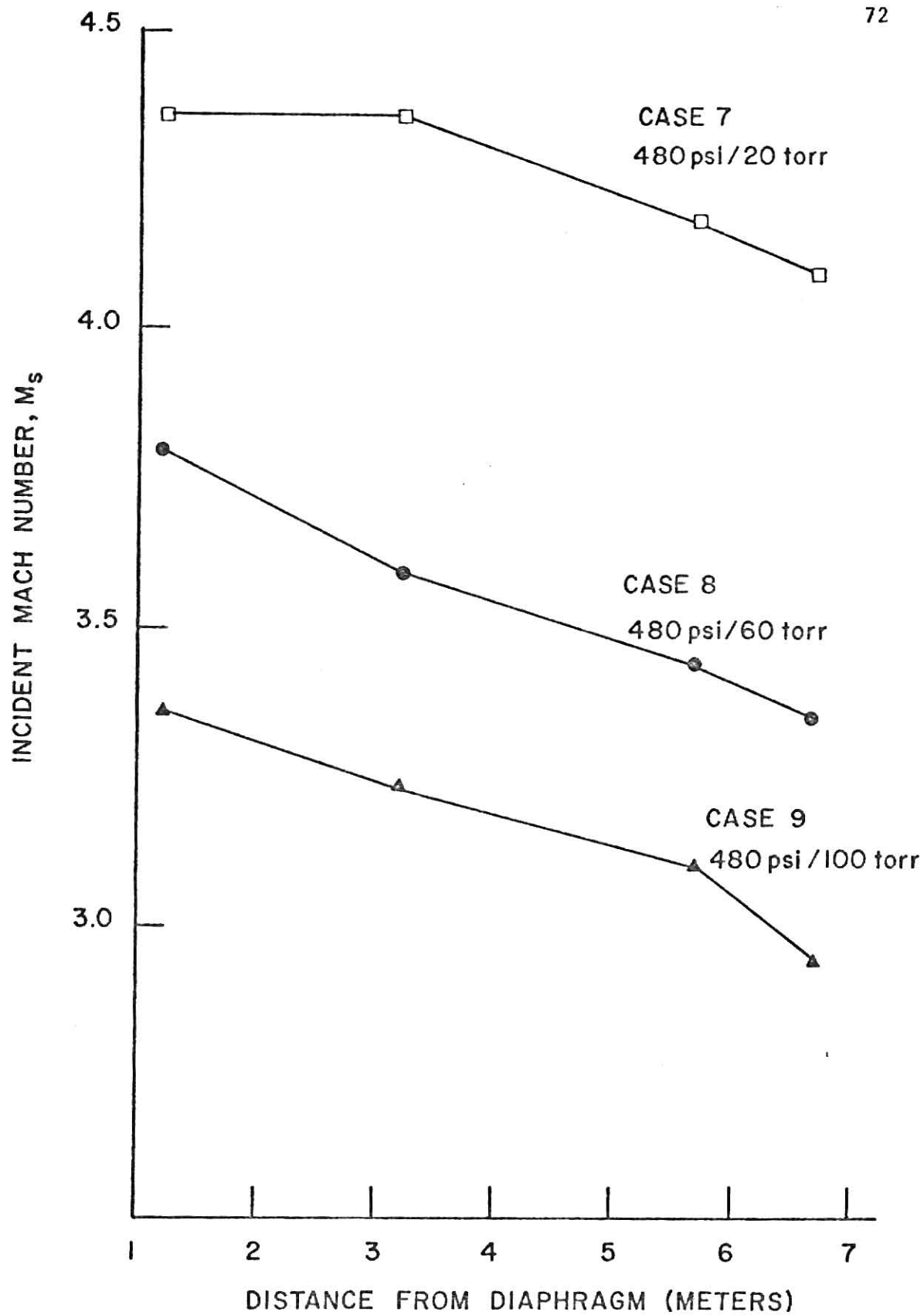
Fig. 29

SHOCK ATTENUATION FOR HELIUM/AIR
SHOCKS; CASES 7,8, and 9

TABLE 4
AVERAGE SHOCK ATTENUATION, ΔM_s, PER METER

CASE	OVER FIRST 3 1/2 METERS	OVER SECOND 3 1/2 METERS	OVER FULL TUBE LENGTH	WHOLLY TURBULENT BOUNDARY LAYER THEORY	WHOLLY LAMINAR BOUNDARY LAYER THEORY
1	0.0107 $\pm$ 0.26	0.269 $\pm$ 0.030	0.167 $\pm$ .059	---	---
2	0.302 $\pm$ 0.053	0.176 $\pm$ 0.053	0.165 $\pm$ .034	---	---
3	0.186 $\pm$ 0.12	0.195 $\pm$ 0.031	0.168 $\pm$ .027	---	---
4	---	0.0442 $\pm$ 0.020	0.0442 $\pm$ .020	0.208	0.0479
5	0.0517 $\pm$ 0.032	0.117 $\pm$ 0.018	0.0913 $\pm$ 0.014	0.133	0.0224
6	-0.0167 $\pm$ 0.043	0.115 $\pm$ 0.0009	0.0631 $\pm$ 0.016	0.105	0.0160
7	0.0 $\pm$ 0	0.0761 $\pm$ 0.003	0.0511 $\pm$ 0.011	0.200	0.0352
8	0.1 $\pm$ 0.0	0.070 $\pm$ 0.004	0.0792 $\pm$ 0.004	0.126	0.0169
9	0.065 $\pm$ 0.0	0.0747 $\pm$ 0.012	0.0723 $\pm$ 0.007	0.0975	0.0116

There is agreement between the results of the predicted boundary layer character and the pressure history of the reflected shock. According to Mark (1958; as discussed by Rudinger, 1961) the boundary layer must be laminar in character in order for the conditions to be correct for the reflected shock to develop the bifurcated interaction pattern. As can be observed from Table 4, case 4 (He/Air; P_4=15.5 bars P_1=10 torr) is the only case studied which has a measured attenuation which is in agreement with the laminar boundary layer theory. From a study of the pressure histories of Fig. 26 it can be observed that only part (a), corresponding to case 4 conditons, demonstrates the rise in pressure history in the lateral wall mounting which indicates the presence of bifurcation.

The magnitude of the attenuation for a helium driver was small and would probably not cause large variations from uniform flow although the helium-nitrogen driver could have severe limitations. The tube, as described has a commercial grade inner surface. The usual fabrication procedure is to hone or to chrome plate the tubing so that the seamless stainless steel tubing has a very smooth inner surface since there are some indications (Mirels, 1971) that this delays the transition from laminar to turbulent boundary layer. The measured attenuation for this tube indicated that these machining processes would be desirable, but are by no means imperitive.

Factors Affecting Uniform Flow

In Fig. 30 and Fig. 31 the variation of the measured shock Mach number on the diaphragm rupture-pressure ratio is demonstrated for a helium driver into air and argon test gases, respectively. The ideal
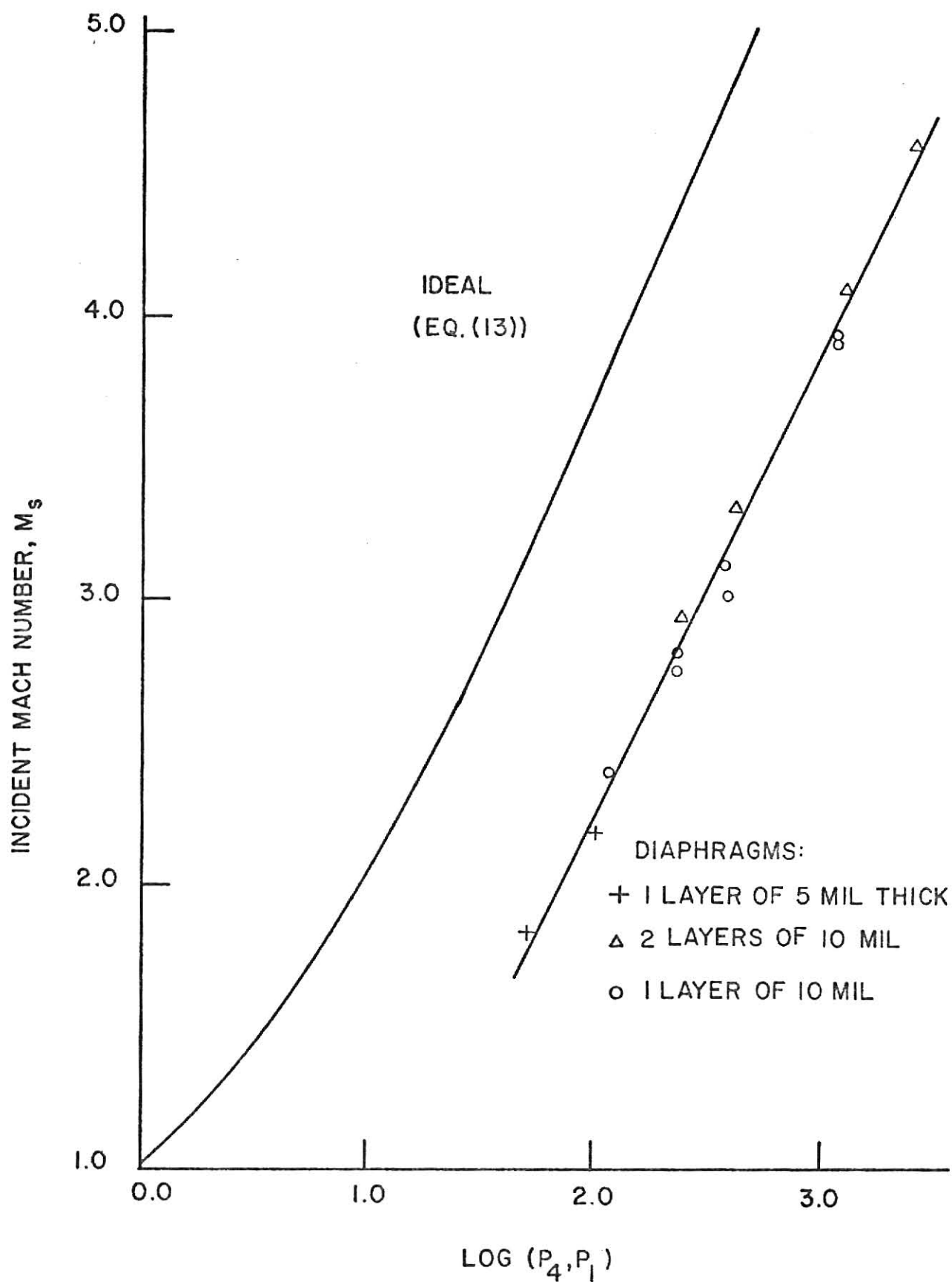
Fig. 30
VARIATION OF SHOCK MACH WITH DIAPHRAGM PRESSURE
RATIO FOR HELIUM INTO AIR TEST GAS
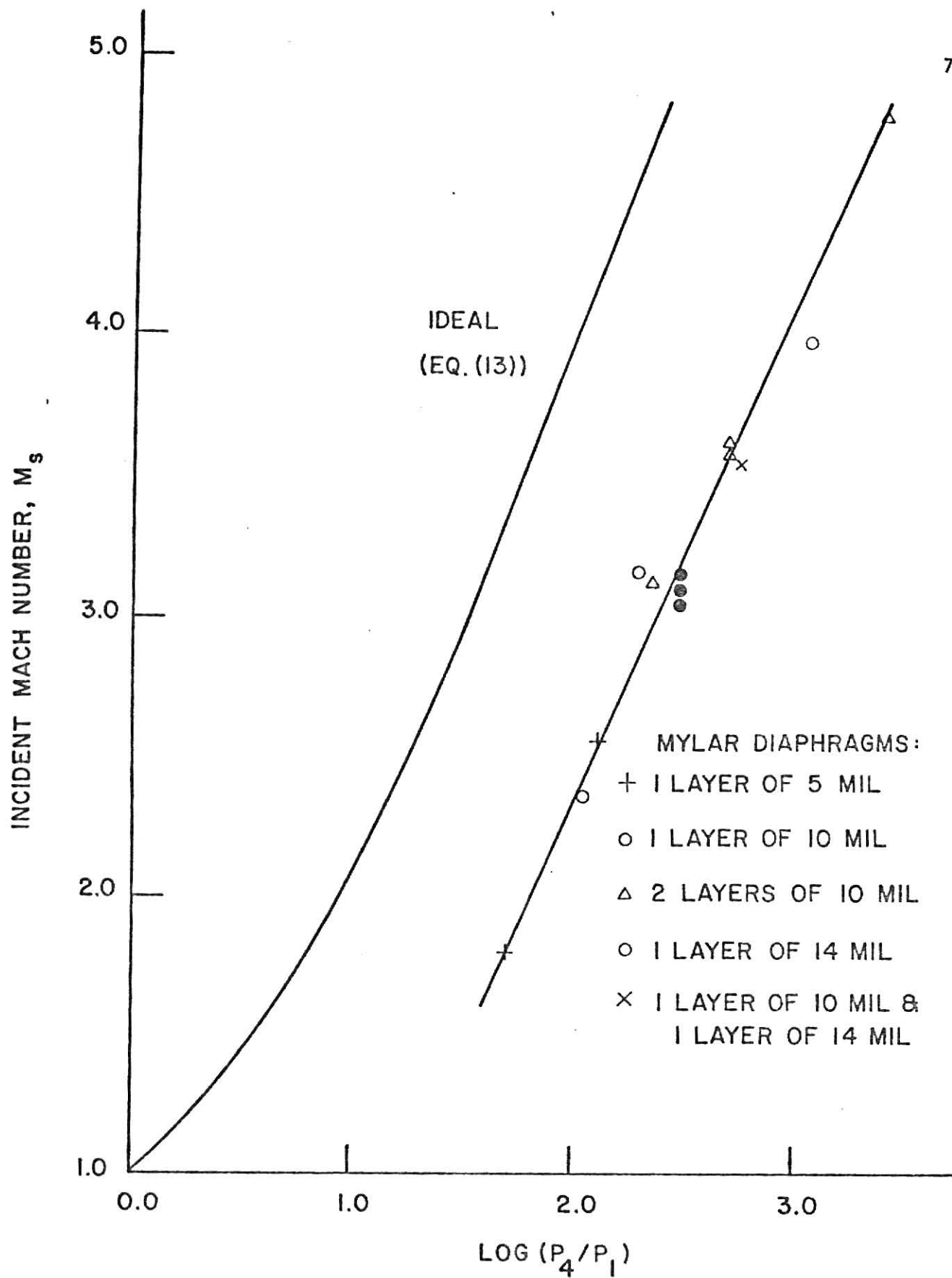
Fig. 31

VARIATION OF SHOCK MACH NUMBER WITH DIAPHRAGM PRESSURE
RATIO FOR HELIUM INTO ARGON TEST GAS

dependence on the pressure ratio, calculated from equation (13), is also plotted. It is seen that nonidealities such as shock attenuation, diaphragm opening processes and real gas effects, cause the shift to higher required diaphragm pressure ratios for a particular shock strength.

An additional factor causing deterioration of the tube performance was the rupture characteristics of thick mylar diaphragm. It was observed that 14 mil thick mylar diaphragms did not open correctly. The fully opened area of the 14 mil diaphragms was only 8.5 cm^2 as compared to 11.9cm^2 for 10 mil diaphragms and 20.3 cm^2 full tube cross section. This caused the effective driver cross sectional area to be reduced and lowered the driver efficiency. The high velocity jet of gas from the smaller opening results in increased mixing of the driver and test gas. It was found that the pressure ratio P_4/P_1 had to be increased by as much as 40 percent to obtain the same shock strength from a 14 mil thick diaphragm as from a combination of thinner mylar sheets.

V. CONCLUSIONS

The shock tube was designed to provide a flexible facility for the study of chemical kinetics and two-phase phenomena. Most of the design features were developed directly from consideration of the character of pulverized coal combustion and the experimental techniques used in the study of combustion reaction kinetics. Other aspects of the design were formulated from general requirements for an easily operated, workable and safe system. All necessary parts have been acquired and the tube constructed. The tube and connections were found to be very leak tight and evacuation of the test section with the roughing pump alone resulted in ultimate pressures of less than a millitorr obtainable in about five minutes. Shock speed measurement instrumentation was developed using manufactured thin film resistance gauges with a suitable time-interval counter system. The time of passage of the shock front over an eight inch length could be determined easily to microsecond accuracy permitting the Mach number of the shock front to be calculated to 1/2 percent precision corresponding to a determination of the ideal reflected shock temperature within 12 °K. A flush lateral wall mounting for the Kistler pressure transducer was developed which allowed correspondence to end-flange mounted pressure histories with little distortion from nonideal effects.

The shock attentuation was measured and the magnitude was found to be within acceptable limits for kinetic studies. When compared to theoretical predictions based on boundary layer effects, it was found that in many cases the laminar boundary layer persisted far down the tube. Only in cases where the initial test gas pressure was high did

the measured attenuation approach the theoretical predictions for a wholly turbulent boundary layer. The attenuation for the same shock strength increased for decreasing initial test gas pressure, indicating a more pronounced boundary layer effect. These observations indicate that the tube material has sufficient internal surface smoothness to accomodate sensitive kinetic measurements.

The observed pressure histories behind the reflected shock demonstrated long pressure plateaus following very sharp pressure steps indicating good shock formation. This plateau was as long as 1.5 milliseconds for initial test gas pressures above 50 torr. The ultimate observation time, due to the arrival of the reflected rarefaction fan was as long as five milliseconds. The intervening plateau was very flat and the pressure rise due to shock attenuation was extremely small, indicating that kinetic measurements over this time span are possible.

VI.   LIMITATIONS AND IMPLICATIONS FOR FUTURE WORK

Shock Tube Modifications

Another method of performing chemical reaction studies which may be more conducive to coal combustion kinetics involves quenching the reaction at specific times during the shock heating with a reinforced rarefaction. As demonstrated in Fig. 23 (a), the rarefaction quickly lowers the pressure as well as the temperature of the shock heated gas. The gas is then sampled and analyzed by use of a gas chromatograph or mass spectrometer for stable species and their concentrations. Glick, Squire and Hertzberg (1955) originally devised a double diaphragm chemical shock tube whose additional diaphragm separated the driver section from a large vacuum chamber. At a predetermined time, after the main diaphragm has ruptured, the second diaphragm is ruptured either by an exploding wire attached to the diaphragm or by puncturing with a sharp mechanically operated plunger. The driver gas then expands into the vacuum chamber and generates a strong expansion wave moving into the test section which has an extremely high cooling rate and quenches any reactions. The second diaphragm may be ruptured at any time so that the reaction may be precisely quenched any point during the reaction. This modification would be relatively simple although somewhat expensive; however, it would add tremendously to chemical kinetic investigation capabilities of the Shock Tube Laboratory.

As mentioned previously, one of the future uses of the shock tube facility will be in the investigation of two phase phenomenon. This requires the addition of a boiling chamber. This chamber, which is to

be attached to the high pressure section of the tube, must have the necessary structural strength to withstand high static pressures under conditions of high wall temperature. The design of such a chamber must include a suitable heating element and observation ports, and must be adapted to the high pressure section of the tube.

Temperature Measurements

In order to predict the complete thermodynamic state of the shock heated gases, two fundamental thermodynamic quantities, pressure, temperature or density, must be known. Thus, in addition to the pressure histories obtainable from the piezo-electric pressure transducer, it is desirable to measure the temperature. Obviously, solid thermometry methods are not functional for the very high and transient temperatures involved so that optical methods are required. These procedures are well developed and include: double-beam line-reversal techniques (Clouston, Gaydon and Hurle, 1959), brightness-emissivity methods (Parkinson and Reeves, 1964; Fairbairn, 1962), and two-line methods (Gaydon and Hurle, 1963). Raman spectroscopy, which has been used recently for temperature determination in flow fields by Lederman, et. al. (1974), could also be adapted for use.

Although it is possible to calculate the temperature from the measured Mach number of the shock front from equation (16) and estimate the correction factor due to real effects, this is not really acceptable. It is much more desirable to have a time resolved temperature determination. Consequently, a sodium double-beam line reversal analysis has been initiated.

Boundary Layer Investigation

In order to obtain a full knowledge of the tube performance, it would be desirable to investigate the growth and characteristics of the boundary layer. This could be accomplished by use of heat transfer gauges similar to the thin film gauges manufactured for this thesis but having a thinner platinum film. The thinner film would allow quicker response time to the heat transfer from the shock heated gases. When mounted flush with the tube wall, the heat transfer gauge would decrease in resistance as they shock front passed, first discontinuously followed by a gentle decrease as the platinum film heated. As the boundary layer passed from the laminar to turbulent regime, the heat transfer gauge resistance would mark the transition with an increase in its rate of change due to the increase in heat transfer (Dumitrescu, Popescu and Brun, 1969). This would allow an accurate determination of the extent of turbulence in the boundary layer.

The shape of the contact surface and the boundary layer can be examined by use of hot wire probes whose position can be varied across the tube diameter (Dumitrescu, Popescu, and Brun, 1969). The voltage on the wire, when submitted to a constant-velocity flow, will vary exponentially. If the exponential time constant is long as compaired to the flow duration, the voltage changes linearly and is only interrupted when the contact surface arrives. The thickness of the boundary layer can be determined because the flow in the boundary layer is nonsteady and therefore the hot wire voltage does not increase linearly. Thus, the boundary-layer thickness and the contact surface shape can be estimated. However, this experimental procedure is complicated by the fragility of the wire.

REFERENCES

American Society of Mechanical Engineer, Bursting pressure seamless tubing, ASME Boiler Code. p. 146.

Clouston, J. G., Gaydon, A. G., and Hurle, I. R., 1959. Temperature measurement of shock waves by spectrumline reversal II, a double-beam method. Proc. Roy Soc. A. 252:143

Daniels, F., and Alberty, R. A., 1975. Physical Chemistry. Fourth edition. New York: John Wiley & Sons.

Dayton, B. B., 1967. High-vacuum pumps. Standard Handbook for Mechanical Engineers. New York: McGraw-Hill. p. 14-62.

Dumitrescu, L. Z., Popescu, C., and Brun, R., 1969. Experimental studies of the shock reflection and interaction in a shock tube. Shock Tubes, Seventh International Shock Tube Symposium. p. 751. Toronto, Canada.

Fairbairn, A. R., 1962. Temperature measurements of C_2 and CN radicals generated in a shock tube I. pyrolysis in absence of oxygen. Proc. Roy. Soc. A. 266:88.

Faizullov, F. S., Sobolev, N. N. and Kudryartsev, E. M., 1960. Spectroscopic investigation of the state of the gas behind a shock wave II. Optics and Spectroscopy. 4:311.

Field, M. A., Gill, D. W., Morgan, B. B., and Howksley, P. G. W., 1967. Combustion of Pulverized Coal. BCURA, Surrey, England: Leatherhead.

Gaydon, A. G. and Hurle, I. R., 1963. The Shock Tube in High-Temperature Chemical Physics. New York: Reinhold.

Glick, H. S., Squire, W. and Hertzberg, A., 1955. A new shock tube technique for the study of high temperature gas phase reactions. Fifth International Symposium on Combustion. p. 393.

Hall, J. G. and Hertzberg, A., 1958. Recent advances in transient surface thermometry. Jet Propulsion. 28, 719.

Halbeche, T. A., and Spencer D. A., 1964. A theoretical and experimental investigation of temperature variation behind attenuated shock waves. Proc. Roy. Soc. A. 279: 111.

Hugoniot, H., 1877. J Ec. Polyt. Paris. 57:1.

Jahn, R. G., and Weimer, D. K., 1958. On the performance of thin-film gauges in high temperature shock tube flows. J. Appl. Phys. 29:4.

Lederman, S., Bloom, M. H., Bornstein, J. and Khosla, P. K., 1974. Temperature and species concentration measurements in a flow field. Int. J. Heat Mass Transfer. 17:1479.

Mark. H., 1958. NACA TM 1418.

Mirels, H., 1971. Boundary layer growth effects in shock tubes. *Shock Tube Research, Proceedings of the Eighth International Shock Tube Symposium*. Imperial College, London.

Mirels, H. and Mullen, J. F., 1964. Small perturbation theory for shock-tube attenuation and nonuniformity. *Phys Fluids*. 7(8):1208.

Nicholls, R. W., and Pritchard, 1969. Spectroscopic and kinetic studies in shock tubes. *Shock Tubes, Seventh International Shock Tube Symposium*. Toronto, Canada, p. 550.

Parkinson, W. H., and Reeves, E. J., 1964. Temperature measurements for powdered solids in reflected shock waves. *Proc. Roy. Soc. A.* 282:265.

Rankine, W. J. M., 1870. *Phil Trans*. 160:288.

Resler, E. L., Lin, S. C., and Kantrowitz, A., 1952. *J. Appl. Phys.* 23:1390.

Rudinger, G., 1961. Effect of boundary-layer growth in a shock tube on shock reflection from a closed end. *Phys. Fluids.* 4(12):1473.

Sage, K., 1975. Comments on "time lag in pressure-measuring system used in short-duration wind tunnel:. *Modern Developments in Shock Tube Research, Tenth International Shock Tube Symposium*. Kyoto, Japan, p. 813.

Soloukin, R. I., 1969. Shock tube diagnostics, instrumentation and fundamental data. *Shock Tubes, Seventh International Shock Tube Symposium*. Toronto, Canada, p. 550.

Vieille, M. P., 1899. On the discontinuities produced by the sudden release of compressed gases. *Comptes Rendus.* 129:1228.

White, D. R., 1958. Influence of diaphragm opening time on shock tube flows. *J. Fluid. Mech.* 4:585.

Wittliff, C. E., Wilson, M. R., and Hertzberg, A., 1959. *J. Aero/space Sci.* 26:4.

Zallen, D. M., 1973. Spectroscopic and Langmuir probe studies of intermediate species in shock induced methane combustion. Unpublished Ph.D. Thesis. Purdue University.

ACKNOWLEDGEMENT

APPENDIXES

APPENDIX A

Dependence of Shock Strength on Diaphragm Pressure Ratio

For an isentropic expansion, it can be shown that the quantity

$$\frac{2a}{\gamma-1} + v \, ,$$

is conserved. Since the rarefaction fan is an isentropic expansion, then it follows that

$$\frac{2}{\gamma_4-1} \cdot a_4 + v_4 = \frac{2}{\gamma_3-1} a_3 + v_3 \, . \tag{A.1}$$

This can be simplified by noting that: the driver gas is initially at rest so that $v_4 = 0$; and for an ideal gas the specific heat ratio is constant so that $\gamma_4 = \gamma_3$. Further, it is noted that since there is no flow through the contact surface then $v_3 = v_2$. Therefore (A.1) can be written as

$$\frac{2}{\gamma_4-1} \cdot a_4 = \frac{2}{\gamma_4-1} \cdot a_3 + v_2 \, . \tag{A.2}$$

For this isentropic process it can also be written from the ideal gas law that

$$\frac{P_4}{P_3} = (\frac{T_4}{T_3})^{\gamma_4/(\gamma_4-1)} \tag{A.3}$$

Using the definition of the characteristic sound speed

$$a = \sqrt{\gamma R T}$$

then (A.3) becomes

$$\frac{P_4}{P_3} = (\frac{a_4}{a_3})^{2\gamma_4/(\gamma_4-1)} \, . \tag{A.4}$$

Further since there is no flow across the contact surface the pressure is continuous or

$$\frac{P_4}{P_3} = \frac{P_4}{P_2} = \frac{a_4}{a_3} \quad 2\gamma_4/(\gamma_4-1) \, . \tag{A.5}$$

Substituting the value of a_3 as a function of a_4 and v_2 from (A.2) into equation (A.5) we have that,

$$\frac{P_4}{P_2} = \left\{ \frac{a_4}{a_4 - \dfrac{\gamma_4-1}{2} \cdot v_2} \right\}^{2\gamma_4/\gamma_4-1} \tag{A.6}$$

From the equation of continuity (1) it is seen that

$$v_2 = U_1 - U_2 = U_1 - (\frac{\rho_1}{\rho_2}) \, U_1 \, . \tag{A.7}$$

then, using the incident shock relation (11)

$$\frac{\rho_2}{\rho_1} = \frac{(\gamma_1+1)M_s^2}{(\gamma_1-1)M_s^2 + 2} \, ,$$

(A.7) can be written as

$$v_2 = \frac{2a}{\gamma_1+1} \quad M_s + \frac{1}{M_s} \, . \tag{A.8}$$

Substituting for v_2 in A.6 then

$$\frac{P_4}{P_2} = \left\{ \frac{a_4}{a_4 - \dfrac{\gamma_4-1}{2} \, [\dfrac{2a_1}{\gamma_1+1} \, (M_s + \dfrac{1}{M_s})]} \right\}^{2\gamma_4/(\gamma_4-1)} \tag{A.9}$$

Finally, combining the incident shock pressure ratio (10)

$$\frac{P_2}{P_1} = \frac{2\gamma_1 M_s^2 - (\gamma_1-1)}{\gamma_1+1}$$

with A.9 the diaphragm ratio is

$$\frac{P_4}{P_1} = \frac{P_4}{P_2}\frac{P_2}{P_1} = \left\{\frac{2\gamma_1 M_s^2 - (\gamma_1 - 1)}{\gamma_1 + 1}\right\}\left\{1 - \frac{\gamma_4 - 1}{\gamma_1 + 1}\left(\frac{a_1}{a_4}\right)(M_s - \frac{1}{M_s})\right\}^{-2\gamma_4/(\gamma_4 - 1)} \quad .$$

APPENDIX B

Ordering Information and Description

A. B. Murray and Co., Inc., Pittsburg, Pennsylvania

--Allegheny Stainless Steel type 304 mechanical hollow bar; extruded,
  cold finished, annealed and pickled; to ASTM A-511; Size 2.500"
  X .250"; Qty 40 ft.

Amersil Inc., Hillside, New Jersey

--Supersil 2 Disc; Ground and Polished; 1/2" Diameter by 1/2" Thick
  T20, Qty 4.

High Pressure Equipment Co., Inc., Erie, Pennsylvania

--Taper Seal Valves, two way straight for 1/4' OD tubing 10-11AF4
  Qty 9
--Taper Seal Valves, two way angle for 1/4" O.D. tubing 10-12AF4 Qty 7
--1/4" Taper Seal to 1/4" NPT male Adapter 10-21AF4NMB Qty 5
--1/4" OD taper seal tube to 1/4" NPT pipe Coupling 10-21AF4NFB Qty 7
--Taper Seal Sleeves for 1/4" OD tubing 10-2A4 Qty 10
--Taper Seal Tee type gauge connector, 1/4" Taper Seal to 1/4" NPT
  10-33AF4NFB Qty 1

Matheson, St. Louis, Missouri

--High Pressure Regulators; Spring loaded; maximum inlet pressure
  4000psi; maximum flow of air 7700 cfh; outlet valve 105 with 1/4"
  NPT outlet; 100-2500 psig delivery pressure; Model 4; Qty 2.

Martech Associates (Huntington Laboratories Representatives), Boulder,
Colorado

--Right Angle Stainless Steel Valve EV-150
  1 1/2" port size with 2-3/4" OD Flange Qty 2
--Nipple 2 3/4" OD Flange, 1 1/2" OD Tubing VF-153
--Tee 2 3/4" OD Flange, 1 1/2" OD Tubing VF-151
--Vac-u-Flat Flange 2 3/4" OD 3/4" ID 275-075
--Gasket kit G-275
--Bolt kit B-275

Mead & Sons, Inc., North Kansas City, Missouri

--ASCO 2-way Solenoid valve; stainless steel body; pipe size 1/4"
  NPT; normally closed, maximum operating pressure 2200 psi; Voltage
  120V A-C/60HZ; 8262A214; Qty 1

Metal Goods, St. Louis, Missouri

--Aluminum Channeling; 6061-T6 extruded channel QQ-A-20018; American
  Standard Aluminum; Size 6" X 0.314" web X 2.034" flange; Qty 35 ft
  (25 ft + 10 ft).

Swan Engineering and Supply, Kansas City, Missouri

--Parker Nitrile (Buna-N) O-rings
  Sizes: 3 3/8 X 3 5/8" 1/8" thick Parker No. 2-237 Qty 12
          1" X 1 1/2"   1/8" thick Parker No. 2-214 Qty 9
          2 3/4" X 3   1/8" thick Parker No. 2-232 Qty 4

Pivan Engineering Sales Co. (Sundstand Data Control Representative)
Shawnee Mission, Kansas

--Miniature Pressure transducer: Pressure range to 3000 psi, 0.366
  picocoulomb per psi sensitivity; rise time of one microsecond;
  Model 603A, Qty 1
--Teflon low-noise Cables, Miniature coaxial cable. 30pF/ft cable
  capacitance, 2 ft with 10-32 plugs, Model 121M2, qty 4
--Cable Adapter, 10-32 Jack to BNC plug, Model 101, Qty 4
--Connector Adapter to 10-32 thd, model 105H, Qty 7

Southwestern Engineering & Equipment. Co. (Edwards High Vacuum) Dallas,
Texas

--"Speedivac" Capsule dial gauge barometrically independent, Range 0-100
  torr, 3 in diameter scale, Code no H180-44, Qty 1

Unistrut Midwest, Inc., North Kansas City, Missouri

--Post Bases; Stock number P2072A; Qty. 12
--Flat Plate Fitting; stock number P1726; Qty 12.
--Channeling; Stock number P1100; Qty. 50 ft.
--Hexagon nuts, 1/2" nuts; Qty 500
--Hex head cap screws; 1/2" X 1 1/2" size; Qty 75
--Unistrut nuts with springs; stock number P1010; Qty 50

Watkins, Inc., Wichita, Kansas

--Hex head Bolts and nuts; heat treated; black finish;
  size 3/4" X 2 1/2", Qty 60; Size 3/4" X 3", Qty 5

Vacao, Vacuum Accessories Corp. of American, Bohemia, L. I., N. Y.

--Angle Type Forged Bellows Sealed Brass High Vacuum Valve Viton-A-
  flat-Disc Seat Seal and "O" ring Bonnet Seal 5/8" Port Diameter
  for 3/4" tube OD sweat fitting ATS-62

APPENDIX C

Construction Schematics

DIAPHRAGM HOLDER DEVICE
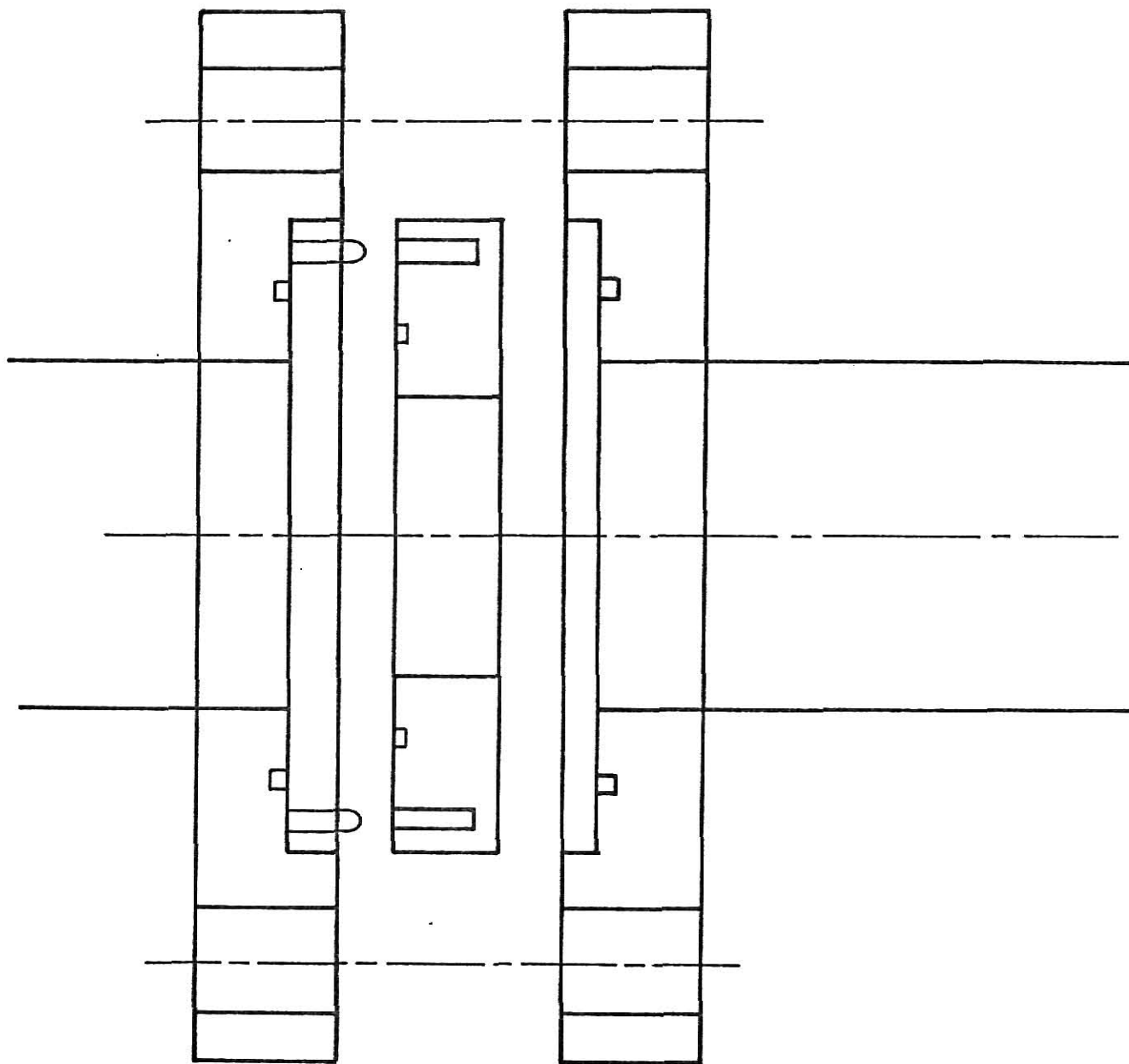
MATERIAL: 7 1/2" O.D. X 2 1/2" I.D. STAINLESS STEEL
SLIP ON FLANGES 15016 (2)

QUANTITY: 1 SET

DIAPHRAGM HOLDER DRIVER FLANGE

O-RING
3 3/8 I.D X 3 5/8 O.D.
1/8" thick

1/8" dia
DOWEL

1/4

3/8

4 1/2

2

5/32

2 1/2

1/8

3 3/8

7 1/2
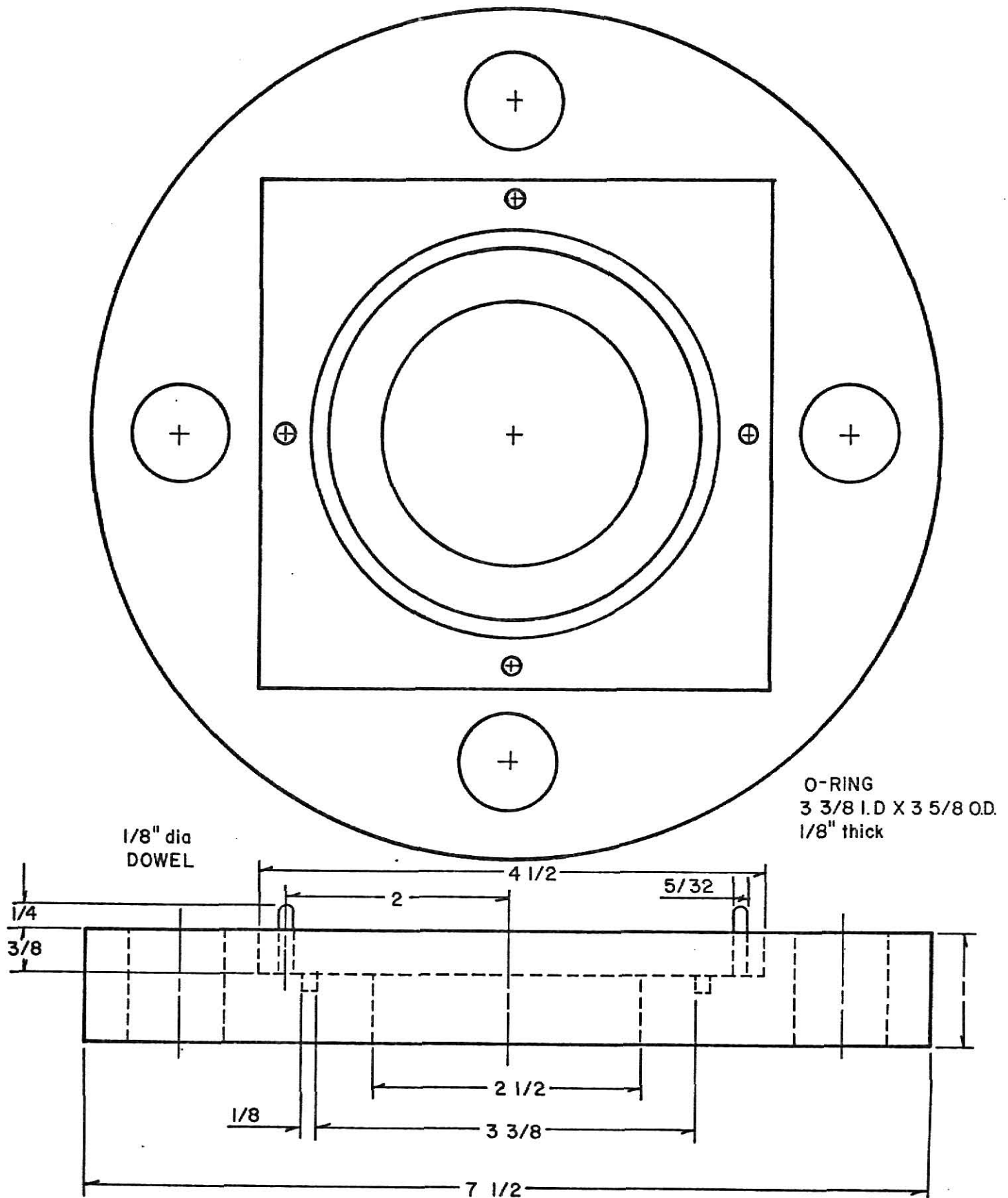
DIAPHRAGM HOLDER CENTER FLANGE
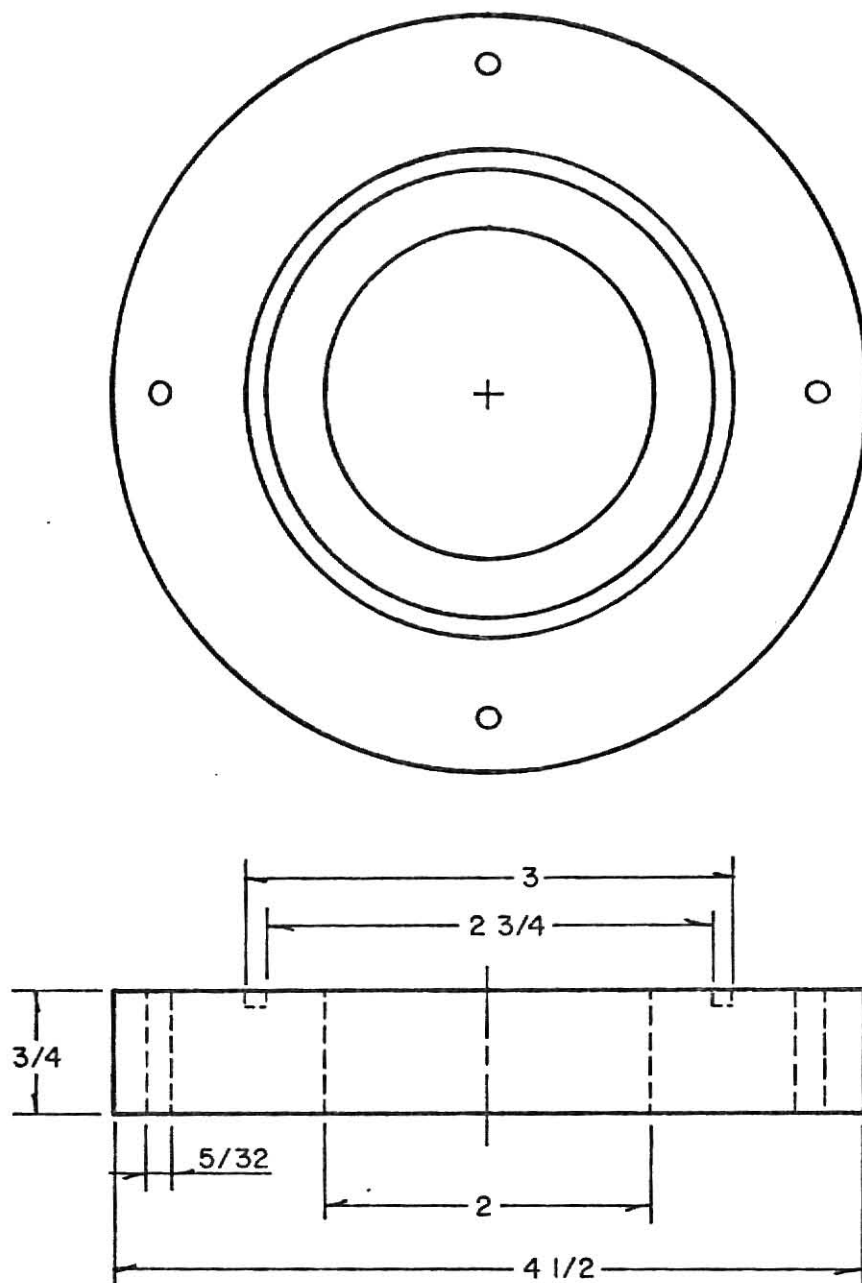
O-RING 2 3/4 I.D. X 3 O.D., 1/8" thick

DIAPHRAGM HOLDER TEST SECTION FLANGE

O-RING
3 5/8 O.D. X 3 3/8 I.D.

4 1/2

1/4

2 1/2

3 3/8

3 5/8

7 1/2
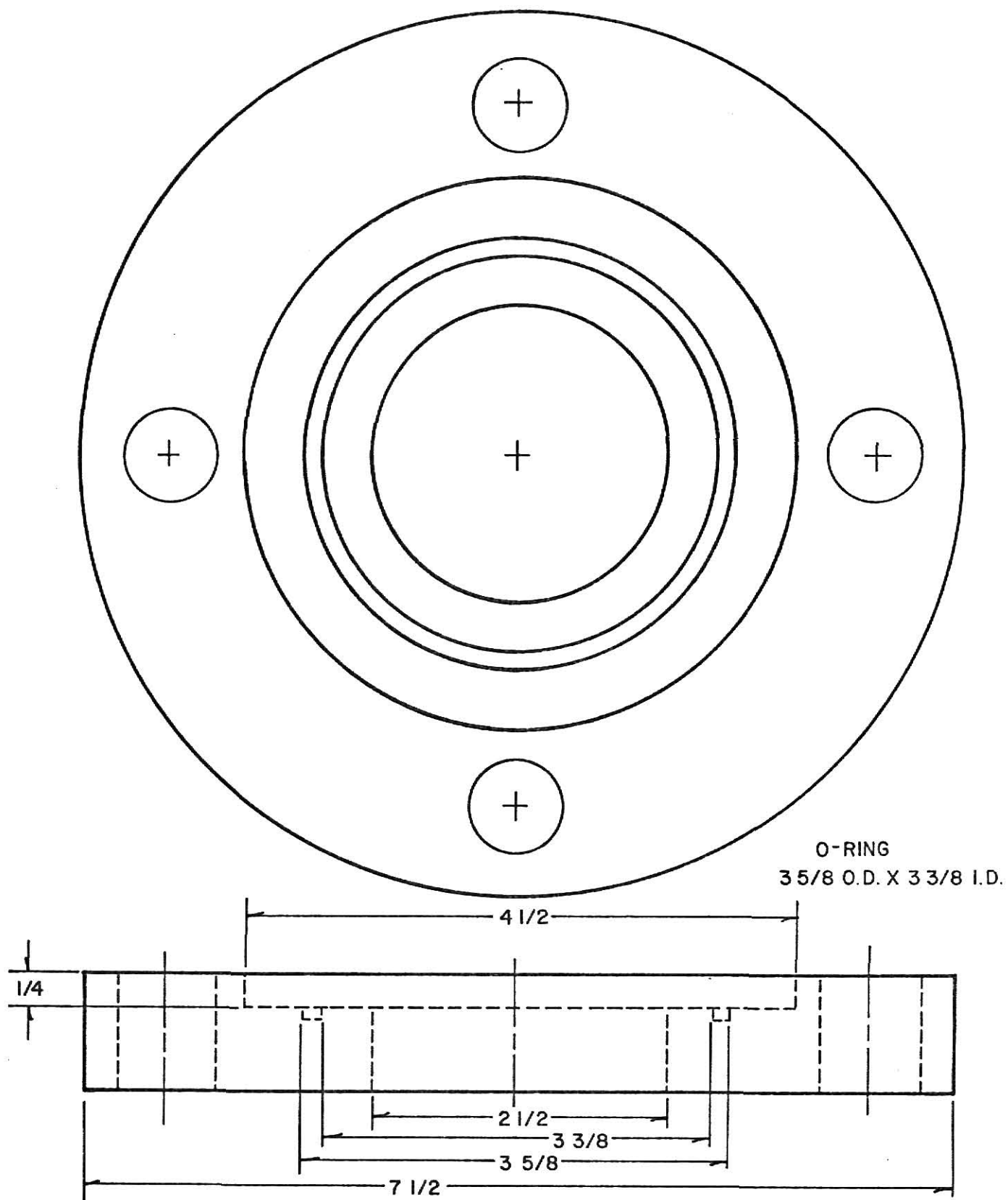
OBSERVATION WINDOW MOUNTING TUBE LOCATION

2"
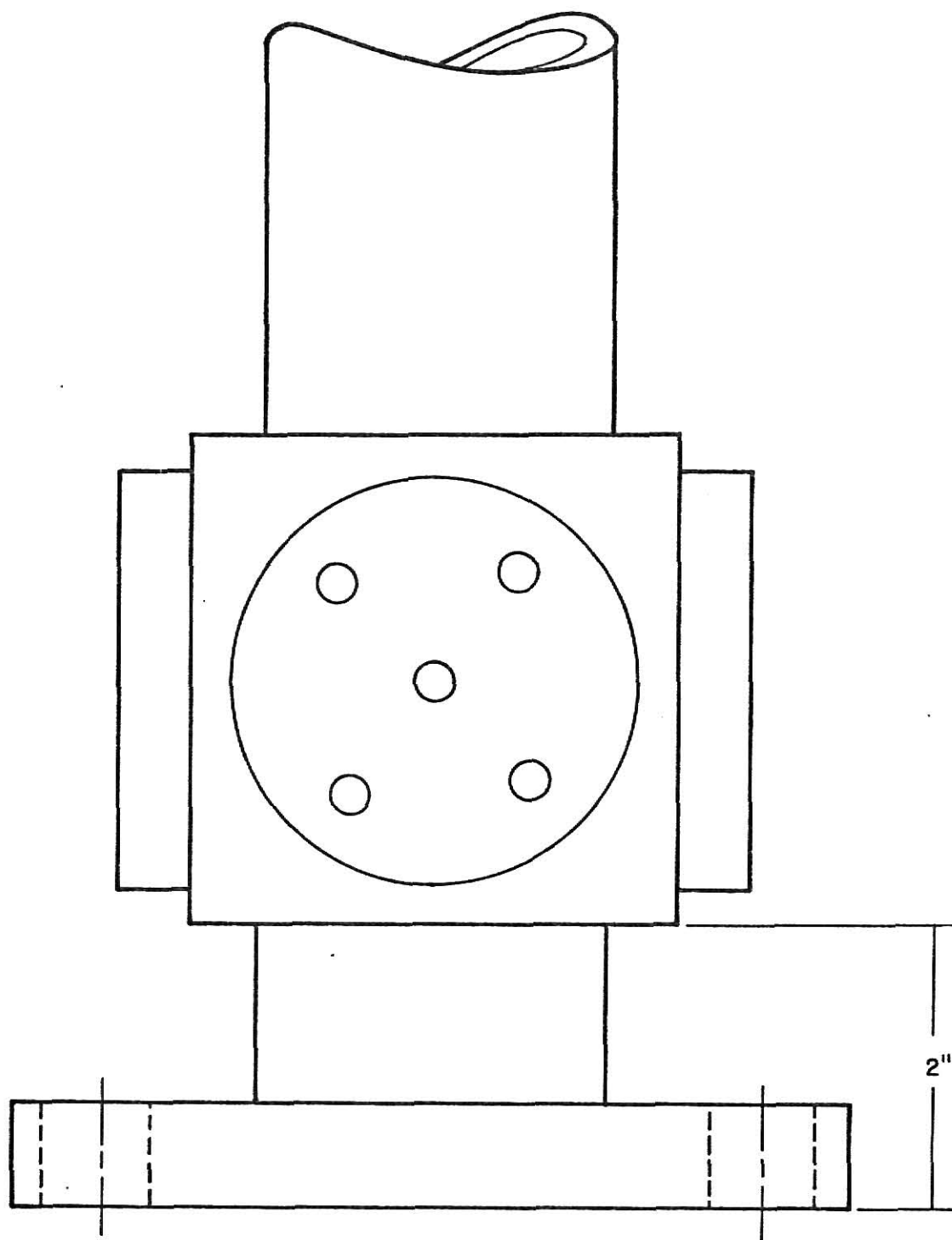
OBSERVATION WINDOW MOUNTING
FLANGE PORTION

EXTREME TOLERANCES
REQUIRED (±.001)

FOR 3/8" BOLT & THREAD
AT LEAST 1/2" DEEP

1.0429   7.50

1.0429

1.0"

3.50

MATERIAL:
    STAINLESS STEEL

QUANTITY: ONE

2.50

3.50
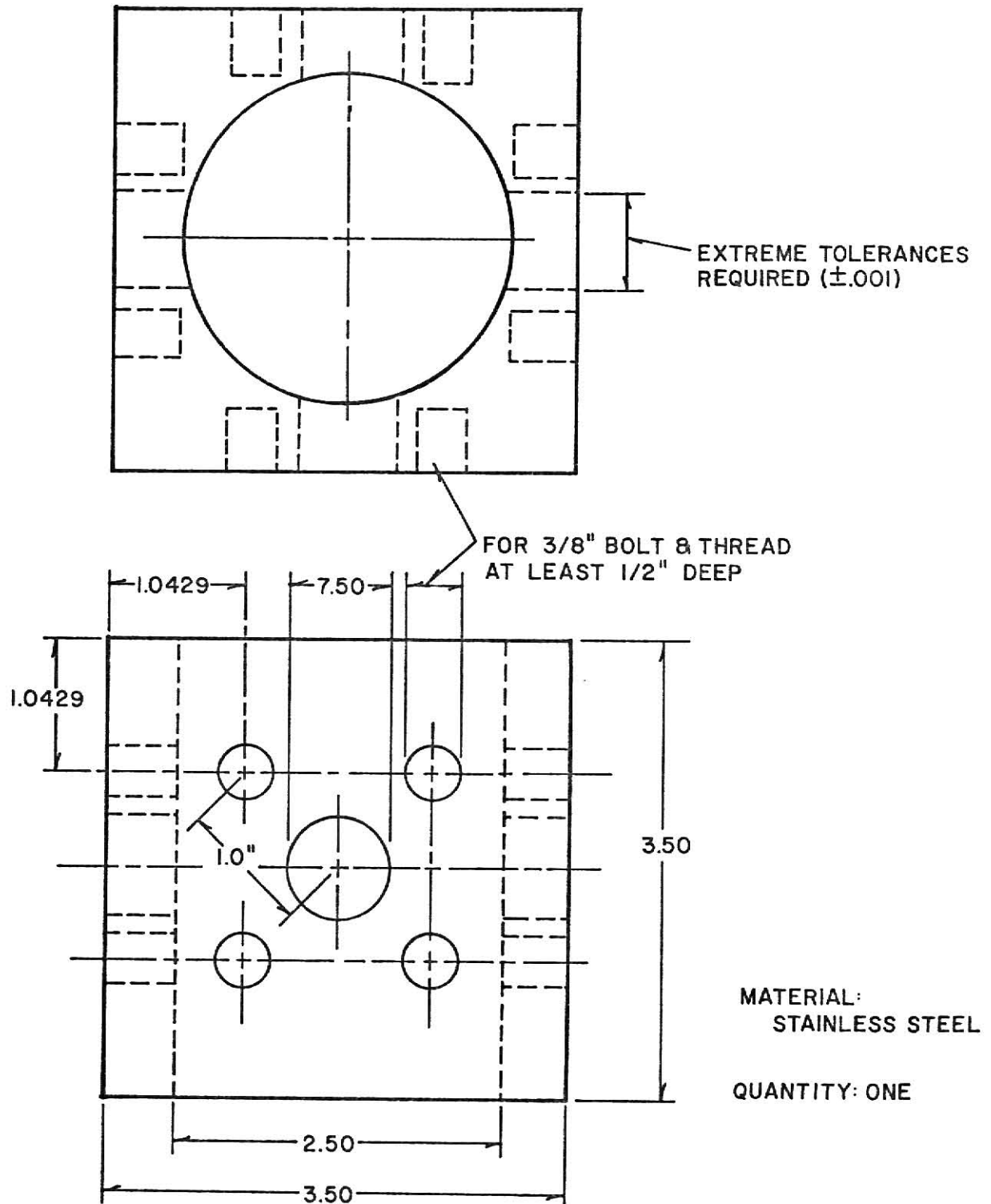
OBSERVATION WINDOW MOUNTING

PLUG ASSEMBLY

O-2 ING
I"X I 1/4"
I/8" THICK

BOLT HOLES ARE FOR
0.0% 3/8"XII BOLTS
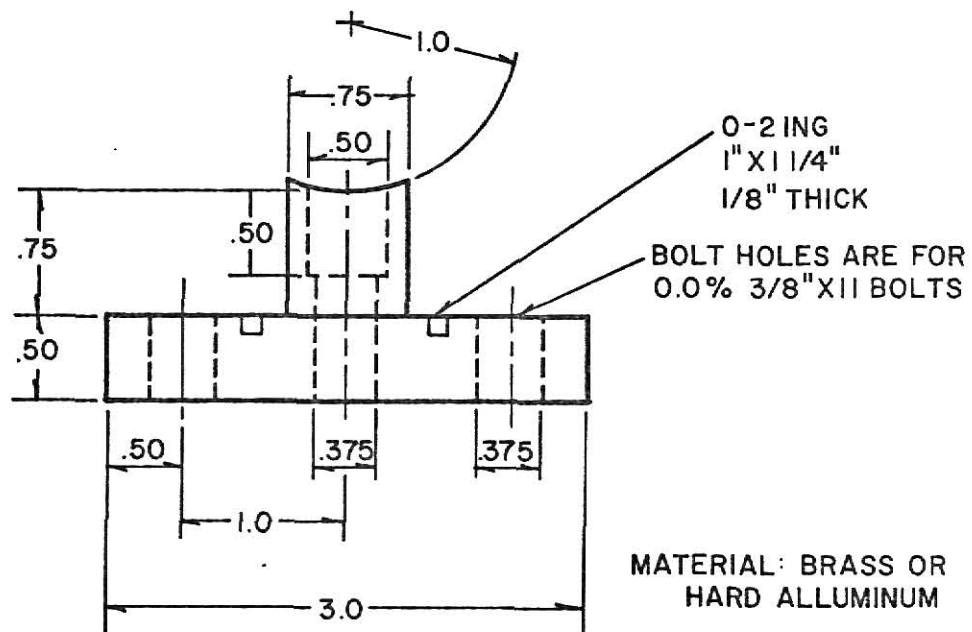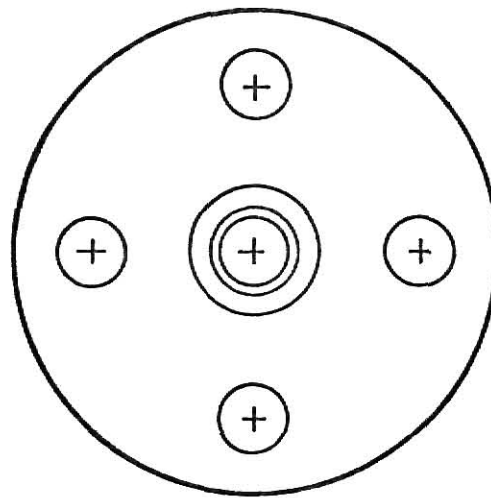
MATERIAL: BRASS OR
HARD ALLUMINUM

QUANTITY: FOUR

BOLTS REQUIRED (good quality)
3/8"XIIXI"
TOTAL QUANTITY FOR ALL
SETS: TWENTY

THIN FILM GAUGES MOUNTING FLANGE

O-RING GROOVE

DRILLED & TAPPED
FOR 1/4" BOLTS

1/2

3/16

1 1/4

3/4

O-RING GROOVE
1" I.D.
1 1/4" O.D.
1/8" thick

1 3/8

15/16

2 3/8
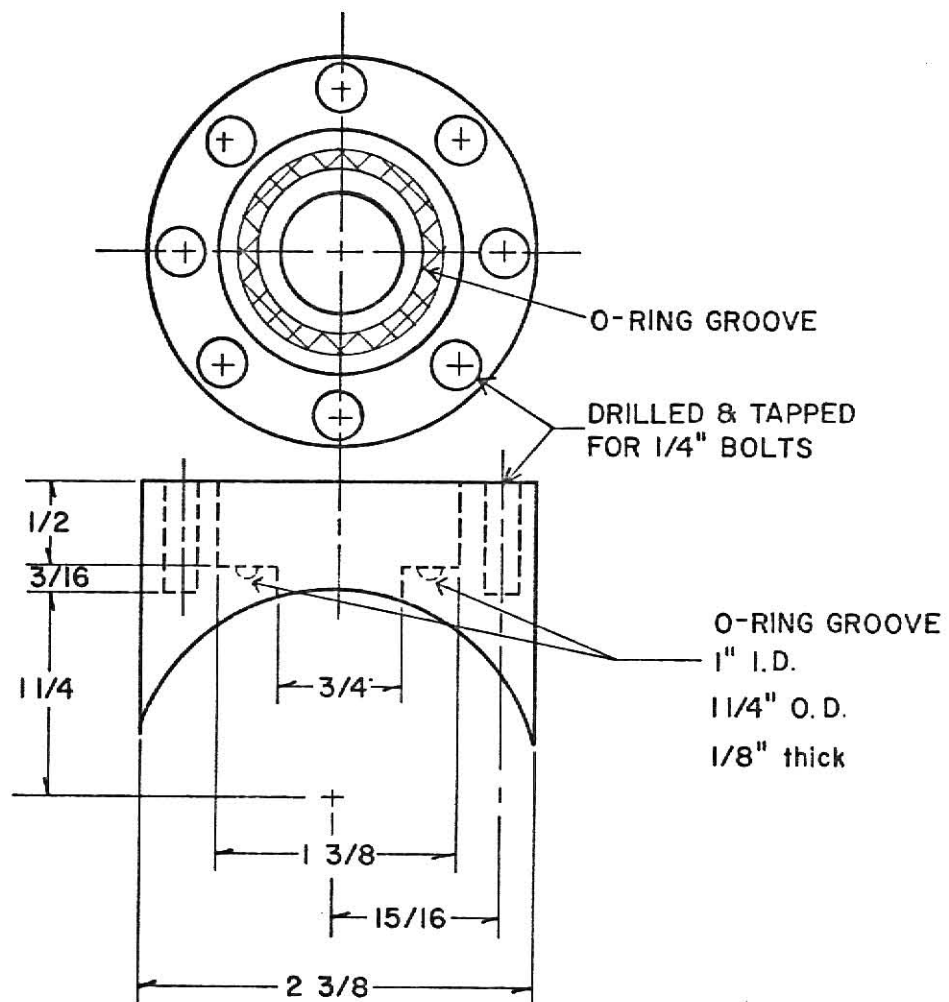
MATERIAL: STAINLESS STEEL

QUANTITY: 4

THIN FILM GAUGE MOUNTING CAP

15/16 ⟶ 1/4 dia

3/8

2 3/8
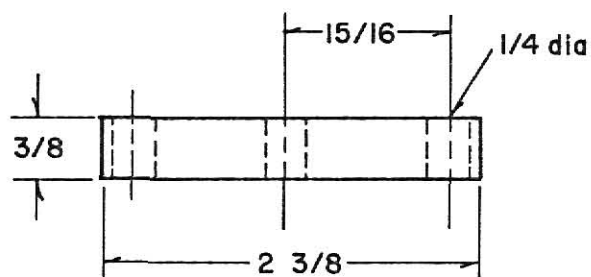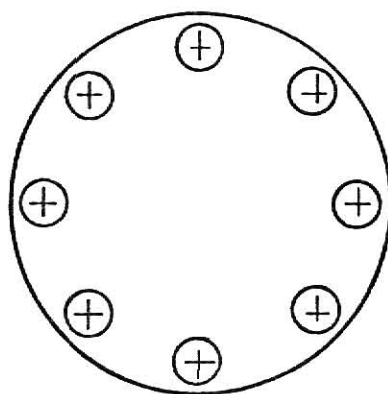
MATERIAL: BRASS (HARD ALLUMINUM)
QUANTITY: 4

THIN FILM GAUGE MOUNTING PLEXIGLASS HOLDER

3/4

1

10 mm

7/16

9/16

1/2

3/8

5/8

1 3/8
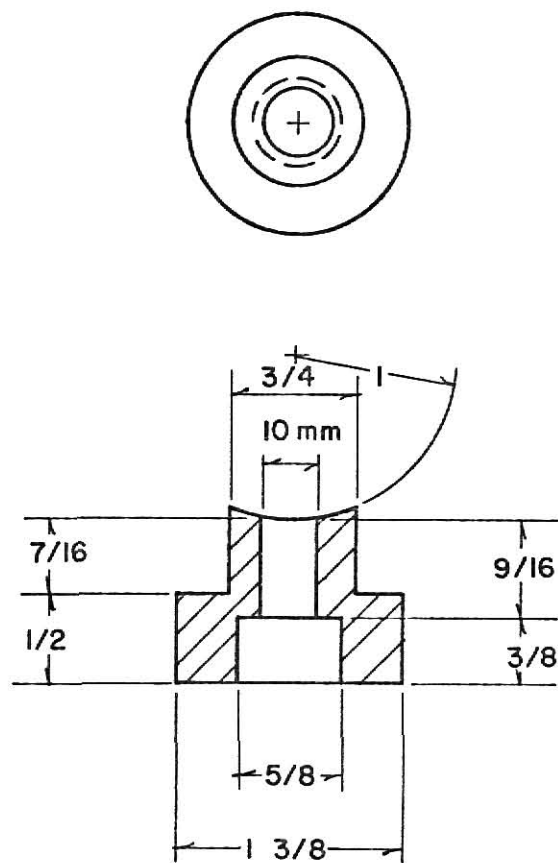
MATERIAL: PLEXIGLASS
QUANTITY: 3
GLASS ROD 10mm X 0.75"

PRESSURE TRANSDUCER MOUNTING

PLUG ASSEMBLY

M7 X 0.75 thd., 0.30 depth
TAP NO. 404-9274-001
(ON ORDER)

1.00

O-RING
1" X 1 1/4", 1/8" thick

0.25
REAM

0.0625

0.375

0.125

0.75

0.70

0.280 min

0.50

.425

0.50 dia
C'BORE

3.00

0.50   1.00
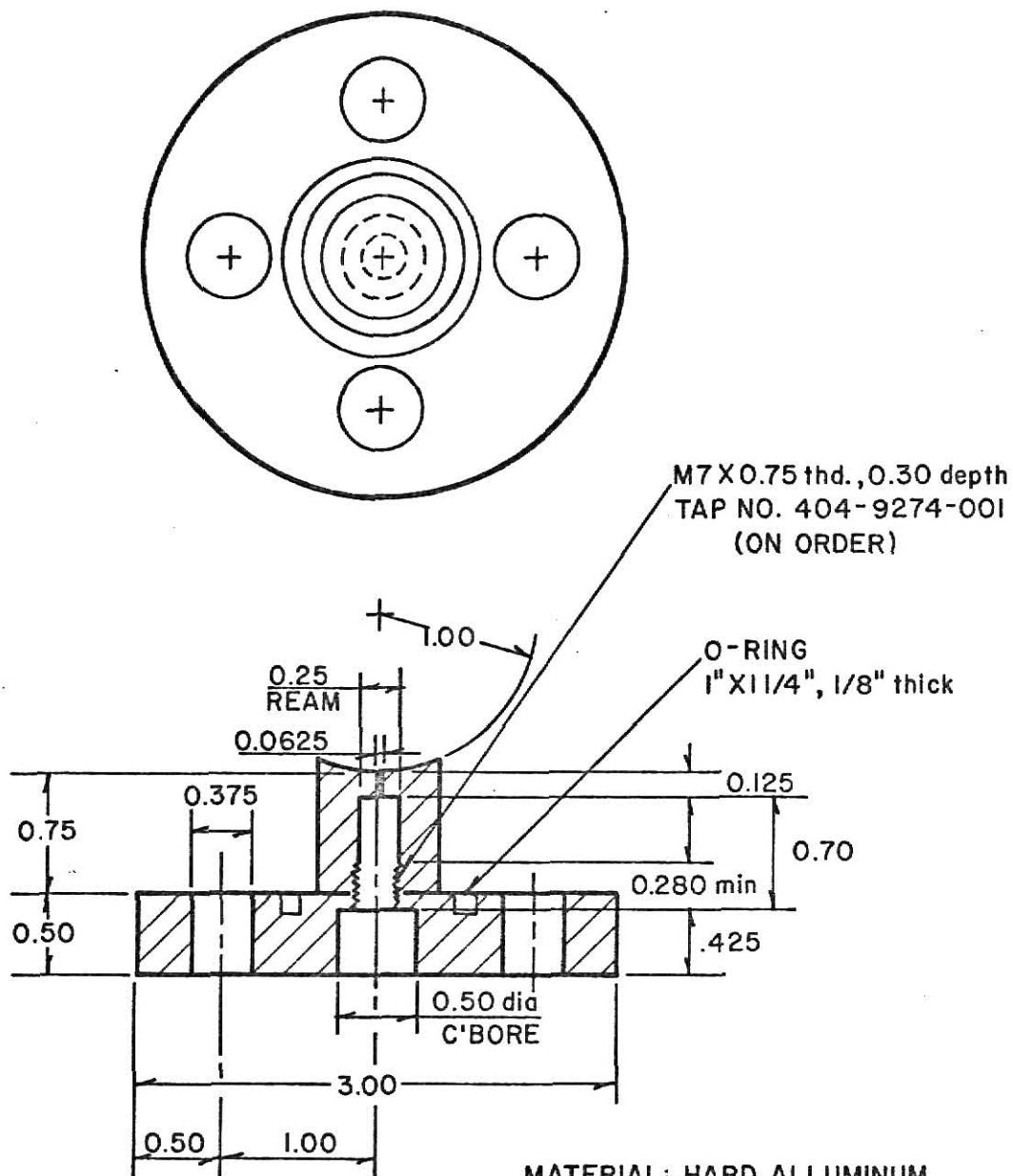
MATERIAL: HARD ALLUMINUM
QUANTITY: ONE
BOLTS: 3/8" X 1", 4 REQUIRED

APPENDIX D

Firing Sequence Check List

FIRING SEQUENCE

Date _____ RUN _____ OPERATOR _____

1. Close valve number 1 _____.

2. Close valve numbers 5 and 6 _____.

3. Using valve number 8, 9, and 10, fill test section to desired pressure and chosen composition for test gas _____.

4. Close valve number 8 _____.

5. Close valve number 4 _____.

6. Double check all inlet valves to test section _____.

7. Using valve number 12 or 13 choose high pressure gas for initial fill of driver section _____.

8. Initial fill driver with gas by opening solenoid valve 15 to pressure below diaphragm bursting pressure and close solenoid valve switch 1 _____.

9. Open gas outlet valve chosen 12 or 13, one-half turn and fire by opening solenoid valve 15 using switch 2 _____.

COMMENTS:

APPENDIX E

Construction Procedures for Thin Film Gauges

(1)   Cut Pyrex rod to desired length (15/16" X 10mm dia)

(2)   Flatten one end by grinding on cutting stone and fire polish to remove sharp edges. Clean with acetone.

(3)   On the flattened end paint the platinum 05-X less than 1mm in width across the diameter and extend slightly over edges.

(4)   Place painted TFG in oven preheated to 600 °C and leave door open until the vehicle, holding the metallic particles in suspension, is driven off and a smooth silvery film is formed. ($\simeq$1min)

(5)   Close door and allow bonding between pyrex and film ($\simeq$2min)

(6)   Take TFG out of oven and allow to cool slowly.

(7)   Repeat (3)-(6) if smooth film is not formed.

(8)   Next paint Platinum along length of rod from point where bonded Platinum stops, full length, to opposite rod face (not on opposite face) in a $\sim$3mm strip width.

(9)   Repeat steps (4), (5) and (6).

(10)   Repeat (8) and (9).

(11)   Check resistance of TFG. If lower than 50ohms polish the front face with a slightly abrasive liquid.

(12)   Apply a spot of silver-loaded solder to the two ends of the Pt strip to enable current-carrying leads to be attached to the element.

(13)   Epoxy into plexiglass holders.

APPENDIX F

Computer Programs

Program: Calculating Shock Gas Parameters for Real and Ideal Effects

Computer: IBM 370

Language: WATFOR

Input: First Card: 80 space title

Second Card:

γ_4	P_1, psi
γ_1	P_4/P_1
T_1, °R	IRUN
T_4, °R	ΔX, ft
R_4, ft^2/s^2 °R	ΔT, sec
R_1, ft^2/s^2 °R	IDEAL

Note: Set IDEAL equal to zero to calculate real effects only
Set IRUN equal to zero for last data set

OUTPUT: See example

```
$JOB
C        CALCULATING SHOCK GAS PARAMETERS FOR REAL AND IDEAL EFFECTS
   1        REAL K4,K1,MS1,MSC,MSA
   2        INTEGER TITLE(20)
   3  10    READ2C,TITLE
   4  20    FORMAT(20A4)
   5        PRINT30,TITLE
   6  30    FORMAT('1',40X,20A4)
   7        READ,K4,K1,T1,T4,R4,R1,P1,P4QP1,IRUN,DX,DT,IDEAL
      C     SET IDEAL EQUAL TC ZERO TO CALCULATE REAL EFFECTS ONLY
      C     SET IRUN EQUAL TO ZERO FCR LAST DATA SET
   8        PRINT 35
   9  35    FORMAT('-',20X,'K(DRIVER)',12X,'K(DRIVEN)',12X,'P4/P1')
  10        PRINT4C,K4,K1,P4QP1
  11  40    FORMAT(1HX,E15.6,7X,E15.6,5X,E15.6)
      C     CALCULATING SOUND SPEEDS
  12        G=32.174049
  13        C1=SQRT(R1*G*K1*T1)
  14        C4=SQRT(R4*G*K4*T4)
  15        ISHOCK=0
  16        IF(IDEAL.EQ.0) GO TO 2dO
      C     FINDING IDEAL MACH NUMBER OF SHOCK FRCM PRESSURE RATIO P4/P1
  17        MSC=3.0
  18        KCUNT=C
  19  50    MSI=MSC
  20        B=MSI-1./MSI)
  21        A=((2.*K1*MS1)-(K1-1.))/(K1+1.)
  22        D=1.-((K4-1.)*C1*B)/((K1+1.)*C4)
  23        E=-2.*K4/(K4-1.)
  24        PRAT=A*(D**E)
  25        RAT=(FRAT-P4QP1)/P4QP1
  26        MSC=MS1
  27        IF(IABS(RAT).LE..0001) GO TO 100
  28        IF(KCLAT.GT.50) GO TO 70
  29        KCUNT=KCUNT+1
  30        IF(RAT.GT.0.) MSC=MSC-(RAT/5.)
  31        IF(RAT.LT.0.) MSC=MSC-RAT
  32        GO TO 50
  33  70    PRINTEC
  34  80    FORMAT(' ','COULD NOT CONVERGE MACH NUMBER/PRESSURE RATIO LOOP')
  35        IF(IIPLN.EG.0) GO TC 300
  36        GO TO 1C
      C     CALCULATING TRUE MACH NUMBER FROM TIME INTERVAL
  37  90    VA=CX/CT
  38        MSA=VA/C1
  39        MSI=MSA
  40        GO TC 110
  41  100   MSI=MSC
      C     CALCULATING GAS PARAMETERS
  42  110   A=((2.*K1*MSI*MSI)-(K1-1.))/(K1+1.)
  43        F=((K1-1.)*MSI*MSI)+2.
  44        G=(K1+1.)*MSI*MSI
  45        H=(((3.*K1)-1.)*MSI*MSI)-(2.*(K1-1.))
  46        G=(2.*(K1-1.)*MSI*MSI)+(3.-K1)
  47        P2QP1=A
  48        RDXAT=G/F
  49        T2QT1=A*F/G
  50        PSQP1=A*H/F
  51        T5QT1=Q*H/(G*(K1+1.))
  52        WRQWS=(2.*(2./(K1-1.))*(1./A))/((K1+1.)/(K1-1.)+(1./A))
```

```
53        P2=P2GP1*P1
54        T2=T2GT1*T1
55        P5=P5GP1*P1
56        T5=T5GT1*T1
57        P4=P4GP1*P1
58        RO1=P1*144./(R1*T1)
59        RC2=RGRAT*RO1
60        WS=MSI*C1
61        WR=WRCGWS*WS
62        V2=2.*C1*(MSI-(1./MSI))/(K1+1.)
63        IF(ISHGCK.NE.0) GO TO 150
64        PRINT120
65  120   FORMAT('C',10X,'**********  PROPERTIES BASED ON IDEAL SHOCK MACH N
     1UMBER **********')
66        PRINT130
67  130   FORMAT('0',20X,'IDEAL SHOCK MACH NUMBER')
68        PRINT140,MSI
69  140   FORMAT(' ',18X,E15.6)
70        GO TO 180
71  150   PRINT160
72  160   FORMAT('0',10X,'**********  PROPERTIES BASED ON ACTUAL SHOCK MACH
     1NUMBER **********')
73        PRINT170
74  170   FORMAT('0',20X,'ACTUAL SHOCK MACH NUMBER')
75        PRINT140,MSI
76  180   PRINT190
77  190   FORMAT(' ',20X,'P2/P1',12X,'P5/P1',12X,'T2/T1',12X,'T5/T1',
     112X,'RHC2/RHO1',12X,'WR/WS')
78        PRINT200,P2GP1,P5GP1,T2GT1,T5GT1,RORA1,WRGWS
79  200   FORMAT(1HX,E15.6,31X,E15.6),2(4X,E15.6))
80        PRINT210
81  210   FORMAT('0',20X,'P1(PSI)',12X,'P2(PSI)',12X,'P4(PSI)',12X,'P5(PSI)'
     1)
82        PRINT220,P1,P2,P4,P5
83  220   FORMAT(18X,E15.6,3(4X,E15.6))
84        PRINT230
85  230   FORMAT('0',20X,'T1(R)',14X,'T2(R)',14X,'T4(R)',14X,'T5(R)')
86        PRINT220,T1,T2,T4,T5
87        PRINT240
88  240   FORMAT('C',20X,'RHO1(LBM/CU-FT)',10X,'RHC2(LBM/CU-FT)')
89        PRINT250,RO1,RO2
90  250   FORMAT(18X,E15.6,12X,E15.6)
91        PRINT260
92  260   FORMAT('C',20X,'WS(FT/SEC)',10X,'WR(FT/SEC)',10X,'V2(FT/SEC)')
93        PRINT270,WS,WR,V2
94  270   FORMAT(17X,E15.6,2(6X,E15.6))
95  280   ISHCCK=ISHOCK+1
96        IF(ISHGCK.GE.2) GO TO 290
97        GO TO 90
98  290   CONTINUE
99        IF(IRUN.GG.0) GO TO 300
100       GO TO 10
101 300   STOP
102       END
$ENTRY
```

TEST RUN .65HE/.35N2 (DRIVER)   ARGON (DRIVEN) P4/P1=364.19

K(DRIVER)   K(DRIVEN)   P4/P1
0.154000E 01   0.166000E 01   0.364190E 03

*********** PROPERTIES BASED ON IDEAL SHOCK MACH NUMBER ***********

IDEAL SHOCK MACH NUMBER
0.377443E 01

P2/P1	P5/P1	T2/T1	P4(PSI)	T5/T1	RHO2/RHO1
0.175330E 02	0.851549E 02	0.527564E 01	0.500033E 03	0.110678E 02	0.332339E 01

P1(PSI)	P2(PSI)	P4(PSI)	P5(PSI)		WR/WS
0.137100E 01	0.240728E 02	0.500033E 03	0.116918E 03		0.536601E 00

T1(R)	T2(R)	T4(R)	T5(R)
0.530000E 03	0.279609E 04	0.530000E 03	0.586592E 04

RHO1(LBM/CU-FT)   RHO2(LBM/CU-FT)
0.963262E-02   0.320130E-01

WS(FT/SEC)   WR(FT/SEC)   V2(FT/SEC)
0.395187E 04   0.210082E 04   0.276216E 04

*********** PROPERTIES BASED ON ACTUAL SHOCK MACH NUMBER ***********

ACTUAL SHOCK MACH NUMBER
0.341119E 01

P2/P1	P5/P1	T2/T1	T5/T1	RHO2/RHO1
0.142753E 02	0.663516E 02	0.466440E 01	0.912586E 01	0.319759E 01

P1(PSI)	P2(PSI)	P4(PSI)	P5(PSI)	WR/WS
0.137300E 01	0.196000E 02	0.500033E 03	0.911007E 02	0.539533E 00

T1(R)	T2(R)	T4(R)	T5(R)
0.530000E 03	0.236613E 04	0.530000E 03	0.483670E 04

RHO1(LBM/CU-FT)   RHO2(LBM/CU-FT)
0.963262E-02   0.308012E-01

WS(FT/SEC)   WR(FT/SEC)   V2(FT/SEC)
0.357156E 04   0.192697E 04   0.245460E 04

CORE USAGE   OBJECT CODE= 5064 BYTES,ARRAY AREA=   80 BYTES,TOTAL AREA AVAILABLE= 50000 BYTES

DIAGNOSTICS   NUMBER OF ERRORS=   0, NUMBER OF WARNINGS=   0, NUMBER OF EXTENSIONS=   0

COMPILE TIME= 0.39 SEC,EXECUTION TIME=   0.06 SEC, WATFIV - JUL 1973 V1L4   15.53.43   MONDAY   24 NOV 75

Program: Shock Parameters

Computer: Tektronix desk top programmable calculator, Model 31

Input: ΔX, inches a_1, m/sec
        Δt, µsec P_1, psi
        γ_1 P_4, psi
        T_1, °K

Notes on use: Stored on magnetic tape cartridge
                Sequence to store program:
                        1)   Put Cartridge in calculator
                        2)   ADDRS
                        3)   GO TO
                        4)   0, 0, 0, 0
                        5)   FROM TAPE
                        6)   2
                Store input in memory
                 ΔX=R00 a_1=R04
                 Δt=R01 P_1=R05
                 γ_1=R02 P_4=R22
                 T_1=R03

Run Program: 1)   RESET
               2)   START

Output: Example

MACH NUMBER
  3.613408920E+00

P2/P1
  1.508288882E+01

P5/P1
  8.527411585E+01

T2/T1
  3.495778374E+00

T5/T1
  6.620408043E+00

P1(PSI)
  .5802631579

P2(PSI)
  8.752044230E+00

P4(PSI)
       225.

P5(PSI)
  4.94812775E+01

T1(K)
       298.

T2(K)
  1.041741956E+03

T5(K)
  1.972881598E+03

0000	R_ _	0051	*	0101	*
0001	0_ _	0052	R_ _	0102	R_ _
0002	1	0053	0_ _	0103	0_ _
0003	*	0054	7	0104	7
0004	R_ _	0055	–	0105	=
0005	0_ _	0056	R_ _	0106	+
0006	4	0057	0_ _	0107	1
0007	=	0058	2	0108	=
0008	1/X	0059	+	0109	R_ _
0009	*	0060	1	0110	1_ _
0010	R_ _	0061	)	0111	0
0011	–_ _	0062	=	0112	CLDP
0012	–	0063	R_ _	0113	R_ _
0013	*	0064	0_ _	0114	0_ _
0014	2	0065	8	0115	2
0015	.	0066	CLDP	0116	*
0016	5	0067	R_ _	0117	/
0017	4	0068	0_ _	0118	5
0018	*10	0069	2	0119	+
0019	4	0070	*	0120	.
0020	=	0071	R_ _	0121	5
0021	R_ _	0072	0_ _	0122	=
0022	0_ _	0073	7	0123	X12
0023	6	0074	–	0124	=
0024	CLDP	0075	(	0125	*
0025	R_ _	0076	R_ _	0126	R_ _
0026	–_ _	0077	0_ _	0127	0_ _
0027	6	0078	2	0128	7
0028	*	0079	*	0129	=
0029	R_ _	0080	.	0130	1/X
0030	0_ _	0081	5	0131	=
0031	6	0082	)	0132	R_ _
0032	=	0083	+	0133	1_ _
0033	R_ _	0084	.	0134	1
0034	0_ _	0085	5	0135	CLDP
0035	7	0086	=	0136	R_ _
0036	CLDP	0087	R_ _	0137	0_ _
0037	R_ _	0088	0_ _	0138	9
0038	0_ _	0089	9	0139	*
0039	2	0090	CLDP	0140	R_ _
0040	+	0091	R_ _	0141	1_ _
0041	1	0092	0_ _	0142	0
0042	=	0093	2	0143	*
0043	1/X	0094	*	0144	R_ _
0044	*	0095	.	0145	1_ _
0045	(	0096	5	0146	1
0046	2	0097	–	0147	=
0047	*	0098	.	0148	R_ _
0048	R_ _	0099	5	0149	1_ _
0049	0_ _	0100	=	0150	2
0050	2				

0151	CLDP	0201	R__	0251	0
0152	3	0202	0	0252	2
0153	*	0203	8	0253	(
0154	R__	0204	=	0254	+
0155	0	0205	R__	0255	2
0156	2	0206	1	0256	=
0157	=	0207	4	0257	R__
0158	–	0208	CLDP	0258	1
0159	1	0209	R__	0259	6
0160	=	0210	0	0260	CLDP
0161	*	0211	2	0261	R__
0162	R__	0212	–	0262	0
0163	0	0213	1	0263	2
0164	7	0214	=	0264	+
0165	–	0215	*	0265	1
0166	(	0216	2	0266	=
0167	2	0217	*	0267	X 2
0168	*	0218	R__	0268	*
0169	R__	0219	0	0269	R__
0170	0	0220	7	0270	0
0171	2	0221	=	0271	7
0172	)	0222	+	0272	=
0173	+	0223	3	0273	1/X
0174	2	0224	–	0274	*
0175	=	0225	R__	0275	R__
0176	R__	0226	0	0276	1
0177	1	0227	2	0277	5
0178	3	0228	=	0278	*
0179	CLDP	0229	R__	0279	R__
0180	R__	0230	1	0280	1
0181	0	0231	5	0281	6
0182	2	0232	CLDP	0282	=
0183	–	0233	3	0283	R__
0184	1	0234	*	0284	1
0185	=	0235	R__	0285	7
0186	*	0236	0	0286	CLDP
0187	R__	0237	2	0287	R__
0188	0	0238	–	0288	–
0189	7	0239	1	0289	8
0190	=	0240	=	0290	*
0191	+	0241	*	0291	R__
0192	2	0242	R__	0292	0
0193	=	0243	0	0293	8
0194	1/X	0244	7	0294	*
0195	=	0245	=	0295	R__
0196	*	0246	–	0296	1
0197	R__	0247	(	0297	7
0198	1	0248	2	0298	CLDP
0199	3	0249	*	0299	R__
0200	*	0250	R__	0300	1

0301 2	0351 PAPR	0401 I
0302 *	0352 P	0402)
0303 R - -	0353 2	0403 R - -
0304 0	0354 /	0404 0
0305 3	0355 P	0405 5
0306 =	0356 1	0406 PRNT
0307 R - -	0357 R - -	0407 CLDP
0308 1	0358 0	0408 PAPR
0309 9	0359 8	0409 P
0310 CLDP	0360 PRNT	0410 2
0311 R - -	0361 CLDP	0411 (
0312 1	0362 PAPR	0412 P
0313 4	0363 P	0413 S
0314 *	0364 5	0414 I
0315 R - -	0365 /	0415)
0316 0	0366 P	0416 R - -
0317 5	0367 1	0417 1
0318 =	0368 R - -	0418 8
0319 R - -	0369 1	0419 PRNT
0320 2	0370 4	0420 CLDP
0321 0	0371 PRNT	0421 PAPR
0322 CLDP	0372 CLDP	0422 P
0323 R - -	0373 PAPR	0423 4
0324 1	0374 T	0424 (
0325 7	0375 2	0425 P
0326 *	0376 /	0426 S
0327 R - -	0377 T	0427 I
0328 0	0378 1	0428)
0329 3	0379 R - -	0429 R - -
0330 =	0380 1	0430 2
0331 R - -	0381 2	0431 2
0332 2	0382 PRNT	0432 PRNT
0333 1	0383 CLDP	0433 CLDP
0334 CLDP	0384 PAPR	0434 PAPR
0335 M	0385 T	0435 P
0336 A	0386 5	0436 5
0337 C	0387 /	0437 (
0338 H	0388 T	0438 P
0339	0389 1	0439 S
0340 N	0390 R - -	0440 I
0341 U	0391 1	0441)
0342 M	0392 7	0442 R - -
0343 B	0393 PRNT	0443 2
0344 E	0394 CLDP	0444 0
0345 R	0395 PAPR	0445 PRNT
0346 R - -	0396 P	0446 CLDP
0347 0	0397 1	0447 PAPR
0348 6	0398 (	0448 T
0349 PRNT	0399 P	0449 1
0350 CLDP	0400 S	0450 (

```
0452    K
0452     )
0453    R _  _
0454    0
0455    3
0456    PRNT
0457    CLDP
0458    PAPR
0459     T
0460     2
0461     (
0462     K
0463     )
0464    R _  _
0465    1
0466    9
0467    PRNT
0468    CLDP
0469    PAPR
0470     T
0471     5
0472     (
0473     K
0474     )
0475    R _  _
0476    2
0477    1
0478    PRNT
0479    CLDP
0480    PAPR
0481    PAPR
0482    PAPR
0483    STOP
```

APPENDIX G

Thin Film Gauge Preamp Schematic

27μf

.001

3.3k

5pf

CA3023

.01

1N4789

1.2k

200

56μ

1N4734

1000μf

IN2994

100,5W

300μf

300μf

MDA920-3

1/2 A
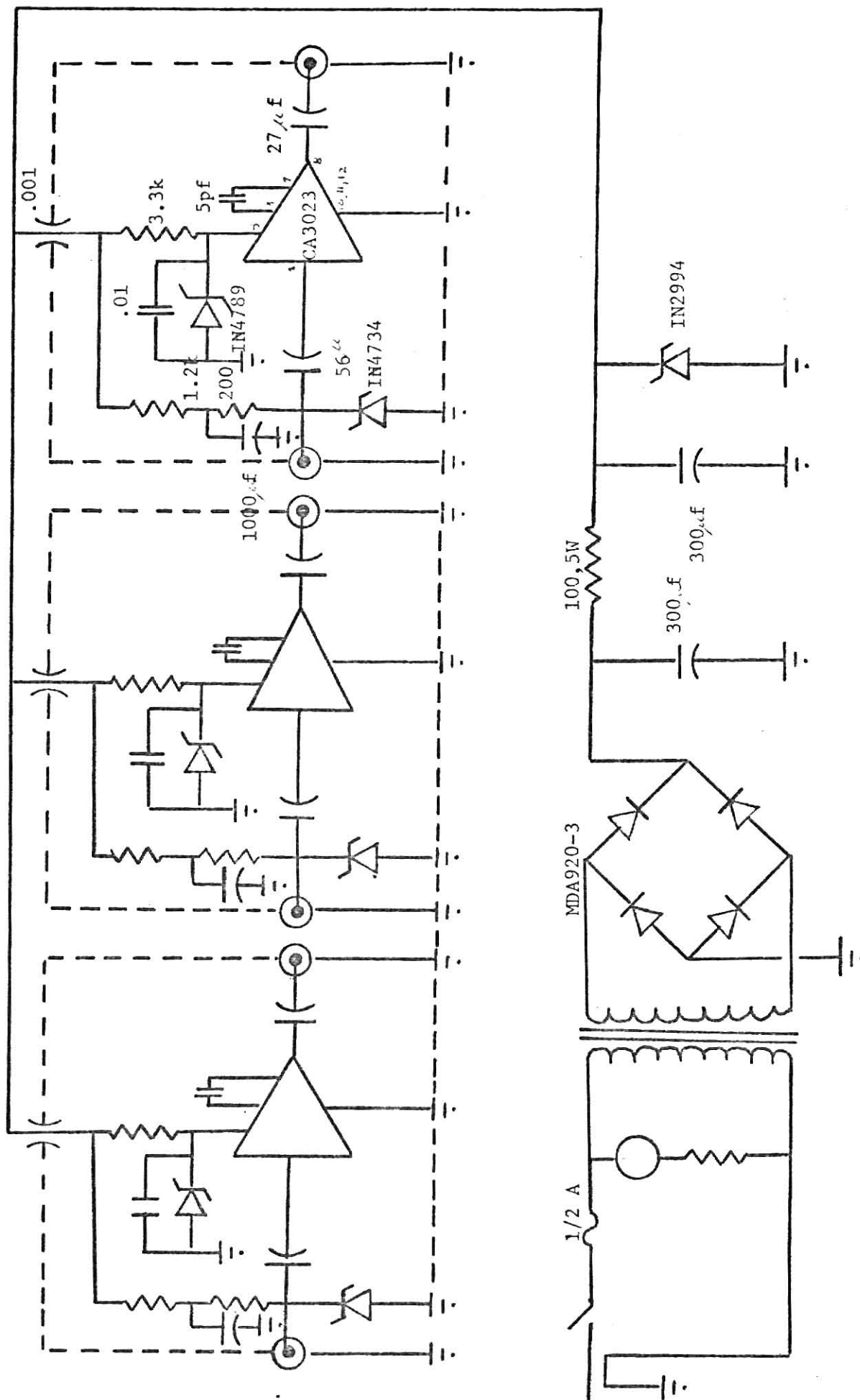
THREE CHANNEL WIDE BAND AMPLIFIER

THE DESIGN, ASSEMBLY, AND TESTING OF A
SHOCK TUBE FOR STUDY OF COAL
COMBUSTION KINETICS

by

WILLIAM RANDALL SEEKER

B. S., New Mexico State University, 1974

AN ABSTRACT OF A MASTER'S THESIS

submitted in partial fulfillment of the
requirements for the degree

MASTER OF SCIENCE

Department of Nuclear Engineering

KANSAS STATE UNIVERSITY

Manhattan, Kansas

1976

ABSTRACT

The objectives of this investigation were to design, contruct, develop operating procedures, and test the performance of a conventional shock tube which could be used for the study of coal combustion kinetics and two-phase boiling phenomenon. The tube was designed to be ten meters in length with driver and test section lengths of three meters and seven meters, respectively. The 2 inch (5.08 cm) I.D. circular stainless steel tube consisted of subsections of various lengths for versatility. The support system, gas manifold systems, vacuum systems, and materials were developed and chosen using normal engineering practices to facilitate the correct performance of the shock tube. Diagnostics were developed to investigate the shock wave strength and formation behind the reflected shock wave.

Operating procedures were developed which allowed repeatability of the shock speed for various runs within 5 percent. The diagnostics were capable of determining the incident shock Mach number with 0.5 percent percision. The effect of the mounting of the pressure transducer was studied and a flush lateral wall mounting was proven acceptable. Pressure histories behind the reflected shock were studied and demonstrated up to 1.5 msec of uniform flow with no observable pressure rise due to shock attenuation. Degradation of this uniform flow time was noted for initial test gas pressures below 50 torr. The reflected rarefaction ultimately limited the observation time to 5 msec. A comparison of the measured and theoretically predicted shock speed deceleration revealed that for low initial test gas pressures the laminar boundary layer persisted far down the tube. The attenuation was observed to increase for the same shock speed in lower initial test gas pressures.